DISCLAIMER NOTICE

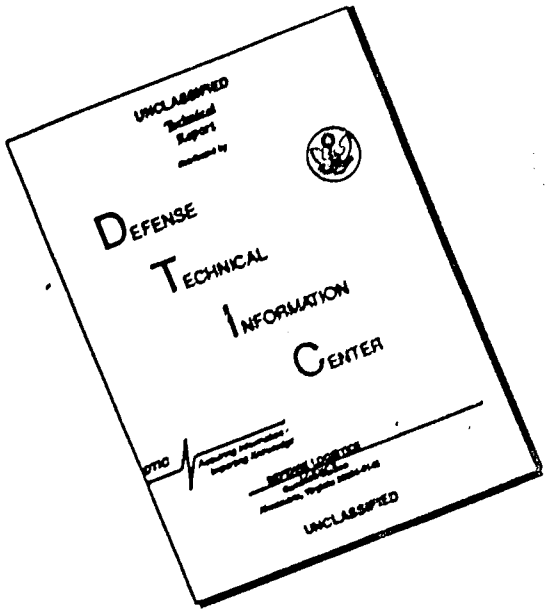

THIS DOCUMENT IS BEST QUALITY AVAILABLE. THE COPY FURNISHED TO DTIC CONTAINED A SIGNIFICANT NUMBER OF PAGES WHICH DO NOT REPRODUCE LEGIBLY.

Final Report

SUDDEN IONOSPHERIC DISTURBANCES AND THE PROPAGATION OF VERY-LOW-FREQUENCY RADIO WAVES

Part I: Phenomenology and Relevant Ionospheric Theory

Prepared for:

UNITED STATES AIR FORCE
AIR FORCE OFFICE OF SCIENTIFIC RESEARCH
WASHINGTON 25, D.C.

CONTRACT AF 49(638)-1081

By: *Edward T. Pierce* *Helen R. Arnold*

STANFORD RESEARCH INSTITUTE
MENLO PARK, CALIFORNIA

SRI

STANFORD RESEARCH INSTITUTE
MENLO PARK, CALIFORNIA
SRI

July 1963

Final Report

SUDDEN IONOSPHERIC DISTURBANCES AND THE PROPAGATION OF VERY-LOW-FREQUENCY RADIO WAVES

Part 1: Phenomenology and Relevant Ionospheric Theory

Prepared for:

UNITED STATES AIR FORCE
AIR FORCE OFFICE OF SCIENTIFIC RESEARCH
WASHINGTON 25, D.C.

CONTRACT AF 49(638)-1081
CONTRACT DATE: 11 MAY 1961
CONTRACT EXPIRATION DATE: 30 APRIL 1963
PROJECT CODE 8200

By: *Edward T. Pierce* *Helen R. Arnold*

Project Scientists: *A. L. Whitson* *DA 6-6200, Ext. 2529*
E. T. Pierce *DA 6-6200, Ext. 2087*

SRI Project No. 3684

AFTAC PROJECT AUTHORIZATION VELA T/1148/E/OSR
ARPA ORDER 159-61, AMENDMENT NO. 7

Approved:

W. R. VINCENT, MANAGER, COMMUNICATION LABORATORY

D. R. SCHEUCH, DIRECTOR, ELECTRONICS AND RADIO SCIENCES DIVISION

Copy No. 11
SERIES B

ABSTRACT

The changes in VLF radio noise accompanying a solar flare and its associated sudden ionospheric disturbance (SID) are surveyed. The onset time of the effects is about 10 minutes, but may be less than 2 minutes for perhaps 5 percent of the incidents. The alteration in propagation conditions implies an increase in noise on frequencies exceeding 20 kc and a decrease below 10 kc. If a local thunderstorm develops, the time phasing is very similar to that of an SID incident, but noise at all frequencies is enhanced.

A detailed examination of the formative processes of the lower ionosphere is made. Values of the rate coefficients for attachment, detachment (photo, collisional, and associative), electron-ion recombination, and ion-ion recombination, are deduced for heights from 40 to 100 km. Over the same height range, the ionizing contributions due to the major influences of cosmic rays, solar X rays, and solar Lyman α and to certain subsidiary causes are examined. The balance equations for the lower ionosphere are solved for the cases of equilibrium conditions and of the departure from equilibrium associated with the approach of night. Two specific examples indicate that contours of electron density, and therefore of ionospheric conductivity, are far from parallel to the surface of the earth. It follows that the attenuation coefficient for VLF propagation by day can differ according to the solar zenith angle by as much as 20 percent from the mean daytime value.

A model of the solar X-ray flux during a flare is derived and its ionizing effects examined. The flux peaks in 5 minutes but it is found that the maximum ionospheric effect lags behind, especially at the lower heights. Surprisingly

enough, the persistence of the added ionization does not increase monotonically with increasing height.

The ionization produced by an X-ray burst from a nuclear explosion in space is deduced. Differences in the onset phase, the spectral distribution of the X rays, and the zenith-angle dependence, as compared with a natural SID, are demonstrated. The decay of the additional ionization is examined and it is shown that this often involves three phases: the establishment of an attachment-detachment balance, a plateau with little decay, and a final decrease by recombination. An example indicates that if the same amount of extra ionization is introduced at heights of 70, 75, and 80 km, then, after about an hour, more of the additional ionization remains at 70 km than at either of the other heights.

CONTENTS

CONTENTS

CONTENTS

ILLUSTRATIONS

ILLUSTRATIONS

ILLUSTRATIONS

ILLUSTRATIONS

TABLES

TABLES

ACKNOWLEDGEMENTS

Mr. Robert F. Daly of Stanford Research Institute assisted us greatly by preparing suitable computing programs. Dr. T. Kamada of the Research Institute of Atmospherics, Nagoya University, Japan, was very helpful in explaining some aspects of his work. Valuable discussions on rate coefficients were enjoyed with Mr. S. D. Abercrombie and his colleagues of the Atomic Weapons Research Establishment, England, and with Mr. Warren S. Knapp of General Electric TEMPO.

1. INTRODUCTION

The very-low-frequency (VLF) band in the radio spectrum is officially defined as covering the frequency range of 3 to 30 kc. Radio waves of these frequencies are normally propagated in the quasi-waveguide represented by the earth and the lower ionosphere. The special case of the whistler mode [Helliwell and Morgan (1959)],* in which the VLF signals are guided along a magnetic line of force and penetrate the ionosphere, will not be considered in this report.

Experimental work upon VLF propagation is reasonably consistent in suggesting that sky waves are reflected from a height of about 70 km by day; at night the reflection height is some 90 km [Bracewell et al. (1951)]. Also, the theoretical approach in which the ionosphere is considered to be a homogeneous conductor sharply bounded at the heights quoted above has been effective in explaining many of the major features experimentally observed in VLF propagation [Wait (1957, 1960)]. The model is that of a waveguide in which the walls--spherically concentric--are formed by the earth and the lower ionosphere: both of the walls are of uniform finite conductivity. Later theoretical work by Wait (1958) suggests that a better agreement with experimental results is found if an increase of ionization, and hence of conductivity, with penetration into the ionospheric boundary is postulated. However, it is still true that the dominant factor in VLF propagation, especially by day, is the ionization at heights below 100 km.

The lower ionosphere, which may be roughly identified with the D region, is complicated and far from being entirely understood. The principal ionizing agencies are cosmic rays and the solar X-ray and Lyman-α (wavelength 1216A) radiations; the latter are, of course, absent at night. Subsidiary ionization

*References are given at the end of each section.

results from the action of meteors, of other solar ultraviolet radiations, and of incoming particles with origins in the sun or in the van Allen belts around the earth. The immediate action of the ionizing influences is to produce free electrons and positive ions of molecular or--above about 90 km--atomic size. Subsequently, the electrons may become attached to neutral particles thus forming negative ions; the reverse process of detachment may operate: and there will be recombination between electrons and positive ions, and also between positive and negative ions. Under quiet solar conditions, balance equations, in which all the above processes are represented, can be formulated and solved. There are, however, many uncertainties in the coefficients involved. Also, it is quite possible that ions of larger size than single molecules are present in the lower ionosphere, a fact that would further complicate the balance equations. It is known that above 90 km the ions are of molecular or atomic character; at 30 km the dominant ion is the small or cluster ion of atmospheric electricity consisting of a single molecular ion surrounded by a group of perhaps 4 to 12 neutral molecules; the height at which the transition from cluster ions to molecular ions takes place remains uncertain.

When a flare is observed upon the sun, normally in the light of the hydrogen Hα line (6563A), a sudden ionospheric disturbance (SID) usually follows within a few minutes. The SID is almost certainly due to an enhancement, associated with the flare, especially of the solar X-ray flux [Friedman (1959)]. Additional ionization is produced in the ionosphere, this being detectable in several ways: for example, a sharp kick known as a crochet occurs upon records of the earth's magnetic field. There are also pronounced absorption effects upon radiowaves passing through the D region; this is because the absorption coefficient for such nondeviating waves is proportional to the product of electron density, N, and electron collisional frequency, ν, so that the increase in N represents an intensified absorption. The absorption is usually detected in two ways. Sources of cosmic noise may be monitored, normally at a frequency (about 20 Mc) slightly above the lower limit that would penetrate the F layer; the drop in

signal accompanying an SID is then often referred to as a sudden cosmic noise absorption (SCA or SCNA). Alternatively, signals generated by ground-based transmitters, at frequencies (3-15 Mc) that are usually reflected from one of the ionospheric layers above D (E or F), may be observed. In this case there is a multiple path through the D region and the absorption produces a short-wave fade-out (SWF).

The effects of an SID upon VLF propagation are also marked. Here the influence of the increased ionization is to depress the lower boundary of the D region and thus to narrow the earth-ionosphere waveguide from its normal daytime dimension of 70 km. At the same time, the conductivity of the ionosphere may be enhanced. There are two principal SID phenomena detectable at VLF. The first of these is the sudden phase anomaly (SPA); when the phase of a long-wave transmitter is continuously monitored, a rapid change, resulting from the lowering of the reflection points for sky waves, is observed. Secondly, an SID alters the propagation characteristic of the earth-ionosphere waveguide so that the attenuation of some frequencies in the VLF band (3-30 kc) is increased while that of others is diminished. The changes are most conveniently detected by recording the radio-noise or VLF atmospherics generated by lightning: this source radiates at all frequencies in the VLF band so that the influence of the SID can be determined as a function of frequency. The phenomenon is often referred to as a sudden enhancement of atmospherics (SEA), although this description is somewhat misleading: the enhancement is only at certain frequencies while at others there is a decrease in signal strength.

This report represents Part I of the Final Report under U. S. Air Force Contract AF 49(638)-1081. The complete Final Report will be concerned with various aspects of the interrelation between an SID, either of natural or man-made origin, and the associated changes in attenuation coefficients for propagation at frequencies within the VLF band. The SEA phenomenon will receive principal attention. This report (Part I) considers two main subjects. First,

the phenomenology of a natural SID and its associated changes in VLF radio noise are discussed. Second, a model of the lower ionosphere and of its changes under various conditions is derived; in particular, variations during an SID and following a nuclear explosion in space are considered. The application to VLF propagation is examined. Part II of the Final Report will mainly deal with the experimental data obtained from an analysis of whistler tapes, and with the development of simple instruments for monitoring the changes in VLF radio noise accompanying an SID.

1.1 REFERENCES FOR SEC. 1

Braecwell, R. N., K. G. Budden, J. A. Ratcliffe, T. W. Straker, and K. Weekes, "The Ionospheric Propagation of Low and Very-Low-Frequency Radio Waves over Distances Less than 1000 km," Proc. IEE (London), Vol. 98 (III), pp. 221-236 (1951).

Friedman, H., "Rocket Observations of the Ionosphere," Proc. IRE, Vol. 47, pp. 272-280 (1959).

Helliwell, R. A., and M. G. Morgan, "Atmospheric Whistlers," Proc. IRE, Vol. 47, pp. 200-208 (1959).

Wait, J. R., "The Attenuation vs. Frequency Characteristics of VLF Radio Waves," Proc. IRE, Vol. 45, pp. 768-771 (1957).

Wait, J. R., "An Extension to the Mode Theory of VLF Ionospheric Propagation," J. Geophys. Research, Vol. 63, pp. 125-135 (1958).

Wait, J. R., "Terrestrial Propagation of Very-Low-Frequency Radio Waves," J. Research NBS, Vol. 64D, pp. 153-204 (1960).

2. PHENOMENOLOGY OF SUDDEN IONOSPHERIC DISTURBANCES AND THE ASSOCIATED CHANGES IN VLF RADIO NOISE

2.1 INTRODUCTION

The solar outburst, known as a flare, usually occurs in association with an active spot-group upon the sun. The flare region, as observed in Hα light, brightens and increases in area for a few minutes; subsequently there is a return to normal which may occupy perhaps half an hour. Flares are classified primarily in terms of area, and the basic categories in order of increasing importance are denoted by 1, 2, and 3. The supplementary designations 1−, 1+, 2+, and 3+ are widely employed. Although the classification is based upon area, increasing flare importance also implies an increase in total duration, in the line-width of Hα at the maximum, and in the intensity of Hα from the flare region as compared with the continuum from adjacent areas. These features are illustrated in Fig. 2.1. When flares are divided into Categories 1, 2, and 3, it is found that 72 percent of the incidents are of the first importance; 25 percent are in Category 2; and only 3 percent are classified as large flares.

Hα light penetrates to the surface of the earth without effective absorption, and thus enables the development of a flare to be readily monitored. However, any solar radiations that influence the ionosphere must suffer appreciable absorption there; it follows that such radiations are not easily detectable, except in the high atmosphere. Direct information upon their variation during an SID must be largely obtained from rocket and--especially--satellite observations. Little such information is presently available. Inferences from ionospheric phenomena still supply most of the knowledge regarding the behavior of solar ionizing radiations during flares.

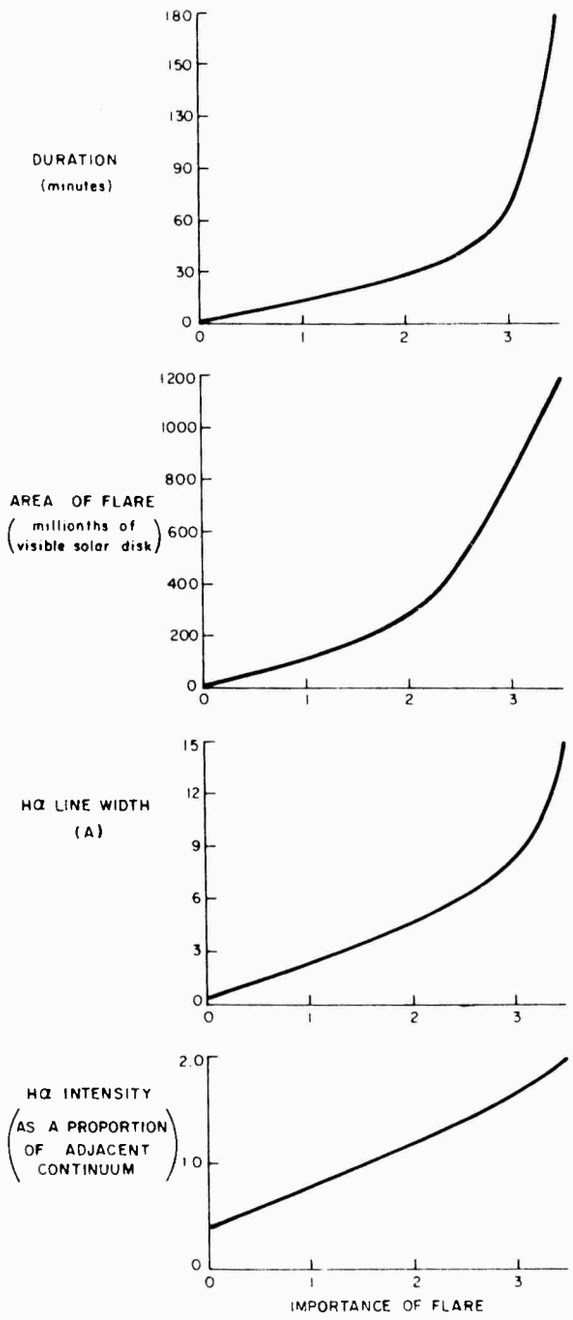

FIG. 2.1 SOME FEATURES OF SOLAR FLARES

For ionization to be produced somewhere in the ionosphere, the ionizing radiation must have a photon energy >9.5 ev, the energy representing ionization of the most easily ionizable molecule, NO. In terms of wavelength, λ, this implies a wavelength of less than some 1300Å. Within this range the harder X rays (λ<8Å) and Lyman -α radiation (λ= 1216Å) are capable of produeing ionization well below 100 km; the intermediate X-ray and ultraviolet radiations are mostly absorbed in the E and F regions. Direct evidenee from the NRL roeket program [Chubb, Friedman and Kreplin, (1960)] has shown that there is eertainly an enhaneement of the solar X-ray flux during a flare. The increase extends over a range of X-ray wavelengths eapable of giving ionization in both the D and E regions. Also the NRL roeket program has failed to indicate any appreeiable ehange, associated with a flare, in the Lyman -α flux. No direet evidenee is available for the wavelength range between Lyman α and X ray, but the observation, at HF, of flare-induced frequeney shifts, by Kanellakos, Chan, and Villard (1962), strongly suggests that extra ionization is produeed at heights between 120 and 200 km. This in turn would imply an inerease in the ultraviolet flux in the wavelength range of 100 to 1000 Å.

There is little evidenee for the ph .sing of the ionizing radiations with regard to Hα during a flare. One of the few direet observations was obtained by the solar satellite SR 1 [Kreplin, Chubb, and Friedman (1962)], for a flare on August 6, 1960. This indicated that the X-ray (<8Å) flux started to rise at about 1510 U.T. reaehing a maximum at approximately 1513; the Hα start was at 1506 and the maximum at 1514; and the Lyman -α flux remained constant between 1509 and 1514. The work of Kanellakos et al. (1962) shows that the maximum HF shift occurs 1 to 4 minutes before the maximum phase in Hα. Generally, the available observations and inferenees are eonsistent in suggesting that any ultraviolet radiation is likely to preeede the Hα, but that the X-ray and Hα phasing almost coineide. The hardest (highest-frequeney) X rays are most pronouneed when the total X-ray intensity is maximum: a similar hardening to maximum with a subsequent softening probably also holds for the ultraviolet flux.

The ionospheric consequences of the ionizing radiations depend, of course, upon their relative penetration. The VLF effects, namely the SPA and SEA, are controlled by hard X radiation and the consequent increase in ionization below about 70 km. Phase and frequency changes at megacycle frequencies, on the other hand, are caused by ionization at considerably higher levels, perhaps even above 150 km [Morriss (1960)]; this is presumably due to ultraviolet radiation. Absorption is an integrated effect throughout much of the ionosphere and in consequence the SWF and SCNA phenomena cannot be easily related to increases in ionization at specific heights.

Since a broad range of ionizing radiations, and consequently of ionospheric phenomena, is involved in a solar flare, the various effects are, inevitably, not very closely related. Although there is an interconnection in the average behavior, as shown, for example, in the straight-line relationship postulated by Shain and Mitra (1953) between SPA and SCNA magnitudes, there are wide differences between the individual cases. Some flares, for instance, give strong VLF effects, but minor absorption changes; others may show considerable absorption, but little alteration in VLF propagation. This variability cannot be overstressed; it is entirely incorrect to assume that the relative importance of the ionospheric effects associated with a solar flare is rigidly fixed.

2.2 SOME SID STATISTICS

The spread in the phenomena accompanying a flare has been emphasized in the preceding section; nevertheless, the average behavior can still be instructive, particularly if the statistical variability incorporated in the averaging procedure is also considered. Accordingly, the six-month period of January-June 1959 was selected and the information available in "Compilations of Solar-Geophysical Data," CRPL-F, Part B, issued by the National Bureau of Standards, was examined. Over a hundred incidents were chosen for which SCNA and SEA statistics (at 27 kc) were available, the SEA being regarded as

representative of VLF effects and the SCNA being considered as indicative of absorption; in about 50 percent of cases, Hα flare information could also be definitely associated with the ionospheric incident. The statistics examined consisted of duration for SCNA, SEA, and Hα flare; the rise time (time from start to maximum) for the same three phenomena; the delay in the start of the SEA and SCNA as compared with that for Hα; and the delay in the maximum of the SEA and SCNA again as compared with that for Hα.

The results obtained are shown in Figs. 2.2 to 2.6. They are in fair agreement (see Table 2.1) with some of the previous work of Ellison (1957, 1960) who tabulated SWF and SEA statistics. The agreement is best for the two sets of SEA data, and, in view of the fact that both the SWF and SCNA are basically absorption effects, some of the differences indicated between Ellison's results for SWFs and the present results for SCNAs are suprising.

Certain features of the data are worth mentioning. It seems likely that the peak in ionospheric phenomena will lag somewhat behind the maximum of the ionizing radiation, since until equilibrium is established between production and dissipation of electrons, the effects will be cumulative. It is certain that upon cessation of the ionizing flux the ionosphere will take an appreciable time--depending upon the height concerned--to return to normal. Many of the SID incidents examined show the Hα flare commencing before either the SEA or the SCNA, the maximum in the Hα flux preceding that of the SEA and SCNA, and the Hα light returning to normal well before complete recovery of the ionosphere. Such incidents are entirely compatible with the concept that the variation of the ionizing radiation is closely related to that of Hα. However, Fig. 2.4 indicates that in a small but significant proportion of instances the onset of an SCNA or SEA precedes that of the Hα flare. Furthermore, it is not uncommon for the SEA and SCNA effects to have ceased while the Hα emission is still active; in some instances the duration of the Hα flare may exceed that

TABLE 2.1

SID STATISTICS

Phenomenon	Average Duration*		Average Rise Time*		Average Starting Delay* Compared with Hα		Average Delay* of Maximum Compared with Hα	
	Present Results	Ellison	Present Results	Ellison	Present Results	Ellison	Present Results	Ellison
SCNA	37.4		8.4		2.8		2.3	
SEA	44.5	57.4	11.8	11.0	2.9	7.5	7.8	7.1
Flare seen in Hα	35.4	53.2	8.7	11.4				
SWF		88.1		13.9		4.8		7.3

*In minutes

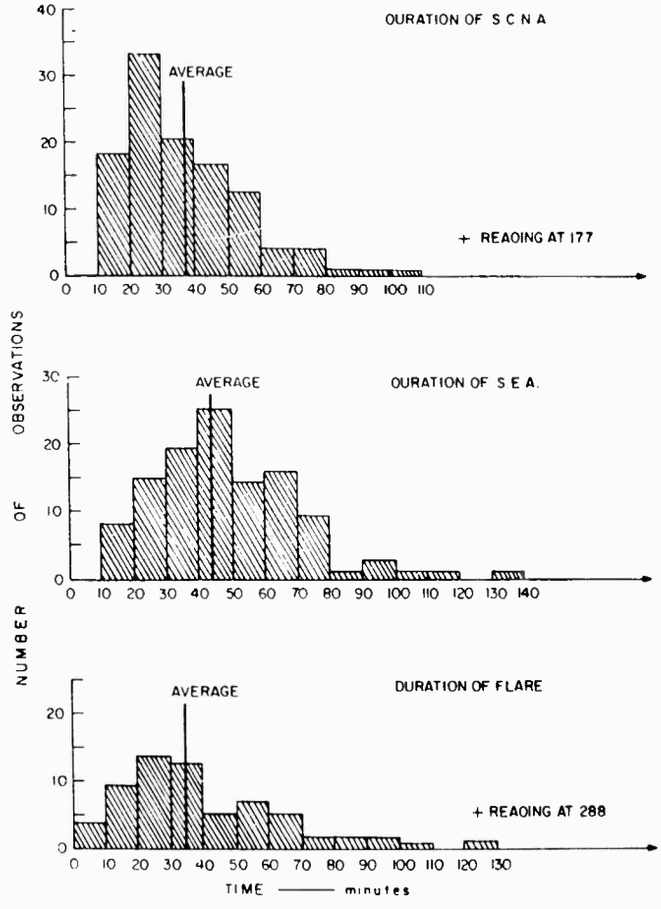

FIG. 2.2 DURATION STATISTICS FOR SID INCIDENTS

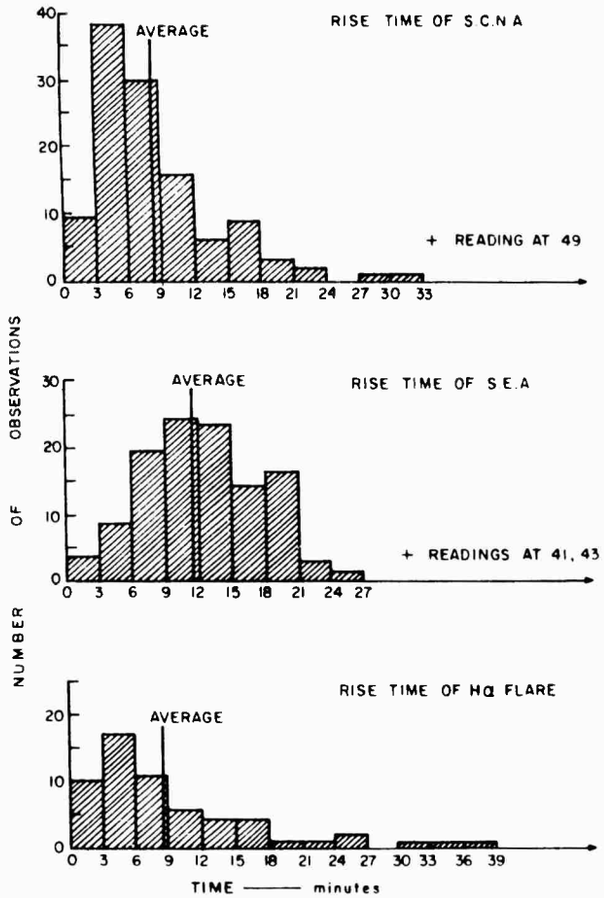

FIG. 2.3 RISE TIME STATISTICS FOR SID INCIDENTS

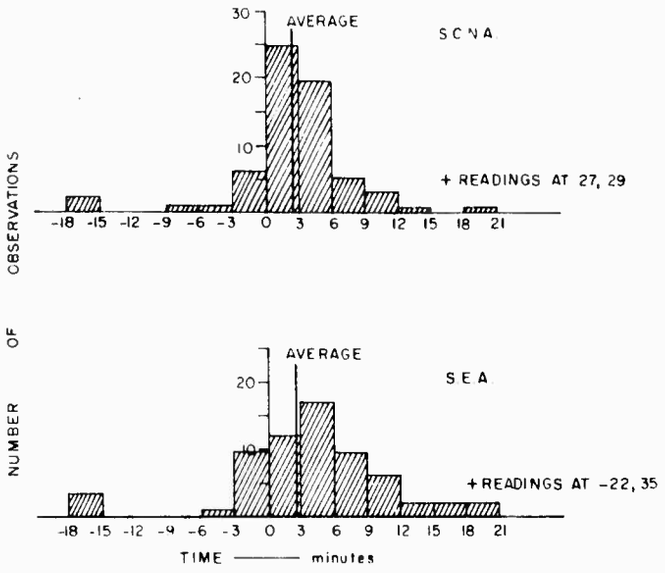

FIG. 2.4 STARTING DELAY STATISTICS FOR SID INCIDENTS

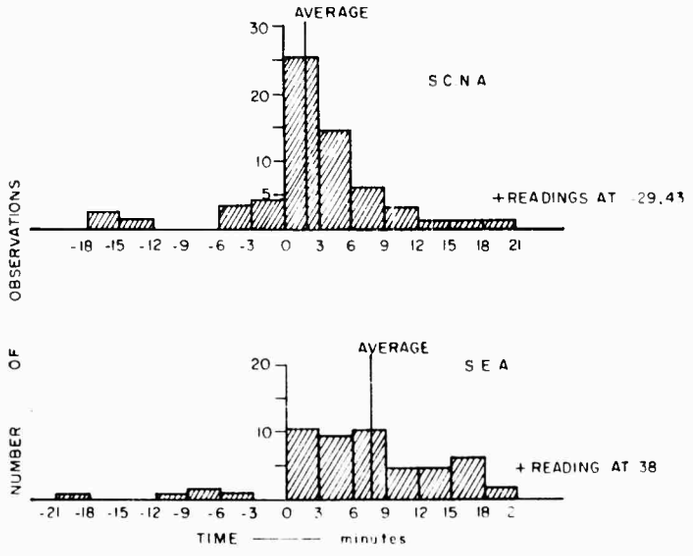

FIG. 2.5 STATISTICS FOR DELAY OF MAXIMUM FOR SID INCIDENTS

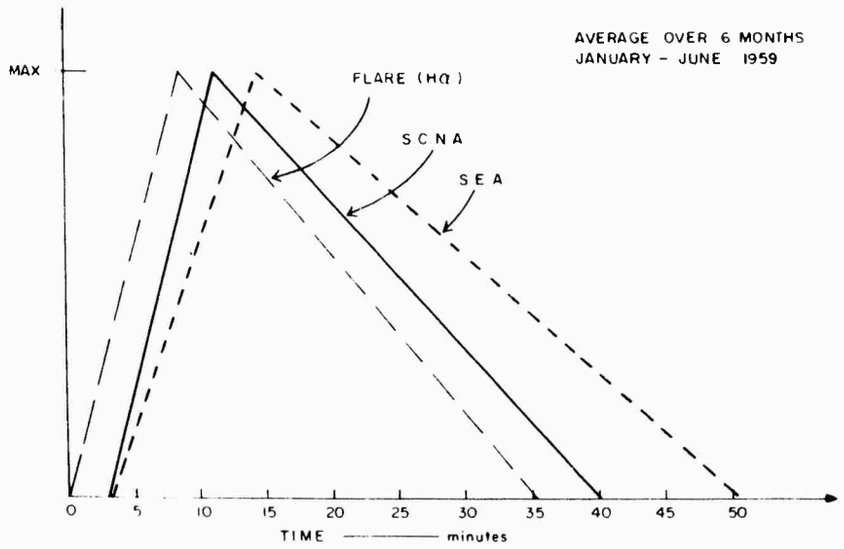

FIG. 2.6 AVERAGE PHASING OF Hα FLARE, SCNA, AND SEA, DURING AN SID INCIDENT

of the SEA and SCNA by 60 minutes or more. All these considerations confirm the conelusion that although the Hα behavior is a guide to that of the ionizing radiations, there is no exact eorrespondence.

One aspect of SID phenomena that could be instructive as regards the ionizing radiation involved is the dependenee upon solar zenith angle. Accordingly, the SCNA incidents for the period March 1958 to September 1961 were examined, the data being obtained as before from the solar-geophysical compilations of the NBS. For each occurrence, the solar zenith angle at the time of the SCNA and the percentage of absorption were obtained for the reporting station, and a plot (Fig. 2.7) made of the information. (One point was obtained for each SCNA.) It was anticipated that a trend toward increasing absorption with decreasing zenith angle would be detected: no such trend is apparent on Fig. 2.7, either in the individual points or in the 10-degree averages. The reason may be that present SCNA techniques involve threshold levels that tend to mask true variations. Perhaps the best method of ascertaining the zenith angle dependence in a SCNA would be to employ results for the same SCNA from several widely dispersed stations.

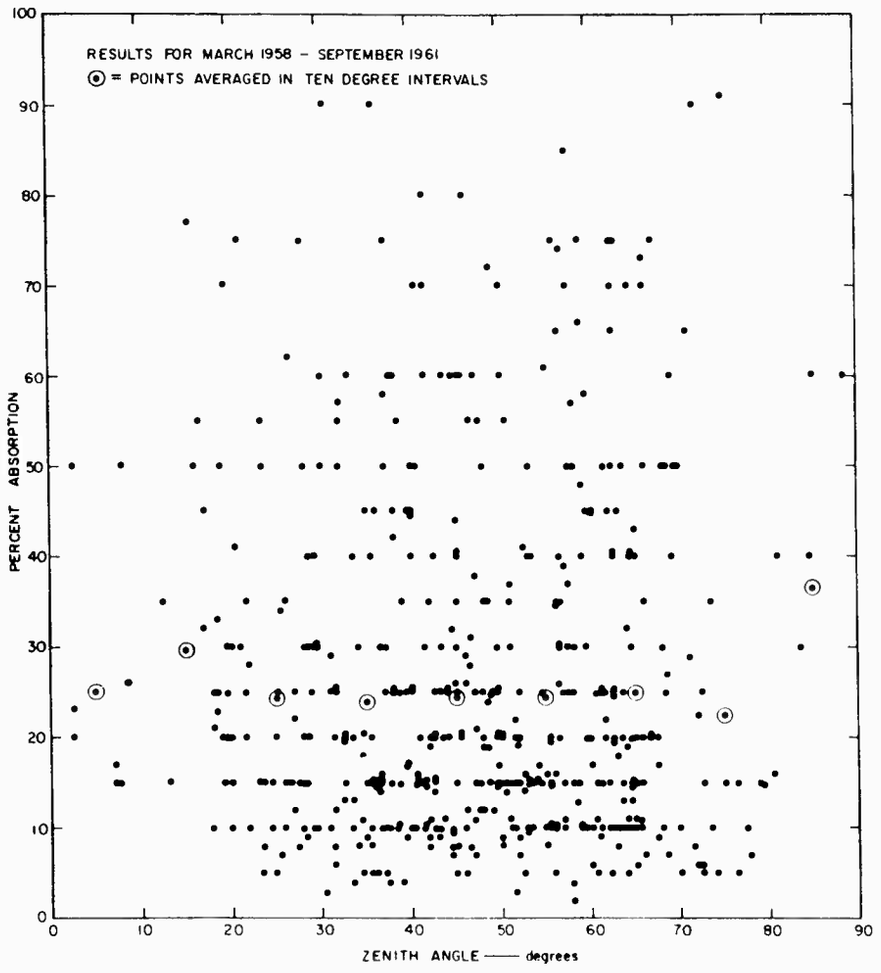

FIG. 2.7 RELATION BETWEEN SOLAR ZENITH ANGLE AND PERCENTAGE ABSORPTION FOR SCNA INCIDENTS

2.3 THE BEHAVIOR DURING AN SEA

2.3.1 Introduction

Almost all the routine information upon an SEA has been derived from recordings at a frequency of 27 kc. Observatories in most countries employ an instrument tuned to this frequency and integrating the received atmospheric noise over a period of a few seconds. The enhancements are reported upon a regular basis and the results, which involve world-wide coverage, are reproduced in publications such as "Compilations of Solar-Geophysical Data" of NBS. Information upon the behavior of SEAs as a function of frequency is scanty. Some data are available from research investigations, and the results from Japan, where it is common practice to record atmospheric noise continuously upon several frequencies, are especially valuable.

2.3.2 The Rise Time of an SEA

The rise times, that is, the time from onset to maximum, of the SEAs tabulated in the NBS publications have been examined. In these tabulations each SEA is classed in terms of magnitude according to the 1, 2, 3, scale with intermediate + or - signs. Ignoring the latter, Fig. 2.8 shows histograms giving the distribution of the results according to class. The information covers the period from March 1958 to February 1962 and includes 896 SEA incidents. The mean value of the rise time increases with class; for SEA incidents of importance 1, 2, and 3, the respective average rise times are 10.0, 12.5, and 14.8 minutes. The distributions are not symmetrical but are skewed in the sense that small values less than the mean tend to be more common than large rise times. The asymmetry seems to be most pronounced for the smaller incidents, but this may merely reflect the limited number of large SEAs. A normal distribution centered upon the mean has been plotted upon each of the histograms; this assists in emphasizing the skewness of the actual observations. The standard deviations appropriate to Classes 1, 2, and 3 are 5.5, 6.8, and 7.6 minutes, respectively.

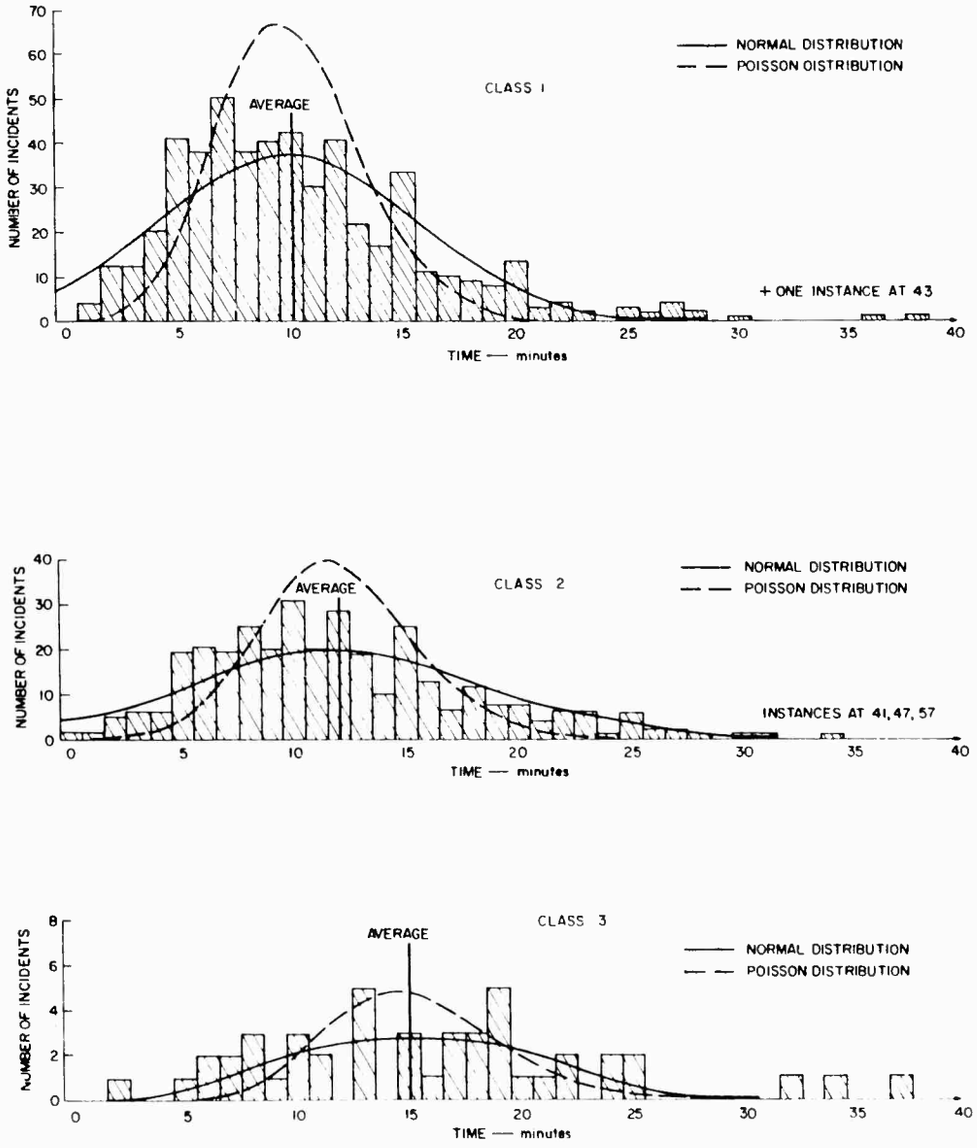

FIG. 2.8 DISTRIBUTION OF RISE TIMES FOR SEA INCIDENTS

Poisson distributions are also given on Fig. 2.8; these might be expected to fit the data better than normal curves, but the agreement is not good. For all the 896 incidents examined, only 11 have rise times of a minute or less while there are 19 SEAs with rise times between 1 and 2 minutes. Thus the chance of an SEA having a rise time equal to a minute or smaller is 1.2 percent; for less than or equal to 2 minutes the chance is 3.4 percent. These statistics are for a 4-year period of high solar activity. It may thus be confidently stated that taken as a whole over the complete solar cycle of 11 years, SEA incidents with rise times of less than 2 minutes are unlikely to occur more often than seven per annum.

Kamada (1960) has examined SEA data, obtained in Japan over the 5 years of 1955 to 1959, on the three frequencies of 10, 21, and 27 kc. For each frequency the distribution of the rise times is skewed towards the smaller values in a manner somewhat similar to that of Fig. 2.8. However, the average rise times are somewhat less than those given in the preceding paragraph. For the frequencies of 10, 21, and 27 kc, the mean rise times are, respectively, 7.8, 7.9 and 7.4 minutes. Also, the proportions of small rise times are rather more than those previously quoted. For rise times less or equal to 1 minute, and less or equal to 2 minutes, the respective percentages are 2.3 and 13.0.

2.3.3 Behavior as a Function of Frequency

The vertical electric field, E (mv/m), at a great-circle distance d (in km) from a source radiating P kw is given approximately [Wait (1958)] by

$$E = \frac{300}{h}\left\{\frac{P\lambda}{a \sin d/a}\right\}^{1/2} \exp(-\alpha d) \qquad (2.1)$$

where a is the radius of the earth (km), h the height of the ionospheric reflecting layer (km), λ the wavelength concerned (km), and α the attenuation factor.

Equation (2.1) assumes the dominance of a single mode which is approximately true for d > 1000 km and frequencies in the VLF range. The application to VLF atmospheric noise is therefore reasonably valid. It follows that if the suffix N represents normal conditions and S the SID, then

$$(\alpha_S - \alpha_N) \quad \frac{1}{d}\, 2 \times 10^4 \log \left(\frac{h_N E_N}{h_S E_S}\right) - \frac{1}{d}\, 2 \times 10^4 \log (1.08\, E_N/E_S). \tag{2.2}$$

In Eq. (2.2) the units for α_S and α_N are db/1000 km, and the fields E_N and E_S are taken as being compared at a definite frequency. The factor $h_N/h_S \approx 1.08$; this is the average value given by Bracewell and Straker (1949).

Pierce (1961) has applied Eq. (2.2) to various sets of research data in order to obtain the variation of $(\alpha_S - \alpha_N)$ with frequency. The three sources of information originally considered by Pierce were Gardner (1950), Obayashi (1960), and Obayashi, Fujii, and Kidokoro (1959). The corresponding results are shown on Fig. 2.9 together with an additional curve deduced from the work of Bowe (1951). It is evident from Fig. 2.9 that at frequencies of 20 kc and greater $(\alpha_S - \alpha_N)$ is negative; in other words, the attenuation is less during an SID than under normal conditions, and there is an enhancement of atmospheric noise. For frequencies of 10 kc and less, $(\alpha_S - \alpha_N)$ is positive, and atmospheric noise will therefore decrease in intensity with the onset of SID conditions. The range from 10 to 20 kc represents the intermediate zone where the transition from a decrease to an enhancement occurs.

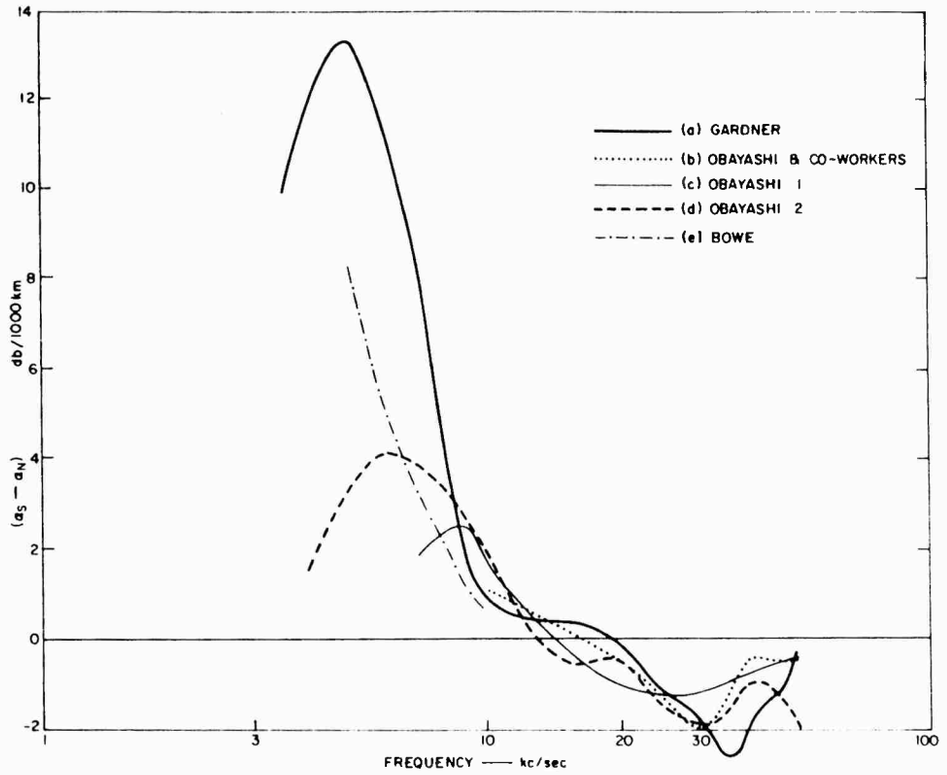

FIG. 2.9 DIFFERENCE BETWEEN VLF ATTENUATION COEFFICIENTS FOR NORMAL DAYTIME AND FOR SID CONDITIONS

The extensive observations of Kamada (1960, 1961) on the three frequencies of 10, 21, and 27 kc show that when a well-authenticated SID occurs there is an increase of noise on 21 and 27 kc and a decrease at 10 kc. This result is entirely consistent with Fig. 2.9. Kamada estimates that the transitional or turnover frequency, which is unaffected during a SEA, lies between 14 and 18 kc. This suggestion is again in agreement with Fig. 2.9, but it should be emphasized that Kamada's estimate is based on interpolation, and also that the amount of data represented by Fig. 2.9 is very limited. There are some indications that the transitional frequency may vary between individual flares in a manner apparently unrelated to other characteristics or to associated ionospheric effects. More data are necessary before such questions can be entirely clarified.

2.3.4 Local Thunderstorms

An SID produces an SEA on a frequency exceeding 20 kc by changing propagation conditions, hence reducing the value of α in Eq. (2.1), and consequently increasing E. Obviously alterations in the other factors in Eq. (2.1) can also have the effect of enhancing E; such alterations are due to changes in the level of thunderstorm activity. For instance, if existing storms increase in intensity, this implies a greater value of P and hence an enhancement in E; if the storms move closer to the recording station, this gives a decrease in the effective d and again an increase in E; if new thunderstorms develop, particularly at short ranges, once more E is enhanced. In the absence of other information, observations of atmospheric noise, at the frequency of 27 kc usually employed, cannot distinguish between an SEA associated with an SID and one due to changes in thundery activity, unless there are characteristic differences between the two types of SEA.

The frequency dependence enables the two types of SEA to be readily distinguished. Section 2.3.3 indicates that, accompanying an SID, a reciprocal effect applies; there is an enhancement of noise at some frequencies and a decrease at others. Changes in the level of thundery activity will, however, produce uniform behavior; at all frequencies, noise will either be increased or diminished.

Japanese observations for the year 1958 [IGY Data (1959)] are available, the sudden changes in atmospheric noise observed at frequencies of 10, 21, and 27 kc being listed. By means of the criterion of reciprocal or similar amplitude behavior at 10 and 27 kc, it is easy to separate the SEA incidents associated with solar disturbances from those probably due to changed thunderstorm activity. Various statistics derived for the two types of SEA are shown on Table 2.2.

TABLE 2.2

COMPARISON OF AVERAGE CHARACTERISTICS FOR SEAS ASSOCIATED RESPECTIVELY WITH SIDS AND CHANGES OF THUNDERY ACTIVITY

Type of SEA	Mean Rise Time*		Mean Duration*		Mean Time* That Onset at 10 kc Precedes That at 27 kc
	10 kc	27 kc	10 kc	27 kc	
Associated with SID	11.8	8.6	46.1	41.9	-0.1
Associated with Thunderstorms	11.4	11.7	40.4	42.6	+0.2

*In minutes.

It is evident that, although their origins are different, there is very considerable similarity in the characteristics of the two types of SEA. Slight distinctions can be identified which mainly represent the correlation between the phasing of the phenomena on the two different frequencies; this connection is much closer for the SEAs due to thunderstorms than it is for those associated with SIDs. For instance, although the means in the final column of Table 2.2 are nearly identical and represent in each instance an almost symmetrical distribution of positive and negative values about zero, the average of the individual differences (irrespective of sign) between the onset times at 10 and 27 kc is significantly divergent as between the two types of SEA. This and other similar points are illustrated in Table 2.3.

TABLE 2.3

COMPARISON OF PHASING OF BEHAVIOR AT 10 AND 27 KC
FOR THE TWO TYPES OF SEA

Type of SEA	Mean Difference* in Onset Times at 10 and 27 kc**	Mean Difference* in Rise Times at 10 and 27 kc**	Mean Difference* in Duration at 10 and 27 kc**
Associated with SID	4.4	4.8	17.4
Associated with Thunderstorms	1.5	2.2	4.6

*In minutes.
**Ignoring sign.

Table 2.3 indicates that if there are appreciable differences at 10 and 27 kc in the time phasing of onset, maximum, and end, then the SEA concerned is probably associated with an SID. However, the most reliable indicator that the SEA is of solar origin remains the reciprocal behavior of an increase in noise at 27 kc and a decrease at 10 kc.

2.3.5 Various Aspects of SEA Behavior

The forms of SEAs as a function of time have been subdivided by Kamada (1960). Kamada's subdivision is somewhat complicated but can be simplified into two classes, A and B. In Class A the rise time of the SEA is much smaller than the decay time and the maximum is a sharp peak. For Class B the rise is comparable with that for Class A, but is followed by an appreciable period where the changes from the maximum value are not very pronounced, until ultimately there is a sudden decay to the origin; this takes much the same time as the rise. Class A changes usually have a sawtooth shape: typically the Class B variations appear as inverted Us or Ws.

When the results at 10, 21, and 27 kc are divided into Classes A and B, there are some interesting features. Table 2.4 has been constructed using 63

SEA incidents which, by the criterion of an increase in noise on 21 and 27 kc and a decrease at 10, are definitely to be associated with an SID.

TABLE 2.4
CLASSIFICATION OF SEA INCIDENTS ACCORDING TO SHAPE

Sawtooth (A) Inverted U (B)

Frequency (kc)	10	21	27	Number of Incidents
	-B	B	B	13
	-B	B	A	6
	-B	A	B	0
	-B	A	A	21
	-A	B	B	6
	-A	B	A	0
	-A	A	B	0
	-A	A	A	17

Incidents where all three frequencies have the same class are common; this is probably a reflection of the temporal variation in the incident flux. The class on 21 kc is always similar either to that on 27 kc or to that on 10 kc; this shows a systematic behavior with frequency. When the class on 10 kc differs from that on 27 kc, usually 10 is of Class B and 27 of Class A; this is consistent with the idea that 10 kc is affected by ionization lower in the ionosphere than is 27 kc, and the recovery is therefore, perhaps, more sudden.

Rough rules can be formulated relating the magnitude of an SEA to the parameters of the causative flare. These rules should be taken only as indicative; obviously, since an SID changes the propagation characteristic, the size of an SEA will depend upon the distance of the sources of atmospheric noise. However, the following average relations apply to the Japanese observations for 1958 [IGY Data (1959)].

At 27 kc, enhancement = 2.5 + 0.5 (S-1) db

at 10 kc, enhancement = - $\{0.2 + 0.4\ (S-1)\}$ db

where S is the importance of the flare. In the Japanese equipment the bandwidth is 500 cps; the 0-db level is 1 $\mu\nu$/m; and the enhancement is defined as 20 log E_S/E_N, where E_S is the maximum intensity of the SEA and E_N the pre-SEA value.

The Japanese 1958 observations were also examined in an effort to determine any relationship between solar zenith angle and the size of an SEA. Such a relationship cannot be expected to be pronounced. Although it is probable that a solar flare produces its maximum ionospheric effect at the subsolar point, the measurement of atmospheric noise involves integration over many propagation paths, and therefore a wide area and a considerable range of zenith angles. Table 2.5 shows the relationship between the average size of an SEA observed at 27 kc and Japanese local time.

TABLE 2.5

RELATIONSHIP BETWEEN SIZE OF SEA OBSERVED AT 27 KC AND LOCAL TIME

Local Time	Number of SEA Incidents	Average Magnitude (db)
800	12	2.8
1000	13	3.5
1200	12	3.0
1400	16	2.8
1600	11	2.4
1800	14	2.4

There is a slight tendency for the larger SEAs to occur near local noon, that is, when the solar zenith angle is least, but the trend is not marked. Kamada's (1960) results show an interesting distinction in behavior between 10, 21, and 27 kc. This is illustrated in Table 2.6.

TABLE 2.6

OCCURRENCE OF SEA INCIDENTS AS A FUNCTION OF LOCAL TIME

	Number of SEA Incidents Observed		
Local Time	10 kc	21 kc	27 kc
0500-0700	1	20	23
0700-0900	7	113	151
0900-1100	23	118	167
1100-1300	48	112	165
1300-1500	51	137	185
1500-1700	31	137	179
1700-1900	12	81	87
1900-2100	0	7	9

Obviously there is a pronounced maximum for the 10-kc observations near local noon. At 21 and 27 kc, on the other hand, the rate of occurrence of SEAs is almost uniform throughout the day. This suggests that the radiation responsible for the 10-kc enhancement, which presumably penetrates to lower heights than that affecting 27 kc, is fairly sensitive to the value of the solar zenith angle.

One further aspect of the Japanese SEA observations is worth noting. This is the close correlation [Kamada (1960)] between outbursts of solar radio noise at centimetric wavelength (> 3000 Mc) and SEA incidents. The start of the solar radio outburst usually precedes that of the SEA by a few minutes.

2.4 REFERENCES FOR SEC. 2.

Bowe, P. W. A., "The Waveforms of Atmospherics and the Propagation of Very Low Frequency Radio Waves," Phil. Mag., Vol. 42, pp. 121-138 (1951).

Bracewell, R. N., and T. W. Straker, "The Study of Solar Flares by Very Long Radio Waves," Monthly Notices Roy. Astron. Soc., Vol. 109, pp. 28-45 (1949).

Chubb, T. A., H. Friedman, and R. W. Kreplin, "Measurements Made of High-Energy X-Rays Accompanying Three Class 2+ Solar Flares," J. Geophys. Research, Vol. 65, pp. 1831-1832 (1960).

Ellison, M. A., "Solar Flares," Vistas in Astronomy, Vol. 2, pp. 799-807 (Pergamon Press, New York, 1957).

Ellison, M. A., Susan M. P. McKenna, and J. H. Reid, "Light-Curves of 30 Solar Flares in Relation to Sudden Ionospheric Disturbances," Dunsink Observatory Publications, Vol. 1, No. 1 (1960).

Gardner, F. F., "The Use of Atmospherics to Study the Propagation of Very Long Radio Waves," Phil. Mag., Vol. 41, pp. 1259-1269 (1950).

"IGY Data on Atmospherics, Whistlers, and Solar Radio Emissions," Vols. II and III for January-June and July-December 1958, National Committee for the IGY, Japan (1959).

Kamada, T., "Statistical Properties of the Sudden Enhancement of Atmospherics in V.L.F. Range," Proc. Research Inst. Atmospherics, Nagoya University (Japan), Vol. 7, pp. 28-39 (1960).

Kamada, T., "SEA and Hiss Associated with Great Bursts of Solar Radio Emission in November 1960--II. Mode IV Sudden Enhancement of Atmospherics," Proc. Research Inst. Atmospherics, Nagoya University (Japan), Vol. 8, pp. 7-12 (1961).

Kanellakos, D. P., K. L. Chan, and O. G. Villard, Jr., "On the Altitude at Which Some Solar-Flare-Induced Ionization is Released," J. Geophys. Research, Vol. 67, pp. 1795-1804 (1962).

Kreplin, R. W., T. A. Chubb, and H. Friedman, "X-Ray and Lyman-Alpha Emission from the Sun as Measured from the NRL SR-1 Satellite," J. Geophys. Research, Vol. 67, pp. 2231-2253 (1962).

Morriss, R. W., "Observations of Sudden Ionospheric Disturbances," Proc. Phys. Soc. (London), Vol. 76, pp. 79-92 (1960).

Obayashi, T., S. Fujii, and T. Kidokoro, "An Experimental Proof of the Mode Theory of VLF Ionospheric Propagation," J. Geomag. Geoelec. (Kyoto), Vol. 10, pp. 47-55 (1959).

Obayashi, T., "Measured Frequency Spectra of Very Low Frequency Atmospherics," J. Research NBS, Vol. 64D, pp. 41-48 (1960).

Pierce, E. T., "Attenuation Coefficients for Propagation at Very Low Frequencies (VLF) During a Sudden Ionospheric Disturbance (SID)," J. Research NBS, Vol. 65D, pp. 543-546 (1961).

Shain, C. A., and A. P. Mitra, "The Measurement of Ionospheric Absorption Using Observations of 18.3 Mc/s Cosmic Radio Noise," J. Atmos. Terrest. Phys., Vol. 4, pp. 204-218 (December 1953).

Wait, J. R., "A Study of VLF Field Strength Data: Both Old and New," Geofis. pura e appl. (Milan), Vol. 41, pp. 73-85 (1958).

3. BALANCE EQUATIONS FOR THE LOWER IONOSPHERE

3.1 THE ION BALANCE EQUATIONS

The equations governing the production and disappearance of electrons and ions in the ionosphere may be written in the following convenient form essentially due to Crain (1961):

$$\frac{dN}{dt} = Q - AN - BNN^+ + (C + D)\,N^- \qquad \text{(a)}$$

$$\frac{dN^-}{dt} = AN - (C + D)\,N^- - EN^-N^+ \qquad \text{(b)} \qquad (3.1)$$

$$\frac{dN^+}{dt} = Q - BNN^+ - EN^-N^+ = \frac{d}{dt}\,(N + N^-)\,. \qquad \text{(c)}$$

In these equations N, N^-, and N^+ represent the densities, respectively, of electrons, negative ions, and positive ions, while Q is the rate of production for electrons (and for positive ions). The rate coefficients, A, B, C, D, and E, govern the loss and gain of the various electrified constituents. A represents the loss of electrons (gain of negative ions) by the attachment of free electrons to neutral particles: C and D involve the reverse processes, being detachment coefficients for the removal of an electron from a negative ion. C is the photodetachment coefficient, while D represents all other detachment processes. B is the electron-ion recombination coefficient, the process entailing a loss both of electrons and of positive ions. E is the ion-ion recombination coefficient, the loss now being of both positive and negative ions.

It is usual, in attempting solutions of the balance equations, to consider that over-all electrical neutrality is always maintained and that Eq. (3.1c) implies

$$N^{+} = N + N^{-}. \tag{3.2}$$

Q and the rate coefficients are all functions of height. In addition, Q is a function of time, since much of the ionizing radiation is of solar origin; during an SID the variation of Q with time will be very rapid. Some of the rate coefficients, for example, C, are also time dependent since a solar flux is involved.

3.2 THE RATE COEFFICIENTS

Before discussing the individual coefficients in detail, it is convenient to tabulate some of the relevant properties of the atmosphere for the height range involved. This is done in Table 3.1, for daytime conditions.

The information in the first five columns is essentially that given in the U.S. Air Force ARDC Handbook of Geophysics (1960). The next two columns represent a compromise between the ARDC Atmosphere and the survey of Barth (1961); these models are similar in that both give a maximum of atomic oxygen concentrations near 100 km. There is, however, a significant difference in that Barth indicates that the number density for O never exceeds that of O_2 over the height range of 40 to 160 km; the ARDC Handbook, on the other hand, shows more O than O_2 above 90 km.

Column 8, the NO concentration, is taken from the paper of Barth. The figures given lie between those of the ARDC Handbook and those quoted by Nicolet and Aikin (1960); they are approximately two orders of magnitude less than the former, and one order of magnitude greater than the latter.

It will be assumed that Table 3.1 applies to both night and day. Barth (1961) has shown that the main alteration with the change to night is a rapid fall in

TABLE 3.1

PROPERTIES OF THE ATMOSPHERE

Ht (km)	Temp (°K)	Pressure (microbar)	Number Density cm^{-3}				
			Total	N_2	O_2	O	NO
40	261	3000	8.32×10^{16}	6.50×10^{16}	1.74×10^{16}	2.5×10^{10}	2.5×10^{7}
45	276	1600	4.20×10^{16}	3.28×10^{16}	8.81×10^{15}	4.0×10^{10}	2.0×10^{7}
50	283	879	2.25×10^{16}	1.76×10^{16}	4.72×10^{15}	5.0×10^{10}	1.6×10^{7}
55	276	484	1.27×10^{16}	9.91×10^{15}	2.66×10^{15}	7.5×10^{10}	1.3×10^{7}
60	254	257	7.33×10^{15}	5.72×10^{15}	1.54×10^{15}	8.2×10^{10}	7.9×10^{6}
65	232	129	4.02×10^{15}	3.14×10^{15}	8.42×10^{14}	1.2×10^{11}	5.0×10^{6}
70	210	60.2	2.08×10^{15}	1.70×10^{15}	4.37×10^{14}	1.6×10^{11}	3.2×10^{6}
75	188	25.9	1.00×10^{15}	7.81×10^{14}	2.10×10^{14}	2.5×10^{11}	1.6×10^{6}
80	166	10.1	4.41×10^{14}	3.45×10^{14}	9.26×10^{13}	3.5×10^{11}	6.3×10^{5}
85	166	3.69	1.61×10^{14}	1.26×10^{14}	3.37×10^{13}	8.1×10^{11}	2.0×10^{5}
90	166	1.35	5.92×10^{13}	4.64×10^{13}	1.14×10^{13}	1.0×10^{12}	7.9×10^{4}
95	180	0.512	2.06×10^{13}	1.61×10^{13}	3.13×10^{12}	1.2×10^{12}	6.3×10^{4}
100	199	0.214	7.78×10^{12}	6.08×10^{12}	1.00×10^{12}	6.5×10^{11}	7.9×10^{4}

the concentration of atomic oxygen at heights of 70 km and below. This is not of great significance in the calculation of rate coefficients, but has been included as a slight modification in Sec. 3.2.5.

3.2.1 The Attachment Coefficient A

Negative ions are readily formed in the atmosphere by the attachment of electrons to atomic (O) or molecular oxygen (O_2). It does not appear, however, that any of the other common atmospheric gases are active in the formation of negative ions. Three attachment processes occur:

Three-body	$e + O_2 + X \rightarrow O_2^- + X^*$	(a)	(3.3)
Radiative	$e + O_2 \rightarrow O_2^- + h\nu$	(b)	
Dissociative	$e + O_2 \rightarrow O^- + O$	(c)	

In Eq. (3.3) e represents an electron; $h\nu$ is a quantum of radiation; X denotes a third body, and X* is an excited state of that body. The first two processes occur both for atomic and molecular oxygen, but the dissociative mechanism is, of course, confined to the molecular case.

When electrons are formed, the spread in energies is wide. However, there is a conversion into thermal energies of a few hundredths of an electron-volt within a time of less than 10^{-8} sec. Attachment occurs subsequently; this implies that the process of dissociative attachment, which, at the altitudes concerned, is only comparable with the three-body process for electron energies exceeding some 0.5 ev, can be neglected.

The coefficient of radiative attachment for atomic oxygen has been given [Branscomb et al.(1958)] as (1.3) x 10^{-15} cm^3/sec at temperatures between 200° and 400° K. The corresponding coefficient for molecular oxygen is very uncertain; it is believed to be between 10^{-15} and 10^{-19}.

Biondi (1961) has discussed the three-body attachment coefficient for molecular oxygen. His results show that molecular oxygen is about thirty times as effective as N_2 in stabilizing the three-body process. The dependence on electron energy is such that the attachment reaches a maximum for energies of about 0.10 ev. This is considerably higher than thermal energies in the lower ionosphere, so that electrons initially formed with energies exceeding 0.10 ev have to pass the attachment maximum before becoming thermalized. Many will not succeed in doing this, and consequently the effective attachment

coefficient may be expected to be somewhat higher than the value corresponding to thermalization. Biondi's results suggest that 3×10^{-30} is a not unreasonable maximum value for an effective attachment coefficient. Biondi has also investigated the dependence of the attachment coefficient upon gas temperature; the results are somewhat uncertain but indicate that in the D region the coefficient becomes less as the temperature decreases.

Three-body processes involving atomic oxygen occur but are not significant in the lower ionosphere. Where atomic oxygen is present in appreciable proportions, that is, above about 90 km, radiative attachment is the dominant process. The three-body reaction is ineffective both because of the pressure dependence and because the relative concentration of O_2, the most efficient third body, is diminished; an atom such as O is more limited in its degrees of freedom than a molecule, and consequently cannot accept the excess energy involved in Eq. (3.3a) as easily.

Summarizing, the attachment coefficient, A, may be written as

$$A = 1.3\,[O] \times 10^{-15} + [O_2] \times 10^{-17} + \left(\frac{T + 100}{400}\right)[O_2]\left([O_2] + \frac{[N_2]}{30}\right) 3 \times 10^{-30} \quad sec^{-1} \qquad (3.4)$$

In Eq. (3.4) the symbol [ ] represents the number density per cm^3 of the constituent enclosed by the symbol: T is the temperature in °K over the range (150-300°K).

3.2.2 The Electron-Ion Recombination Coefficient B

Three processes may be identified: radiative, three-body, and dissociative. In reaction form they may be written as

Radiative	$M^+ + e \rightarrow M + h\nu$	(a)	(3.5)
Three-body	$M^+ + e + X \rightarrow M + X^*$	(b)	
Dissociative	$M^+ + e \rightarrow A^* + A^{**}$	(c)	

for the case of a molecular positive ion M^+. A denotes an atom. The coefficient for Reaction (3.5a) is about 10^{-12}. Massey and Burhop (1956) give the coefficient for (3.5b) as being 2×10^{-7} at ground level; since the three-body process is directly proportional to pressure, it follows that the three-body coefficient must be less than 10^{-9} at heights exceeding 40 km. Most estimates for the dissociative coefficient are of the order of 10^{-7} to 10^{-8}; hence this is the significant process in the lower ionosphere. The suggestion of Mitra (1952) that the three-body process is dominant below 65 km does not seem to be correct.

The dissociative recombination of N_2^+ has been examined by Bialecke and Dougal (1958) and by Faire and Champion (1959). Their results are in good agreement as to order of magnitude, but differ in the form of dependence on pressure and temperature. Faire and Champion find a value of 4×10^{-7} at a temperature of 400°K, and indicate that the coefficient varies inversely as the square root of temperature, but is independent of pressure at heights above 40 km; these results are consistent with the theoretical work of Bates (1950). On the other hand, Bialecke and Dougal suggest a marked and complicated dependency on both pressure and temperature.

Biondi and Brown (1949) and Holt (1959) have examined the dissociative recombination process for O_2^+. In each paper a value of about 3×10^{-7} is quoted.

However, it seems that rate coefficients for O_2^+ and N_2^+ have little direct application to the lower ionosphere. Although O_2^+ and N_2^+ are formed in

significant quantities, conversion to NO^+ occurs very rapidly by reactions such as

$$N_2^+ + O_2 \rightarrow O_2^+ + N_2 \rightarrow NO^+ + NO$$

$$N_2^+ + O \rightarrow NO^+ + N$$

$$O_2^+ + N \rightarrow NO^+ + O.$$

Direct measurements [Johnson et al. (1958)] show that NO^+ is certainly the dominant ion below 100 km at night, and probably also by day. The experiments of Istomin (1961 a,b) indicate that NO^+ is always the most plentiful positive ion.

Unfortunately the rate coefficient for the dissociative recombination of NO^+ has not been measured. Nicolet and Aikin (1960) have suggested that the coefficient is an order of magnitude less than the value for O_2^+ basing this conclusion upon the relatively long lifetime of the NO^+ ion. This seems a reasonable argument. Accordingly, B will be taken as given by

$$B \approx 3 \times 10^{-8} \left(\frac{400}{T}\right)^{1/2} cm^{-3} sec^{-1}, \qquad (3.6)$$

the temperature and pressure dependence given by Faire and Champion (1959) for N_2^+ being adopted.

Equation (3.6) may, as is evident above, be appreciably in error. An upper limit for B is probably 3×10^{-7}, corresponding to the dissociative recombination of O_2^+, and it is interesting to note that this value was deduced by Whitten and Poppoff (1961) from ionospheric observations. A lower limit cannot be assigned at present.

3.2.3 The C Term Photodetachment

The photodetachment reactions are essentially

$$O^- + h\nu \rightarrow O + e$$

$$O_2^- + h\nu \rightarrow O_2 + e.$$

Burch, Smith, and Branscomb (1958) have determined the coefficient for O_2^- as 0.44; this process involves an integration over the whole solar spectrum. Although a value of 0.15 ev was taken in this work for the electron affinity, E_a, of the O_2^- ion, and this is now believed to be low, it is not thought that a revision of the calculation with $E_a = 0.40$ -- a more likely value -- would make any significant difference. This is because 1.0 ev corresponds to a quantum of wavelength well in the infrared; since the peak of solar radiant energy is in the visible, variation of the lower limit of the photodetachment integral over a wide range in the infrared should have relatively little effect on the value deduced for C.

Photodetachment of O^- can also occur, the coefficient according to Branscomb et al. (1958) being 1.4. Thus the photodetachment coefficient is dependent upon the proportions of the negative ions in atomic and in molecular form. Also, since solar radiation is involved, there is a dependence on solar zenith angle, χ, which may be taken after Mitra (1952) as proportional to $\cos\chi$. Combining these effects, C may be written as

$$C = \left(\frac{0{\cdot}44\,[O_2^-] + 1{\cdot}4\,[O^-]}{[O_2^-] + [O^-]} \right) \cos\chi \ (in\ sec^{-1}) \qquad (3.7)$$

and the proportions of $[O_2^-]$ and $[O^-]$ may be considered as defined by their relative rates of formation by the attachment processes.

3.2.4 The Collisional Detachment Coefficient D_c

At heights below about 90 km, the O_2^- ion is the prevalent negative ion; between 90 and 100 km, O^- ions are important, and indeed in this region the attachment coefficient, A, is dominated by the radiative attachment process for atomic oxygen. Collisional detachment is represented by the reactions

$$O_2^- + M \rightarrow O_2 + M + e$$

$$O^- + M \rightarrow O + M + e.$$

The molecule M must possess sufficient kinetic energy to overcome the detachment energy or electron affinity, E_a, of the ion concerned.

All estimates of the appropriate electron affinities exceed 0.15 ev: that is, the energy required to detach the electron is considerably larger than the mean molecular energy at temperatures of 150°-300°K. Thus the fraction of the total number of molecules that have the necessary detaching energy can be derived from kinetic theory, using the approximation for speeds much greater than the most probable molecular velocity. The fraction is given by

$$\frac{2}{\sqrt{\pi}} \exp\left(-\frac{E_a}{kT}\right) \times \left(\frac{E_a}{kT}\right)^{1/2}$$

where k is Bolzmann's constant and T the temperature: the exponential term is by far the most significant.

Regarding the detachment of O_2^-, Bailey (1959) considered that all molecules in the atmosphere were capable of producing detachment, but Phelps and Pack (1961) find that molecular oxygen is the only effective detaching agent. When this is taken into account and it is recognized that the detachment

coefficient is proportional to the number density and that the ratio of the ionic to the molecular free path is proportional to the square root of temperature, the following expression for D_c for O_2^- ions is obtained:

$$D_c \approx \frac{P}{T} \exp\left(-\frac{E_a}{kT}\right)\left(\frac{E_a}{kT}\right)^{1/2} 2.5 \times 10^6 \qquad (3.8)$$

where P is the pressure in microbars.

The value of E_a remains a subject of controversy. Twenty years ago 1.0 ev was an accepted value [Bates and Massey (1943)]. More recently, Smith, Burch, and Branscomb (1958) suggested an affinity of as low as 0.15 ev, but subsequently there has been a steady reaction in favor of higher values as exemplified by the 0.25 ev of Bailey and Branscomb (1960), the 0.46 ev of Phelps and Pack (1961), and the 0.74 ev of Jortner and Sokolov (1961). The theoretical work of Mulliken (1961) perhaps indicates the start of a second reaction towards lower values again; Mulliken estimates that E_a lies between 0.15 and 0.5 ev. As Crain (1961) has emphasized, because of the exponential factor a slight change in E_a implies a very large alteration in D_c. (The same is true of changes in T and this has an interesting consequence, upon the structure of the lower ionosphere.) Accordingly, in Table 3.2 values of D_c as calculated from Eq. (3.8) are given for three electron affinities, 0.15, 0.40, and 0.65 ev.

As has been indicated, most of the negative ions above 90 km are of atomic oxygen. The electron affinity for the O^- ion is about 1.5 ev. [Branscomb et al. (1958)]. Thus collisional detachment of O^- is a most inefficient process and may be entirely neglected. Since only O_2^- ions can be detached, a correction of D_c is necessary for the larger heights in Table 3.2. This is done approximately by multiplying the deduced D_c by a factor of proportionality given by $A[O_2^-]/A[O_2^-] + A[O^-]$ where $A[\ ]$ is the attachment rate, that is, the rate of formation, of the ionic constituent indicated in the bracket.

TABLE 3.2

DETACHMENT COEFFICIENTS

h(km)	D_c			Corrected D_c (E_a = 0.40)	D_4	
	0.15	0.40	0.65			
40	$2.3.10^{5}$	3.2	$4.9.10^{-5}$	3.2		
45	$1.9.10^{5}$	4.4	$1.9.10^{-4}$	4.4		
50	$1.0.10^{5}$	2.3	$1.0.10^{-4}$	2.3		
55	$5.7.10^{4}$	1.3	$5.7.10^{-5}$	1.3		
60	$2.1.10^{4}$	$2.9.10^{-1}$	$4.4.10^{-5}$	$2.9.10^{-1}$		
65	$6.1.10^{3}$	$2.2.10^{-2}$	$1.3.10^{-7}$	$2.2.10^{-2}$	Day	Night
70	$1.5.10^{3}$	$1.6.10^{3}$	$1.3.10^{-9}$	$1.6.10^{-3}$	$1.6.10^{-3}$	$1.6.10^{-4}$
75	$2.5.10^{2}$	$4.0.10^{-5}$	$4.5.10^{-12}$	$4.0.10^{-5}$	$2.5.10^{-3}$	$8.1.10^{-4}$
80	2.4.10	$3.3.10^{-7}$	$5.3.10^{-15}$	$3.1.10^{-7}$	$3.5.10^{-3}$	
85	8.9	$1.2.10^{-7}$	$1.9.10^{-15}$	$7.8.10^{-8}$	$8.1.10^{-3}$	
90	3.3	$4.1.10^{-8}$	$6.9.10^{-16}$	$7.4.10^{-9}$	$1.0.10^{-2}$	
95	2.1	$8.0.10^{-8}$	$9.3.10^{-15}$	$1.2.10^{-9}$	$1.2.10^{-2}$	
100	2.1	$5.1.10^{-7}$	$4.2.10^{-13}$	$1.6.10^{-9}$	$6.5.10^{-3}$	

This correction is applied for an electron affinity of 0.40 ev in the fifth column of Table 3.2.

3.2.5 Associative Detachment (D_4)

This process is represented by reactions such as

$$O_2^- + O \rightarrow O_3 + e$$

and

$$O^- + O \rightarrow O_2 + e.$$

Estimates of the rate constants concerned range over five orders of magnitude. Whitten and Poppoff (1962) have shown that the selection of a value of about 10^{-14} cm^3 sec^{-1} would enable some aspects of the ionospheric observations of Bailey (1959), during polar cap absorption events, to be interpreted without the necessity of postulating significant collisional detachment and an electron affinity of as low as 0.25 ev for the O_2^- ion. The laboratory value of about 0.40 ev would then be applicable.

Although the uncertainties are very considerable, it seems best, at the present juncture, to adopt the rate constant of 10^{-14} suggested by Whitten and Poppoff (1962). Multiplication by the concentration of atomic oxygen gives the coefficients listed in the last column of Table 3.2; a distinction between day and night is included for heights of 70 and 75 km. At 80 km and above, $D_A >> D_\ell$ for $E_a = 0.40$ ev; below 70 km D_ℓ exceeds D_A.

3.2.6 The E Term Ionic Recombination

There are two significant processes:

two-body, e.g., $O_2^+ + O_2^- \rightarrow O_2^* + O_2^{**}$

and

three-body, e.g., $O_2^+ + O_2^- + M \rightarrow O_2^* + O_2^{**} + M$.

Values of between 10^{-9} and 3×10^{-8} have been quoted for the two-body process. Opinion in Britain [Abererombie (1962)] is in favor of a figure even higher than

3×10^{-8} and that in the U.S.A. [Knapp (1962)] is tending in the same direction. Accordingly, the value of 3×10^{-8} will be adopted.

The three-body coefficient has a pronounced dependency upon pressure and temperature. It decreases as the pressure becomes less, probably leveling off at a value of 3×10^{-9} [Loeb (1955)]. With the pressure, P, in microbars the three-body coefficient may be written as

$$5 \times 10^{-12} \cdot P \cdot \left(\frac{273}{T}\right)^4 + 3 \times 10^{-9}.$$

In this expression the temperature dependency is different, by a factor of $T^{1/2}$, from that given by Ratcliffe and Weekes (1958). The difference arises because in the original Thomson theory the ratio of the ionic to the molecular free path is involved; this is not independent of temperature but varies according to $T^{1/2}$.

Summarizing,

$$\beta = 5 \times 10^{-12} \cdot P \cdot \left(\frac{273}{T}\right)^4 + 3 \times 10^{-9} + 3 \times 10^{-8} \qquad (3.9)$$

3.2.7 Summary

The rate coefficients are listed in Table 3.3 and plotted on Fig. 3.1. D represents the sum of D_f and D_4. Crain (1961) has given the best recent survey of the data on rate coefficients; his work is especially notable for its emphasis upon the great uncertainties of the subject, and is in marked contrast to the tendency of many researchers to ascribe far more precision to selected values than is justifiable. It cannot be overemphasized that, although Fig. 3.1 is believed to represent the optimum development of the information presently (August 1962) available, it is probable that within a year or two some of the quoted values will have been changed by an order of magnitude!

Table 3.3

RATE COEFFICIENTS

h (km)	Attachment Coefficient A (sec^{-1})	Electron-Ion Recombination Coefficient B ($cm^3 sec^{-1}$)	Photodetachment Coefficient C sec χ (sec^{-1})	Combined Associative and Collisional Detachment Coefficient D (sec^{-1})	Ion-Ion Recombination Coefficient E (cm^3 sec^{-1})
40	9.2×10^{2}	$3.7 \cdot 10^{-8}$	$4.4 \cdot 10^{-1}$	3.2	$5.2 \cdot 10^{-8}$
45	$2.4 \cdot 10^{2}$	$3.6 \quad 10^{-8}$	$4.4 \cdot 10^{-1}$	4.4	$4.1 \cdot 10^{-8}$
50	$7.2 \cdot 10$	$3.6 \quad 10^{-8}$	$4.4 \quad 10^{-1}$	2.3	$3.7 \cdot 10^{-8}$
55	$2.3 \cdot 10$	$3.6 \quad 10^{-8}$	$4.4 \quad 10^{-1}$	1.3	$3.6 \cdot 10^{-8}$
60	7.1	$3.8 \quad 10^{-8}$	$4.4 \quad 10^{-1}$	$2.9 \cdot 10^{-1}$	$3.5 \cdot 10^{-8}$
65	1.9	$3.9 \quad 10^{-8}$	$4.4 \quad 10^{-1}$	$2.2 \quad 10^{-2}$	$3.4 \cdot 10^{-8}$
				Day Night	
70	$5.1 \cdot 10^{-1}$	$4.1 \quad 10^{-8}$	$4.4 \quad 10^{-1}$	$3.2 \cdot 10^{-3}$ $1.8 \cdot 10^{-3}$	$3.4 \cdot 10^{-8}$
75	$1.1 \cdot 10^{-1}$	$4.4 \quad 10^{-8}$	$4.4 \quad 10^{-1}$	$2.6 \cdot 10^{-3}$ $8.5 \cdot 10^{-4}$	$3.3 \cdot 10^{-8}$
80	$2.0 \cdot 10^{-2}$	$4.7 \quad 10^{-8}$	$4.6 \quad 10^{-1}$	$3.5 \cdot 10^{-3}$	$3.3 \cdot 10^{-8}$
85	$4.0 \cdot 10^{-3}$	$4.7 \quad 10^{-8}$	$7.0 \quad 10^{-1}$	$8.1 \cdot 10^{-3}$	$3.3 \cdot 10^{-8}$
90	$1.7 \cdot 10^{-3}$	$4.7 \quad 10^{-8}$	1.3	$1.0 \cdot 10^{-2}$	$3.3 \cdot 10^{-8}$
95	$1.6 \cdot 10^{-3}$	$4.5 \quad 10^{-8}$	1.36	$1.2 \cdot 10^{-2}$	$3.3 \cdot 10^{-8}$
100	$8.5 \cdot 10^{-4}$	$4.3 \quad 10^{-8}$	1.40	$6.5 \cdot 10^{-3}$	$3.3 \cdot 10^{-8}$

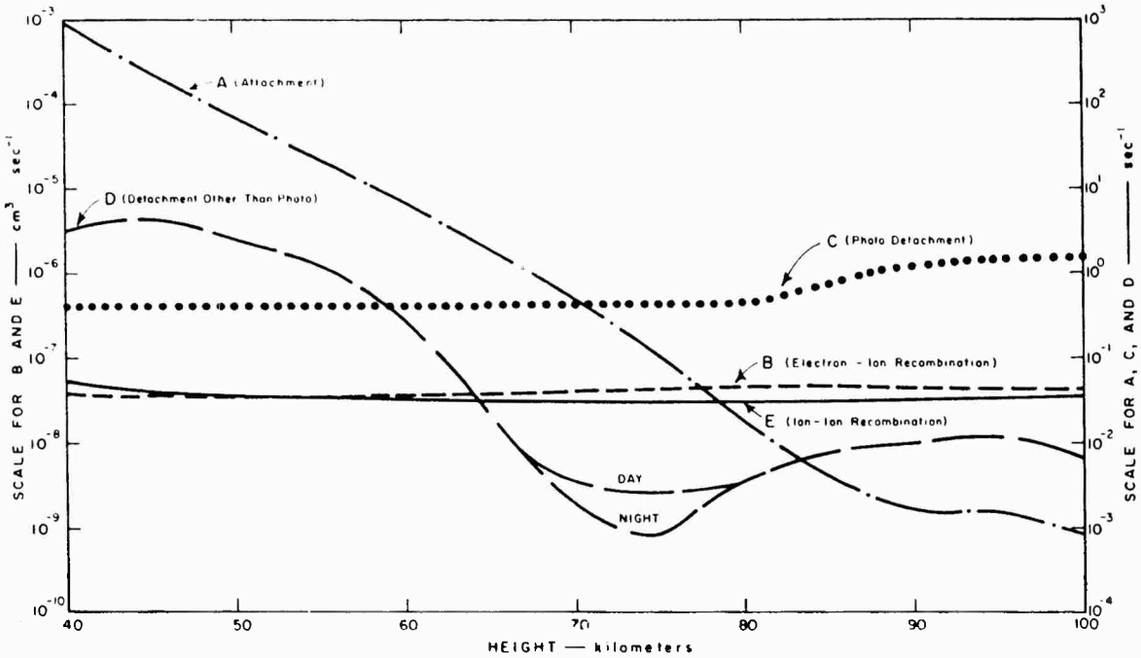

FIG. 3.1 RATE COEFFICIENTS vs. HEIGHT

It is of some interest to examine the differences between Fig. 3.1 and the data given by Crain. As regards the attachment coefficient, A, the two sets of results are in excellent agreement except for heights above about 85 km where the influence of atomic oxygen (not considered by Crain) begins to become significant. The B value is about 40 percent of that given by Crain. The results for the C coefficient are identical below 80 km, but above that level the effective value for C is greater than that of Crain because of the presence of O^- ions. Between 40 and 70 km the coefficient D is primarily due to collisional detachment; the agreement with Crain is reasonable, but the variation on Fig. 3.1 is greater because of the inclusion of the effect of temperature. Above 70 km associative detachment is the principal detachment process represented on Fig. 3.1; this mechanism was not considered by Crain, so that there is an

appreciable divergence between the two sets of data. Finally, the E coefficient is about forty times that given by Crain; this reflects the movement of opinion referred to in Sec. 3.2.6.

3.3 The Ionizing Radiations During Quiet Conditions

3.3.1 Cosmic Radiation

Cosmic radiation is usually separated into the primary rays incoming from extraterrestrial sources and the secondary radiation generated by the interaction of the primary rays with the earth's atmosphere. The incoming primary radiation is deflected towards the magnetic poles by the magnetic field of the earth. Only the most energetic primary particles can avoid such deflection and reach equatorial regions; there is thus a pronounced latitude effect with the dependence being upon a latitude defined geomagnetically rather than geographically. Secondaries are produced in large numbers only at heights below 35 km. However, Meredith, van Allen, and Gottlieb (1955) have shown that the ionizing radiation at considerable attitudes consists of primaries, secondaries generated at lower heights and reflected upwards (the splash albedo), and such secondaries re-entering the atmosphere (the re-entrant albedo). For geomagnetic latitudes of less than 55° the three terms are comparable in magnitude.

Most of the primary cosmic-ray particles are protons and have energies exceeding 1 Bev. For such high-energy particles the rate of energy loss per centimeter of path, and therefore the energy available to produce ionization of the ambient atmosphere, is almost independent of the particle energy. Thus, in the latitude effect, since the albedo secondaries are also of high energy, the proportionality is between ionization production and the number flux rather than the energy flux of the ionizing radiation.

The influence of the earth's magnetic field means that incoming protons with energies (in Bev) less than approximately $15 \cos^4\theta$, where θ

is a geomagnetic latitude, cannot penetrate to the latitude θ. Thus the number flux at any particular latitude could be evaluated by taking an expression such as that of Kaplon et al. (1952) for the energy distribution of the incoming primaries, making allowances for the splash and re-entrant albedos, and integrating between the limits of 15 $\cos^4\theta$ and infinity. Refinements could be introduced into the simple Störmer cut-off criterion of 15 $\cos^4\theta$ as indicated by Winckler et al. (1950).

However, the above procedure although complicated is fundamentally empirical, as there is no sound theoretical basis for the energy spectrum of the incident cosmic radiation. Since an empirical approach is inevitably necessary, it seems easiest to apply it in the following way. Measurements on the latitudinal dependence of the vertical flux of particles near the top of the atmosphere have been summarized by Curtis (1956). Between geomagnetic latitudes of 0° and 60° the latitudinal dependence is fairly well approximated by a simple proportionality with $\cos^{-4}\theta$; at higher latitudes the flux is roughly constant. The loss of energy of the particles by ionization is taken to be 2.2 x 10^3 ev per centimeter traveled, at atmospheric pressure, and 32 ev is accepted as the energy corresponding to the production by cosmic-ray particles of an ion pair in air. By using these figures, the rate of ionization production, q_o, in ion pairs per cm^3 per second per atmosphere is given by

$$q_o \approx 38 \cos^{-4}\theta . \qquad (3.10)$$

Equation (3.10) is in good agreement with three values quoted by van Allen (1952) as shown in Table 3.4.

TABLE 3.4

COSMIC-RAY IONIZATION AS A FUNCTION OF GEOMAGNETIC LATITUDE

θ	3°	38°	51°
q_o (van Allen)	35	90	257
q_o [Eq. (3.10)]	38	98	243

The rate of ionization production, q_c, due to cosmic rays at a height h is readily obtained from Eq. (3.10) since

$$q_c(h,\theta) = q_o \frac{n_h}{n_o} = 38 \cos^{-4}\theta \frac{n_h}{n_o} = 38 \cos^{-4}\theta \frac{n_h}{(2.55) \times 10^{19}} \ cm^{-3} sec^{-1}$$

where n_h and n_o are the number densities at heights h and 0.

It is interesting to note that the differential number spectrum, dN, for incoming primaries of energy E is quoted as $dN = kE^{-\alpha}dE$, where k is a constant and the empirical constant α has a value of between 1.8 and 1.9. It follows that if the shadow cone effect is ignored and the simple Störmer cut-off is adopted, then $N_\theta = \int_{15 \cos^4\theta}^{\infty} kE^{-\alpha}dE$, which is not far removed from the $\cos^{-4}\theta$ dependency of Eq. (3.10).

One important feature of the cosmic-ray latitude dependency is the system of geomagnetic co-ordinates to be selected. Recent information [Sandström (1958)] suggests that the cosmic-ray equator corresponds best with the dip equator. Thus the ion production function is best written as

$$q_c(h, I) = 15 n_h \cos^{-4} I \times 10^{-19}. \qquad (3.11)$$

where I is the angle of dip.

Regular temporal changes in cosmic-ray activity are slight, with the exception of the variations associated with the solar cycle [Simpson (1958)]. It appears that many more low-energy protons reach the earth during solar minimum than at times of maximum. These protons are naturally channeled into high latitudes where the cyclical effects are thus likely to be most pronounced. The variation in ion production near the poles is probably ±25 percent between solar maximum and minimum; for latitudes less than 55°, however, it is much less.

ion production rates derived from Eq. (3.11) are given in Table 3.5.

3.3.2 Lyman α

The sun emits intensely at the wavelength of 1215.7Å, the first line in the Lyman series of hydrogen. It was thought a few years ago that the emission was extremely variable and that many of the short-term fluctuations in the ionosphere, such as SIDs, were associated with rapid changes in the intensity of the Lyman -α radiation. However, as additional information by more reliable methods has become available, notably through the NRL rocket and satellite program [Friedman (1961)] it has become evident that on a short-term basis the flux of Lyman α is remarkably constant, but the possibility of a long-term variation, perhaps by as much as an order of magnitude, in phase with the solar cycle, cannot at present be eliminated. During the solar maximum the flux is about 5 ergs $cm^{-2} sec^{-1}$ at the top of the terrestrial atmosphere. This corresponds to 3×10^{11} photons $cm^{-2} sec^{-1}$.

Lyman-α radiation is capable of ionizing NO and is strongly absorbed by molecular oxygen. Watanabe, Inn, and Zelikoff (1953) give the absorption cross section for molecular oxygen as $1.04 \times 10^{-20} cm^2$, while for nitric oxide the ionization cross section is $2 \times 10^{-18} cm^2$ and the absorption cross section $2.4 \times 10^{-18} cm^2$ [Watanabe (1954)]. For molecular nitrogen, N_2, the Lyman-α absorption coefficient is probably less than $6 \times 10^{-23} cm^2$ [Ditchburn et al. (1954)].

If the incident flux of Lyman α is I_∞ , then the flux, I_h, at any height h may be written as

$$I_h = I_\infty \exp\left(-\sec\chi \sum_j \int_h^\infty \sigma_j n_j dh\right) \qquad (3.12)$$

where σ_j and n_j are the absorption cross section and number density respectively, of the constituent j. Equation (3.12) includes the approximation of

Table 3.5

RATE OF ION PRODUCTION ($cm^{-3}\ sec^{-1}$) BY COSMIC RAYS

h (km)→ Angle of dip I(°) ↓	40	45	50	55	60	65	70	75	80	85	90	95	100
0	1.2×10^{-1}	6.3×10^{-2}	3.4×10^{-2}	1.9×10^{-2}	1.1×10^{-2}	6.0×10^{-3}	3.1×10^{-3}	1.5×10^{-3}	6.6×10^{-4}	2.4×10^{-4}	6.9×10^{-4}	3.1×10^{-5}	1.2×10^{-5}
20	1.6×10^{-1}	8.1×10^{-2}	4.3×10^{-2}	2.4×10^{-2}	1.4×10^{-2}	7.7×10^{-3}	4.0×10^{-3}	1.9×10^{-3}	8.5×10^{-4}	3.1×10^{-4}	1.1×10^{-4}	4.0×10^{-5}	1.5×10^{-5}
40	3.6×10^{-1}	1.8×10^{-1}	9.8×10^{-2}	5.5×10^{-2}	3.2×10^{-2}	1.7×10^{-2}	9.1×10^{-3}	4.4×10^{-3}	1.9×10^{-3}	7.0×10^{-4}	2.6×10^{-4}	9.0×10^{-5}	3.4×10^{-5}
60	2.0	1.0	5.4×10^{-1}	3.0×10^{-1}	1.8×10^{-1}	9.7×10^{-2}	5.0×10^{-2}	2.4×10^{-2}	1.1×10^{-2}	3.9×10^{-3}	1.4×10^{-3}	4.9×10^{-4}	1.9×10^{-4}

replacing the Chapman function for zenith angle, χ by sec χ; this is reasonable for $\chi \leq 80°$. The production, q_h, of ionization at height h is given by

$$q_h = \sum_j \sigma_j' n_j(I_h) \tag{3.13}$$

where σ_j' represents the ionization cross section.

Of the various terms in Eqs. (3.12) and (3.13), only that considering NO is involved in the ionization summation. As regards the absorption summation, the absorption is very slight above 100 km, so that $I_\infty \approx I_{100}$. Below 100 km, a combination of the information on Table 3.1 and on the absorption cross sections shows that the absorption is almost entirely due to molecular oxygen. For the molecular oxygen constituent $\int_h^\infty n_h\, dh = \frac{1}{g\, M_o} \frac{P_h}{4.3}$ where M_O is the molecular weight and P_h the atmospheric pressure at height h. With g taken as 960 cm sec^{-2} over the range of heights concerned and $M_O = 5.31 \times 10^{-22}$ gram, Eq. (3.12) can be rewritten as

$$I_h = I_\infty \exp\left(-\sec \chi \cdot \frac{P_h}{21.2}\right). \tag{3.14}$$

By using Eqs. (3.13) and (3.14) and the information of Table 3.1, Table 3.6 giving ion production rates due to Lyman α may be calculated.

Table 3.6 has not been continued below about 60 km, because cosmic-ray ionization is dominant at these lower heights. The minimum at 95 km follows from the minimum of NO indicated by Barth (1961) at this height.

3.3.3 X Rays

X rays are capable of ionizing all constituents of the atmosphere, and it is usually taken that all the absorbed energy is converted into ionization.

Table 3.6

RATE OF ION PRODUCTION ($cm^{-3}\,sec^{-1}$) BY LYMAN-α RADIATION

Solar Zenith angle X	h(km)--> 60	65	70	75	80	85	90	95	100
0	$2.5.10^{-5}$	$6.6.10^{-3}$	$1.1.10^{-1}$	$2.8.10^{-1}$	$2.4.10^{-1}$	1.10^{-1}	$4.5.10^{-2}$	$3.7.10^{-2}$	$4.7.10^{-2}$
20		$4.8.10^{-3}$	$9.4.10^{-2}$	$2.6.10^{-1}$	$2.3.10^{-1}$	$9.9.10^{-2}$	$4.5.10^{-2}$	$3.7.10^{-2}$	$4.7.10^{-2}$
40		1.10^{-3}	$4.8.10^{-2}$	$1.9.10^{-1}$	$2.1.10^{-1}$	$9.7.10^{-2}$	$4.4.10^{-2}$	$3.7.10^{-2}$	$4.6.10^{-2}$
60		$1.5.10^{-5}$	$6.5.10^{-3}$	$8.4.10^{-2}$	$1.5.10^{-1}$	$8.5.10^{-2}$	$4.2.10^{-2}$	$3.6.10^{-2}$	$4.6.10^{-2}$
80			$1.4.10^{-7}$	$8.2.10^{-3}$	$2.5.10^{-2}$	$4.4.10^{-2}$	$3.4.10^{-2}$	$3.3.10^{-2}$	$4.4.10^{-2}$

The computation of X-ray ionization is somewhat more difficult than that for Lyman α because the radiation is not monochromatic, but the basic procedure is essentially similar.

If I_∞ is the intensity of the incident radiation, then $I_h = I_\infty \exp\left[-\sec\chi\,\mu_m \int_h^\infty \rho_h dh\right]$ where μ_m is the mass absorption coefficient, ρ_h the density at height h, and the secant approximation to the Chapman function is used. Now $\int_h^\infty \rho_h dh = \frac{P_h}{g}$, so that the rate, q_h of ion production at height h may be expressed as

$$q_h = \beta\mu_m I_\infty \rho_h \exp\left(\frac{-\mu_m \sec\chi \cdot P_h}{g}\right) \tag{3.15}$$

where β is the yield in ions per unit absorption.

The quantities μ_m and β (to a lesser extent) are functions of wavelength, while the incident solar X-ray flux contains energy over a wide range of wavelengths. In order to obtain solutions for q_h, three approaches are possible. First, elaborate numerical integration can be performed. Second, attempts can be made to obtain functional representations of the quantities that are frequency dependent, with a view to obtaining an expression for q_h in terms of wavelength λ. Third, approximations can be included, where appropriate, in an effort to obtain solutions that are reasonably accurate but still tractable without the necessity for extensive computation; this is the approach that will be adopted.

Rajewsky and Lang (1961) have reviewed the information relating the average energy lost in creating an ion pair to the energy of the incident X-rays. The trend of the results is indicated in Table 3.7.

TABLE 3.7

IONIZING EFFECTIVENESS OF X RAYS

Energy of incident X rays (kev)	0.1	1	10	100
Corresponding wavelength (Å)	127	12.7	1.27	0.127
Energy lost in producing one ion pair (ev)	50	37.5	34.5	33

The energy loss per ion pair varies appreciably with wavelength for the softer X radiation but tends towards constancy as the X rays become harder. Rajewsky and Lang find from their experiments that, between 2.2 and 0.7Å, 35 ev is a good approximation to the energy loss per ion pair, and this value will be taken as applying over the whole X-ray spectrum. The error in this assumption is appreciable at wavelengths greater than about 15 Å, but this wavelength range is mostly absorbed above 100 km and is, therefore, of minor significance as regards the lower ionosphere.

A value indicative of β having been established, it remains to consider μ_m. Appropriate information concerning μ_m as a function of wavelength has been given by Victoreen (1949) and Henke et al. (1957). A composite representation of the available data is given in the curve of Fig. 3.2. For wavelengths exceeding 0.6 Å and less than about 20 Å, that is, over the range most important in the lower ionosphere, the variation in Fig. 3.2 is represented by the empirical relationship $\mu_m = (3.1)\lambda^{(2.8)}$. Below 0.25 Å, a relationship with similar form but different constants applies:

$$\mu_m = (0.36)\lambda^{(0.38)}$$

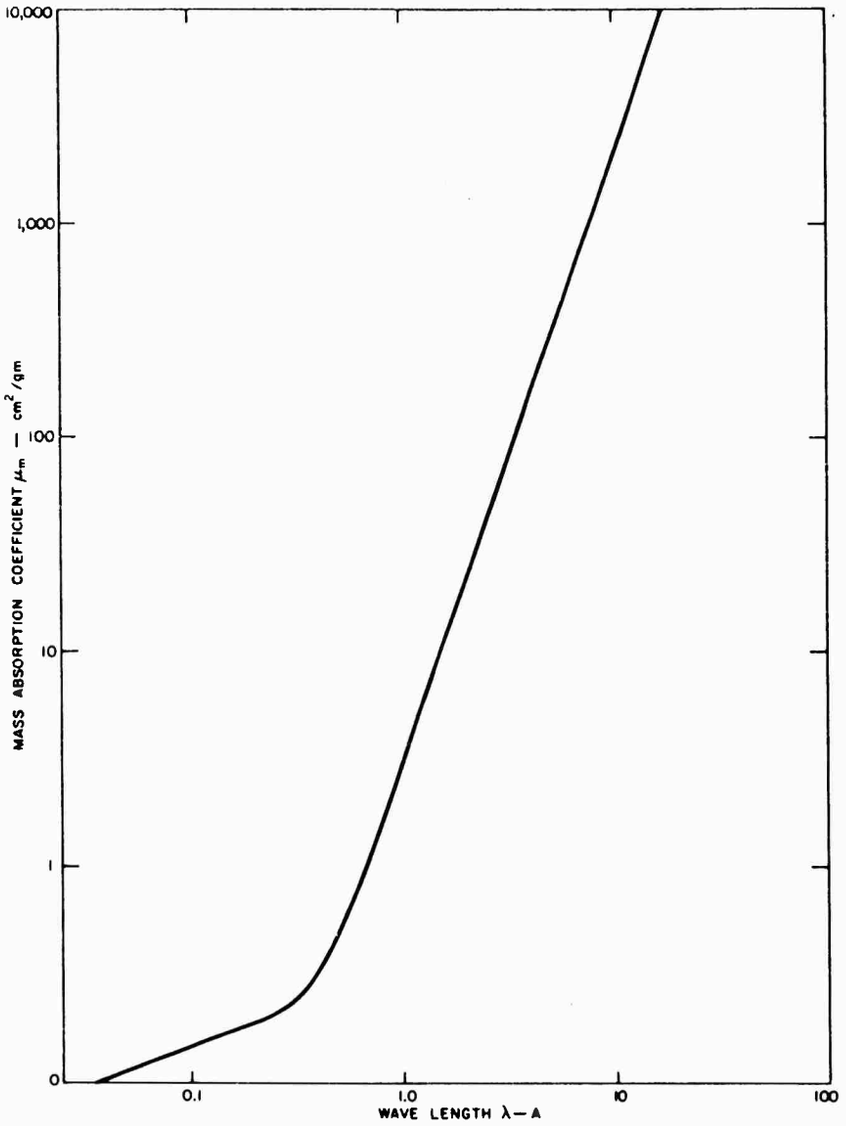

FIG. 3.2 MASS ABSORPTION COEFFICIENT FOR X RAYS IN AIR AS A FUNCTION OF WAVELENGTH

If an incident flux, I_o, of 1 erg cm^{-2} sec^{-1} is taken, with a conversion factor of 35 ev, Eq. (3.15) reduces to

$$q_h = 1.8 \times 10^{10} \mu_m \rho_h \exp\left(-\frac{\mu_m \sec \chi \, p_h}{960}\right) \tag{3.16}$$

where 960 cm sec^{-2} is taken as a mean value of the acceleration due to gravity over the altitude range concerned. Equation (3.16) is plotted as a function of height for five values of χ and seven values of the wavelength of the incoming radiation, in Figs. 3.3 through 3.8. It is evident that the harder the X radiation the lower the height at which the maximum production of ionization occurs. Also, for a given wavelength, a change of zenith angle has a much larger effect at heights below that of maximum production than at those above.

It remains to determine the X-ray flux associated with a quiet sun. Poppoff and Whitten (1962) have estimated the background X-ray flux from data obtained by the Sunflare II Probe of the Naval Research Laboratory. The latest available results from the NRL series of rocket and satellite experiments show that near solar maximum the quiet solar flux in the 2 to 8 Å band never exceeds 6×10^{-4} erg cm^{-2} sec^{-1}. [Kreplin (1962)]. In order to make the Poppoff-Whitten spectrum agree with this observation of Kreplin, it must be reduced by a factor of about 2.5; this has been done and the result is plotted in Fig. 3.9.

In order to determine accurately the rate of ion production represented by the incident flux, a complicated calculation involving summation over all wavelengths is necessary. However, a reasonable approximation may be made by splitting the flux into different wavelength ranges and then applying the information of Fig. 3.3 to 3.7. A convenient subdivision is shown on Fig. 3.9 and also given in Table 3.8. By using this subdivision, the rate of production of ionization for the quiet solar X-ray flux has been calculated for several zenith angles. The results are given in Table 3.9.

3.3.4 Other Ionizing Agents--Watanabe and Hinteregger (1962) have examined the ionization due to solar ultraviolet radiation and soft X rays. Their results show that appreciable ionization can be produced at heights of 95 to 100 km by radiations between 911 and 1027 Å, and by X rays with wavelengths in the range of 30 to 170 Å. At 90 km and below, however, this ionization is insignificant as compared with that already considered due to X rays harder than 30 Å. Table 3.10 indicates the rate of production of ions for these additional radiations.

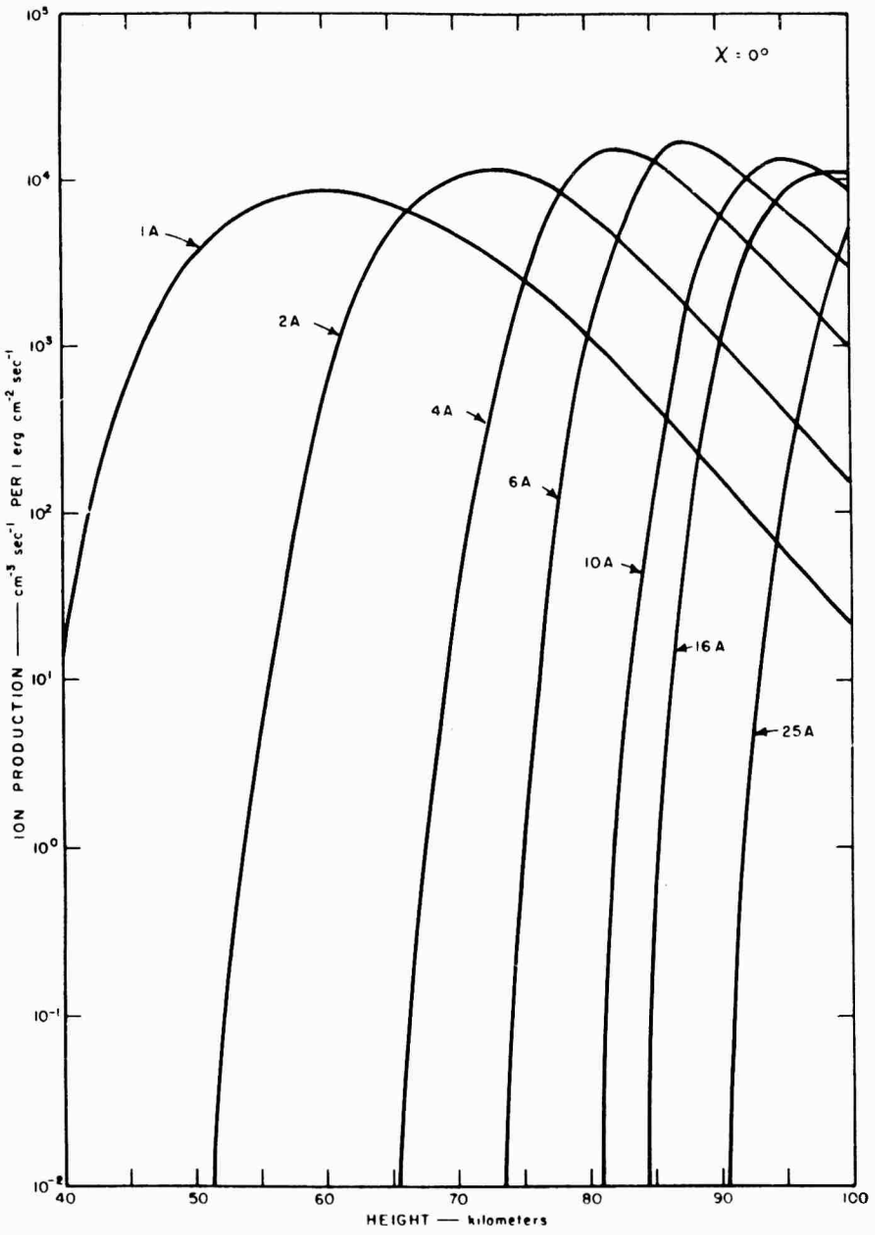

FIG. 3.3 ION PRODUCTION DUE TO X RAYS AS A FUNCTION OF HEIGHT AND WAVELENGTH (Zenith Angle 0°)

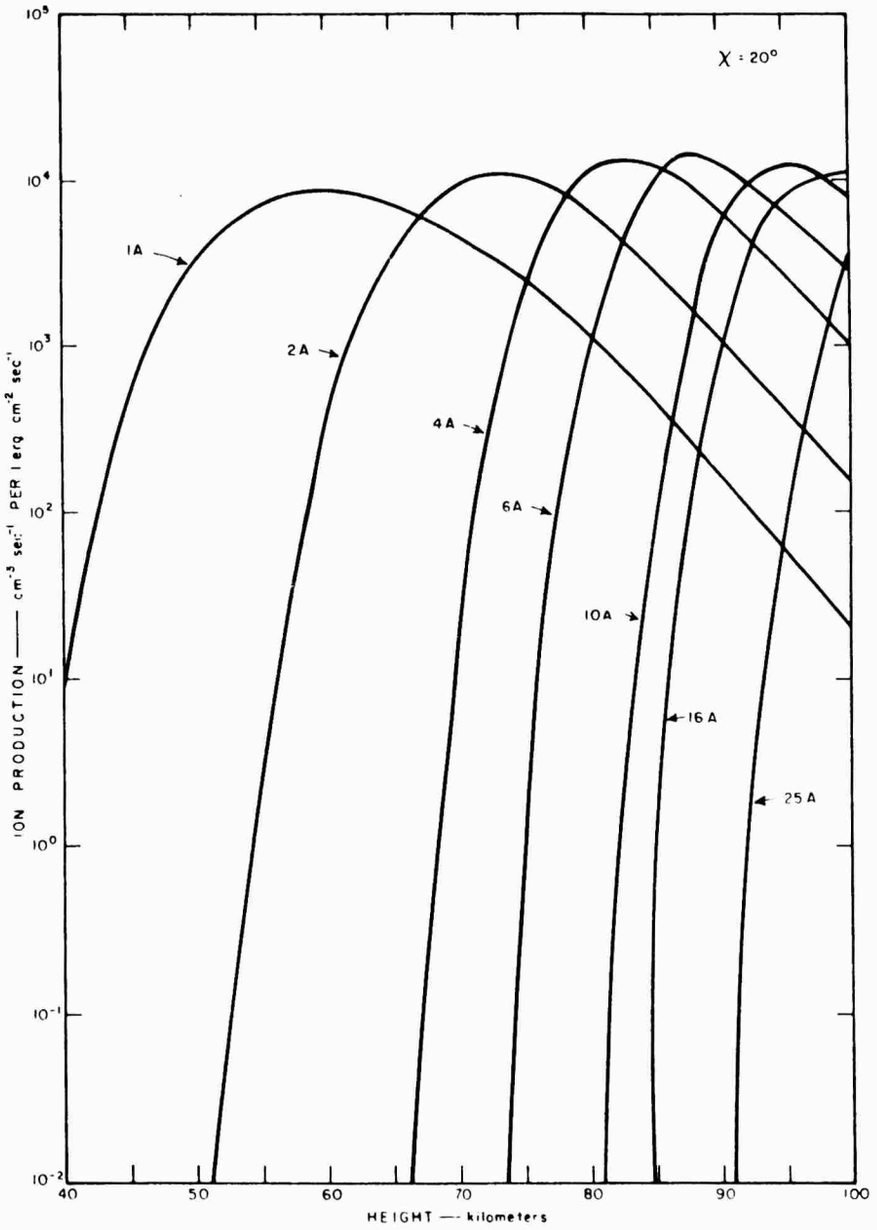

FIG. 3.4 ION PRODUCTION DUE TO X RAYS AS A FUNCTION OF HEIGHT AND WAVELENGTH (Zenith Angle 20°)

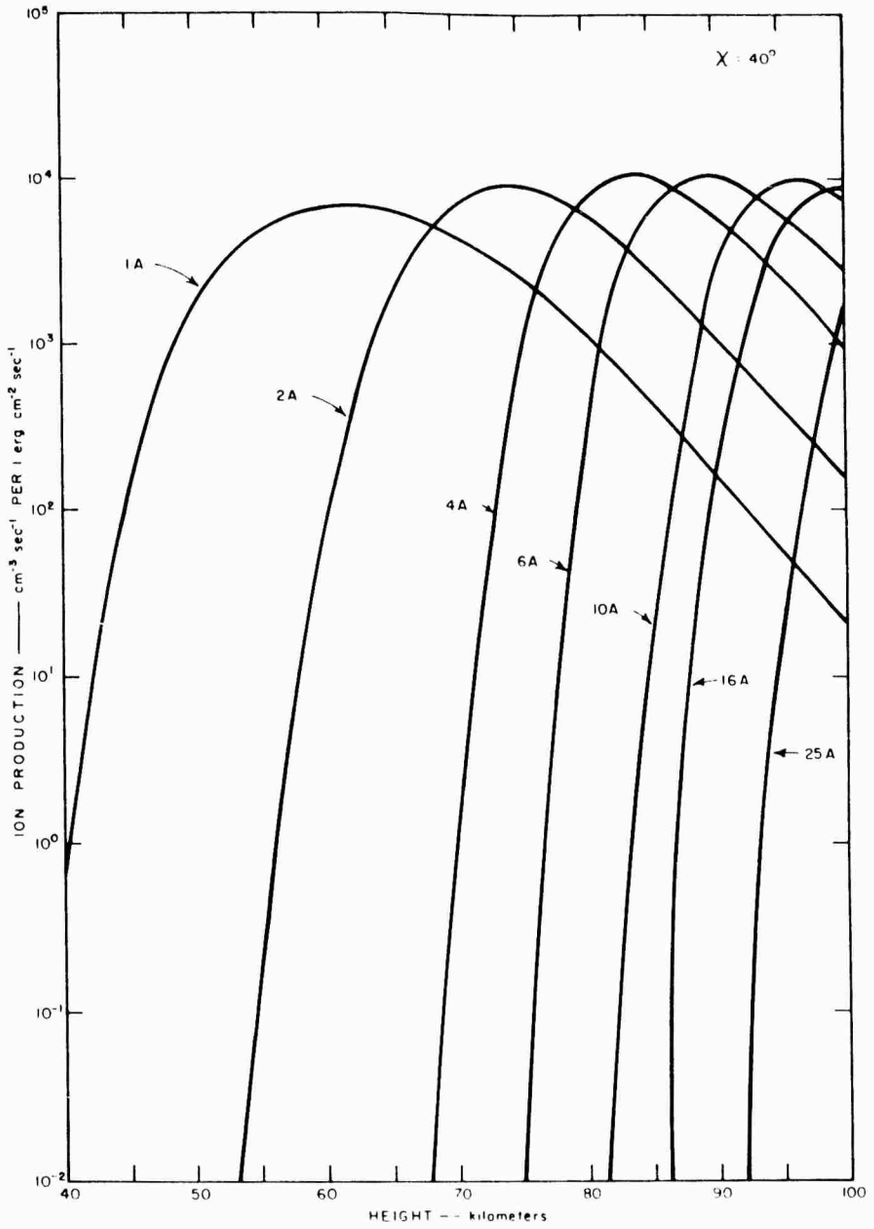

FIG. 3.5 ION PRODUCTION DUE TO X RAYS AS A FUNCTION OF HEIGHT AND WAVELENGTH (Zenith Angle 40°)

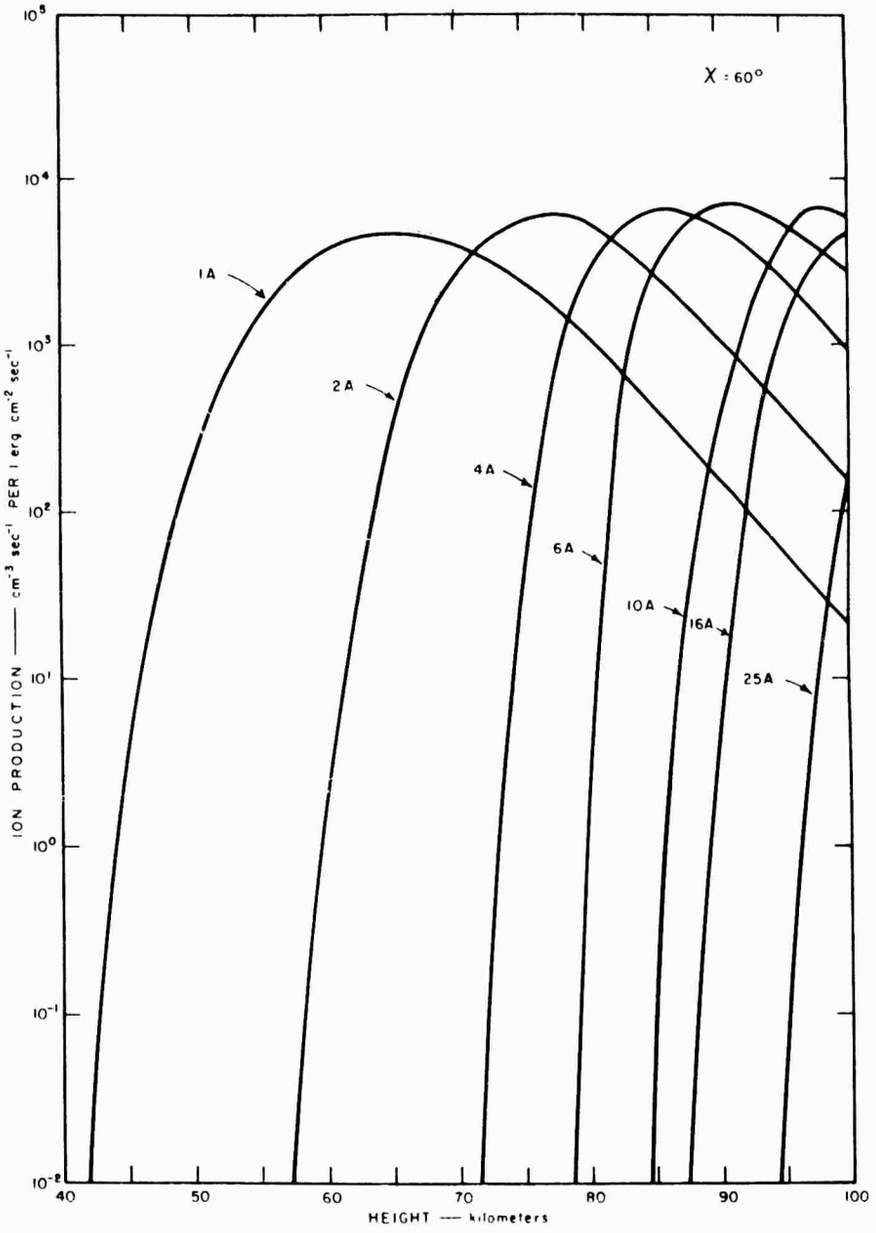

FIG. 3.6 ION PRODUCTION DUE TO X RAYS AS A FUNCTION OF HEIGHT AND WAVELENGTH (Zenith Angle 60°)

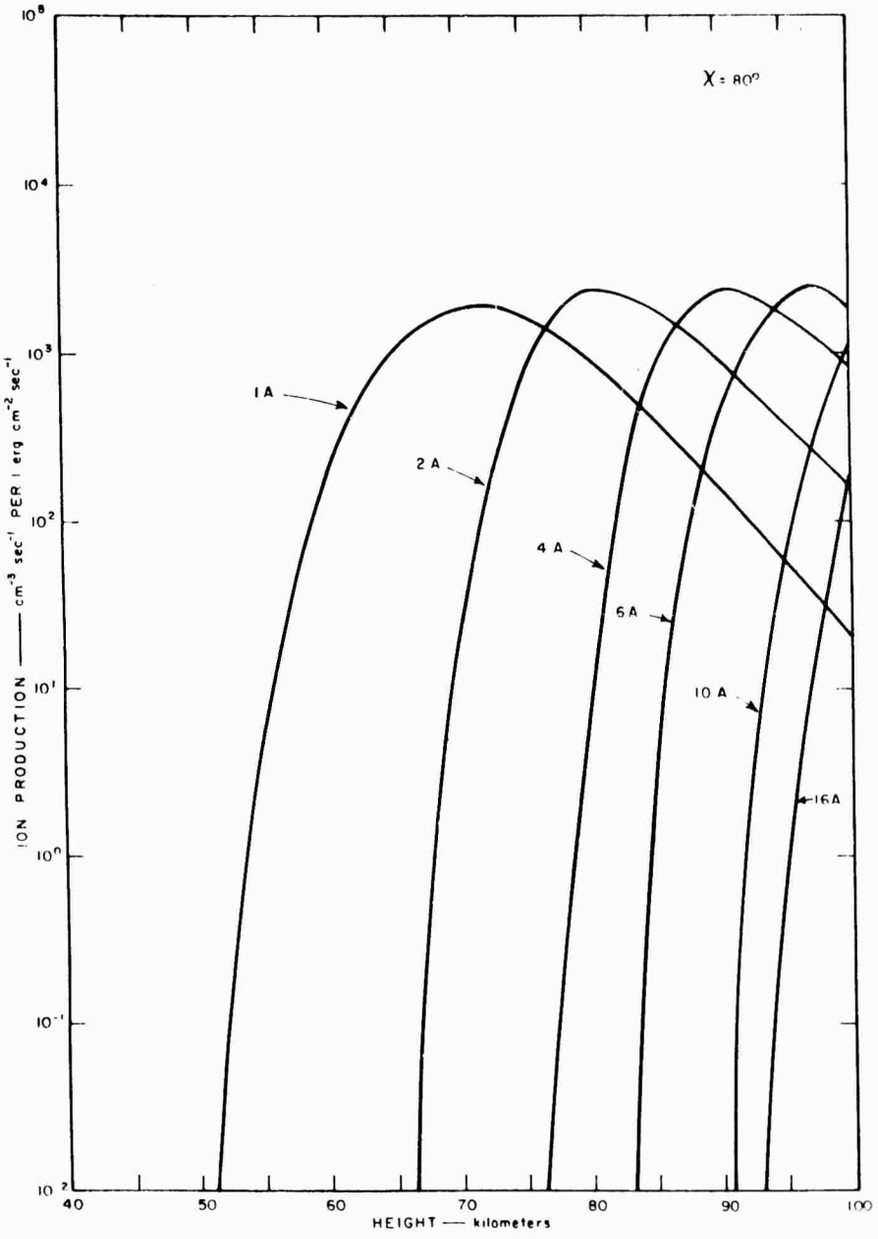

FIG. 3.7 ION PRODUCTION DUE TO X RAYS AS A FUNCTION OF HEIGHT AND WAVELENGTH (Zenith Angle 80°)

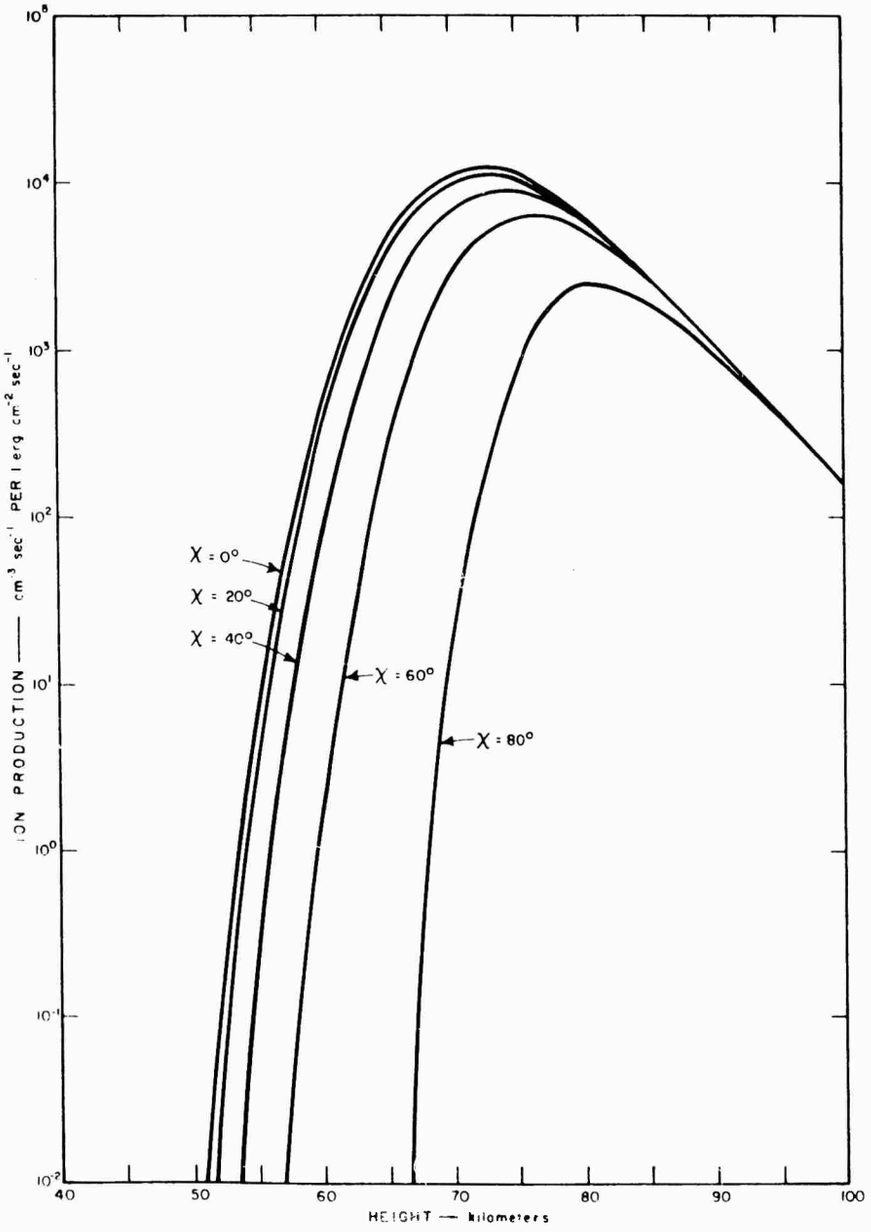

FIG. 3.8 ION PRODUCTION DUE TO 2Å X RAYS AS A FUNCTION OF HEIGHT FOR FIVE ZENITH ANGLES

TABLE 3.8

SUBDIVISION OF X-RAY FLUX FROM QUIET SUN

Wavelength Range (Å)	Center Wavelength (Å)	Mean Flux per A (erg cm^{-2} sec^{-1})	Total Flux in Range (erg cm^{-2} sec^{-1})
19-31	25	$1.4.10^{-3}$	$1.7.10^{-2}$
13-19	16	$9.0.10^{-4}$	$5.4.10^{-3}$
7-13	10	$4.5.10^{-4}$	$2.7.10^{-3}$
5-7	6	$1.3.10^{-4}$	$2.6.10^{-4}$
3-5	4	3.10^{-5}	6.10^{-5}
1-3	2	10^{-6}	2.10^{-6}

The "average" meteor appears at a height of about 110 km and disappears at 80 km. Over this range of altitude the mean rate of ion production for all the sporadic meteors occurring globally is about 10^{-4} cm^{-3} sec^{-1} [Lovell (1957)]. Taking into account the height distribution of the ionization yields Table 3.11. It must be emphasized that meteor ionization is not likely to be uniform below 100 km; it is improbable that the diffusion of the individual trails will be sufficient for them to merge into an isotropic whole. Accordingly, it is somewhat dubious whether meteor ionization should ever be regarded as a continuous source. The average flux of shower meteors is only about 20 percent of that associated with sporadic meteors: however, during the largest showers the ion production rate may rise to as much as a thousand times the rates given in Table 3.10.

TABLE 3.9

RATE OF ION PRODUCTION ($cm^{-3}sec^{-1}$) BY X RAYS FROM QUIET SUN

Height / Solar zenith	60	65	70	75	80	85	90	95	100
0	$8.9.10^{-4}$	$8.5.10^{-3}$	$2.1.10^{-2}$	$1.5.10^{-1}$	1.0	3.9	2.6.10	8.4.10	$1.6.10^{2}$
20	$6.3.10^{-4}$	$7.2.10^{-3}$	$2.0.10^{-2}$	$1.3.10^{-1}$	$8.7.10^{-1}$	3.5	2.1.10	7.8.10	$1.4.10^{2}$
40	--	$3.5.10^{-3}$	$1.4.10^{-2}$	$5.6.10^{-2}$	$5.1.10^{-1}$	2.1	1.1.10	5.2.10	9.4.10
60	--	$4.8.10^{-4}$	$5.4.10^{-3}$	$1.4.10^{-2}$	$1.6.10^{-1}$	$8.4.10^{-1}$	3.0	2.0.10	4.5.10
80	--	--	$3.4.10^{-5}$	$1.4.10^{-3}$	$5.0.10^{-3}$	$4.9.10^{-2}$	$2.7.10^{-1}$	$8.3.10^{-1}$	4.7

TABLE 3.10

RATE OF ION PRODUCTION ($cm^{-3}sec^{-1}$) BY ADDITIONAL RADIATIONS

Solar Zenith Angle χ	Height (km)	
	95	100
0	2.4x10	$1.3x10^{3}$
20	2.1x10	$1.2x10^{3}$
40	1.4x10	$1.0x10^{3}$
60	6.7	$4.0x10^{2}$
80	$7.0x10^{-1}$	4.0x10

3.3.5 Summary--Figure 3.10 summarizes the ionizing contributions of the various radiations. It can be seen that below some 60 km the cosmic ray source is dominant; above 80 km X rays are most important; while between 60 and 80 km the contributions due, respectively, to Lyman α, X rays, and cosmic radiation are of comparable size. The results of Fig. 3.10 confirm the conclusion of Poppoff and Whitten (1962) that X rays are the major factor in the formation of the D region; the opinion of Nicolet and Aikin (1960) that Lyman α is the dominant influence is not supported. However, it should be emphasized that the

TABLE 3.11

RATE OF ION PRODUCTION ($cm^{-3}\,sec^{-1}$) BY METEORS

Height	Ion Production
80	0
85	$2.5x10^{-4}$
90	$1.7x10^{-4}$
95	$1.0x10^{-4}$
100	$0.5x10^{-4}$

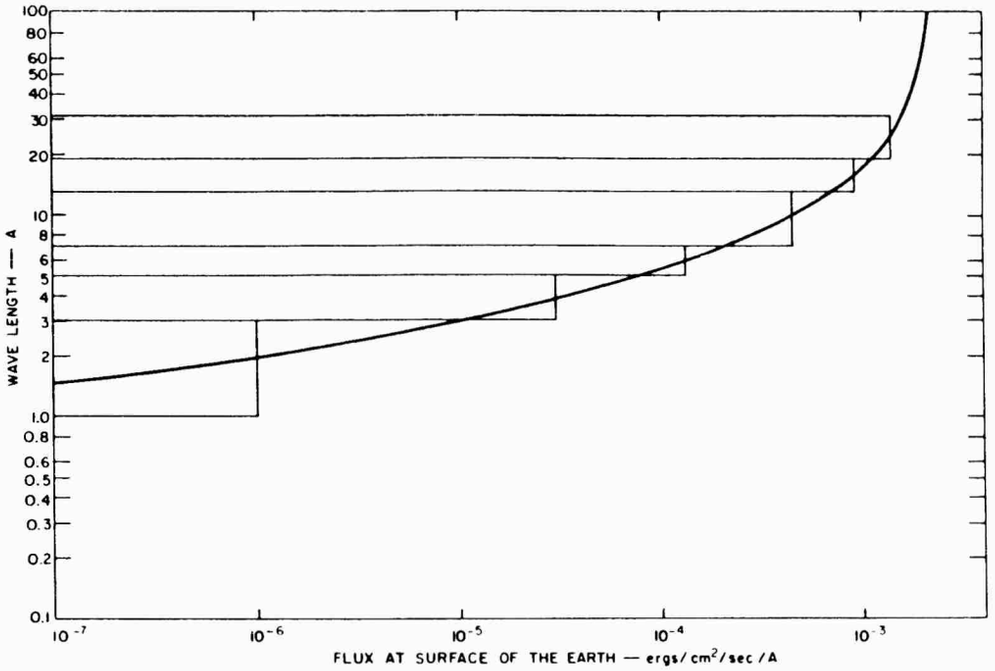

FIG. 3.9 X-RAY FLUX FROM QUIET SUN NEAR MAXIMUM OF SOLAR CYCLE

X-ray flux from which the X-ray contribution to Fig. 3.10 was derived was obtained for quiet solar conditions during a period not far removed from sunspot maximum. If the quiet X-ray flux follows the solar cycle while that for Lyman α remains unchanged, then the relative importance of X rays and Lyman α could be very different at sunspot minimum and at sunspot maximum. Any conclusions on this point are still somewhat indefinite, but it is very significant that Kreplin, Chubb, and Friedmann (1962) in a recent paper estimate that the X-ray flux in the important band of 2-8A changes by a factor of a thousand during the solar cycle; the ultraviolet emission, on the other hand, seems relatively stable.

Above about 95 km, as Fig. 3.10 shows, the radiations forming the E layer, namely solar ultraviolet and soft X rays, are dominant. Below some 70 km, cosmic rays, as pointed out by Moler (1960), are very important, and even at greater heights seem to produce somewhat larger effects than those due to meteors.

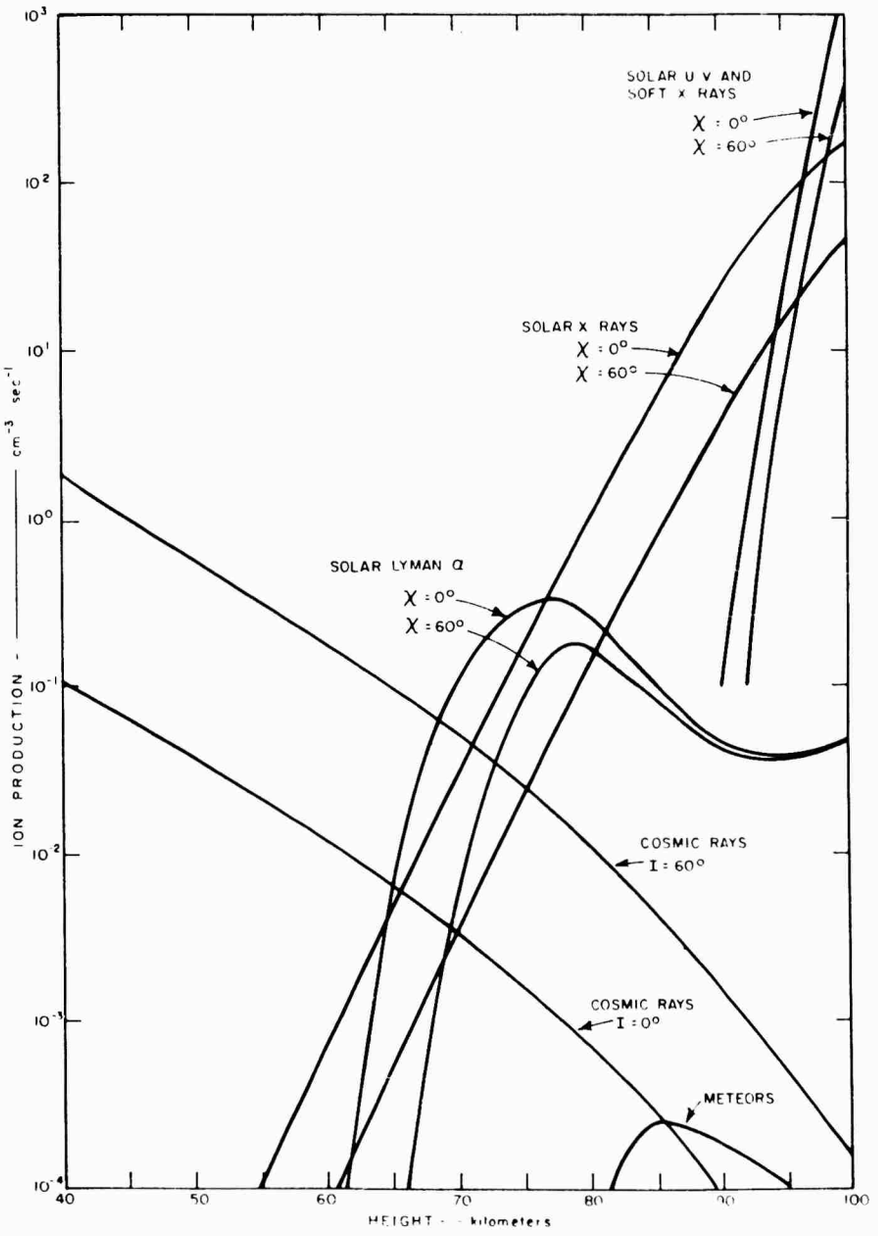

FIG. 3.10 RATE OF ION PRODUCTION AS A FUNCTION OF HEIGHT UNDER QUIET SOLAR CONDITIONS

3.4 REFERENCES FOR SECTION 3

Abercombie, S. D., Atomic Weapons Research Establishment, Aldermaston, England, private communication (1962).

Bailey, D. K., "Abnormal Ionization in the Lower Ionosphere Associated with Cosmic-Ray Flux Enhancements," Proc. IRE, Vol. 47, pp. 255-266 (1959).

Bailey, D. K., and L. M. Branscomb, "Rate Coefficients for 0_2^- Collisional Detachment," Bull. Am. Phys. Soc., Vol. 5, p. 123 (1960).

Barth, C. A., "Nitrogen and Oxygen Atomic Reactions in the Chemosphere," Chemical Reactions in the Lower and Upper Atmosphere, pp. 303-326 (Interscience Publishers, Inc., New York, New York, 1961).

Bates, D. R., "Dissociative Recombination," letter in Phys. Rev., Vol. 78, pp. 493-494 (1950).

Bates, D. R., and H. S. W. Massey, "Negative Ions of Atomic and Molecular Oxygen," Phil. Trans. Roy. Soc., Vol. 239A, pp. 269-304 (1943).

Bialecke, F. P., and A. A. Dougal, "Pressure and Temperature Variation of the Electron Ion Recombination Coefficient in Nitrogen," J. Geophys. Research, Vol. 63, pp. 539-546 (1958).

Biondi, M. A., "Atomic Collision Processes in Atmospheric Gases," Chemical Reactions in the Lower and Upper Atmosphere, pp. 353-369 (Interscience Publishers, Inc., New York, New York, 1961).

Biondi, M. A., and S. C. Brown, "Measurement of Electron-Ion Recombination," Phys. Rev., Vol. 76, pp. 1697-1700 (1949).

Branscomb, L. M., D. S. Burch, S. J. Smith, and S. Geltman, "Photodetachment Cross-Section and the Electron Affinity of Atomic Oxygen," Phys. Rev., Vol. 111, pp. 504-513 (1958).

Burch, D. S., S. J. Smith, and L. M. Branscomb, "Photodetachment of 0_2^-," Phys. Rev., Vol. 112, pp. 171-175 (1958).

Crain, C. M., "Ionization Loss Rates Below 90 km," J. Geophys. Research, Vol. 66, pp. 1117-1126 (1961).

Curtis, H. O., "Effects of the Primary Cosmic Radiation on Matter," Air Force Surveys in Geophysics, No. 78, Air Force Cambridge Research Center (1956).

Ditchburn, R. W., J. E. S. Bradley, C. G. Cannon, and G. Munday, "Absorption Cross-Sections for Lyman α and Neighbouring Lines," Rocket Exploration of the Upper Atmosphere, pp. 327-334 (Pergamon Press, New York, New York, (1954).

Faire, A. C., and K. S. W. Champion, "Measurements of Dissociative Recombination and Diffusion in Nitrogen at Low Pressures," Phys. Rev., Vol. 113, pp. 1-6 (1959).

Friedman, H., "Lyman α Radiation," Ann. Geophys., Vol. 17, pp. 245-248 (1961).

Henke, B. L., R. White, and B. Lundberg, "Semi-empirical Determination of Mass Absorption Coefficients for the 5-50 Å X-Ray Region," J. Appl. Phys., Vol. 28, pp. 98-105 (1957).

Holt, E. H., "Electron Loss Proccesses in the Oxygen Afterglow," Bull. Amer. Phys. Soc., Vol. 4, pp. 112-113 (1959).

Istomin, V. G., "Magnesium and Calcium Ions in the Earth's Upper Atmosphere," Doklady Akad. Nauk SSSR, Vol. 136, pp. 1066-1068 (1961a), Translation NASA TTF-69.

Istomin, V. G., "Nitrogen Ions in the Upper Atmosphere of the Earth and the Nocturnal Ionization of the E Region," Doklady Akad. Nauk SSSR, Vol. 137, pp. 1102-1105 (1961b).

Johnson, C. Y., E. B. Meadows, and J. C. Holmes, "Ion Composition of the Arctic Ionosphere," J. Geophys. Research, Vol. 63, pp. 443-444 (1958).

Jortner, J., and U. Sokolov, "Spectrophotometric Determination of the Electron Affinities of Some Diatomic Molecules," Nature, Vol. 190, pp. 1003-1004 (1961).

Kaplon, M. F., B. Peters, H. L. Reynolds, and D. M. Ritson, "The Energy Spectrum of Primary Cosmic Radiation," Phys. Rev., Vol. 185, pp. 295-309 (1952).

Knapp, W. S., General Electric TEMPO, Santa Barbara, California, private communication (1962).

Kreplin, R. W., "Solar X-ray and Lyman-α Radiation Measured by the NRL SR-1 Satellite Experiment," paper presented at URSI Spring Mecting, Washington, D. C., 1962.

Kreplin, R. W., T. A. Chubb, and H. Friedman, "X-Ray and Lyman-Alpha Emission from the Sun as Measured from the NRL SR-1 Satellite," J. Geophys. Research, Vol. 67, pp. 2231-2253 (1962).

Loeb, L. B., The Basic Process of Gaseous Electronics (University of California Press, Berkeley, California 1955).

Lovell, A. C. B., "Geophysical Aspects of Meteors," Handbuch der Physik, Vol. XLVIII (Springer-Verlag, Berlin, Germany, 1957).

Massey, H. S. W., and E. H. S. Burhop, Electronic and Ionic Impact Phenomena (Oxford University Press, Oxford, England, 1956).

Meredith, L. H., J. A. van Allen, and M. B. Gottlieb, "Cosmic Ray Intensity above the Atmosphere at High Latitudes," Phys. Rev., Vol. 99, pp. 198-209 (1955).

Mitra, S. K., The Upper Atmosphere (The Asiatic Society, Calcutta, India, 1952).

Moler, W. F., "VLF Propagation Effects of a D-Region Layer Produced by Cosmic Rays," J. Geophys. Research, Vol. 65, pp. 1459-68 (1960).

Mulliken, R. S., "Electron Affinity of O_2^-," Phys. Rev., Vol. 115, pp. 1225-1226 (1961).

Nicolet, M. and A. C. Aikin, "The Formation of the D Region of the Ionosphere," J. Geophys. Research, Vol. 65, pp. 1469-1484 (1960).

Phelps, A. V. and J. L. Pack, "Collisional Detachment in Molecular Oxygen," Phys. Rev. Letters, Vol. 6, pp. 111-113 (1961).

Poppoff, I. G. and R. C. Whitten, "D-Region Ionization by Solar X-rays," J. Geophys. Research, Vol. 67, pp. 2986-2988 (1962).

Rajewsky, B., and D. Lang, "Absolute Measurement of Average Energy Lost By Very Soft X-Rays per Ion Pair in Air," Nature, Vol. 190, pp. 249-250 (1961).

Ratcliffe, J. A., and K. Weekes, The Physics of the Upper Atmosphere, p. 305 (Academic Press, New York, New York, 1958).

Sandstrom, A. E., "The Latitude Effect of the Cosmic Ray Nucleonic Component in Relation to the Magnetic Dip," Arkiv. Fysik., Vol. 14, pp. 409-418 (1958).

Simpson, J. A., "Cosmic Ray Program--First Twelve Months," Bull. I.G.Y., Vol. 15, p. 11 (1958).

Smith, S. J., D. S. Burch, and L. M. Branscomb, "Experimental Photodetachment Cross-Section and the Ionospheric Detachment Rate for O_2^-," Ann. Geophys., Vol. 14, pp. 225-231 (1958).

U.S. Air Force, Cambridge Research Center, Handbook of Geophysics for Air Force Designs (MacMillan Co., New York, New York, 1960).

Van Allen, J. A., The Nature and Intensity of the Cosmic Radiation, Physics and Medicine of the Upper Atmosphere, pp. 239-266 (University of New Mexico Press, Albuquerque, New Mexico, 1952).

Victoreen, J. A., "The Calculation of X-Ray Mass Asorption Coeffieients," J. Appl. Phys. Vol. 20, pp. 1141-1147 (1949).

Watanabe, K., "Photoionization and Total Absorption Cross Section of Gases, I. Ionization Potentials of Several Molecules, Cross Sections of NH_3 and NO," J. Chem. Phys., Vol. 22, pp. 1564-1570 (1954)

Watanabe, K., and H. E. Hinteregger, "Photoionization Rates in the E and F Regions," J. Geophys. Research, Vol. 67, pp. 999-1006 (1962).

Watanabe, K., E. C. Y. Inn, and M. Zelikoff, "Absorption Coefficients of Oxygen in the Vacuum Ultraviolet," J. Chem. Phys., Vol. 21, pp. 1026-1030 (1953).

Winckler, J. R., T. Stix, K. Dwight, and R. Sabin, "A Directional and Latitude Survey of Cosmic Rays at High Altitudes," Phys. Rev., Vol. 79, pp. 656-669 (1950).

Whitten, R. C., and I. G. Poppoff, "A Model of Solar-Flare-Induced Ionization in the D Region," J. Geophys. Research, Vol. 66, pp. 2779-2786 (1961).

Whitten, R. C., and I. G. Poppoff, "Associative Detachment in the D Region," J. Geophys. Research, Vol. 67, pp. 1183-1185 (1962).

4. SOLUTION OF THE BALANCE EQUATIONS FOR QUIET CONDITIONS

4.1 SOLUTION ASSUMING BALANCE IS IMMEDIATELY ATTAINED

The survey of the rate coefficients made in Sec. 3.2 shows that the two recombination coefficients B and E are approximately equal over the height range of 40 to 100 km. An assumption that $B = E \approx 4.10^{-8}$ leads to a very considerable simplification of the equations, and to convenient solutions; it will therefore be adopted. Admittedly, the assumption involves approximation, but the resulting solutions are far more accurate than some previous machine computations which employed values of the rate coefficients now demonstrably incorrect. Generally, in this field, there is a dangerous tendency to accept an elaborate machine solution as being entirely correct, whereas there may well be uncertainties of an order of magnitude in some of the parameters upon which the solution is based.

Under quiet conditions the rate of change of the concentrations of electrons and ions is small. Thus, by equating the derivatives to zero and putting $B = E$, Eq. (3.1) simplifies to

$$\left.\begin{aligned} Q - AN - BNN^+ + (C + D)\,N^- &= 0 \\ AN - (C + D)\,N^- - BN^-N^+ &= 0 \\ Q - BNN^+ - BN^-N^+ = Q - B(N^+)^2 &= 0 \end{aligned}\right\} \qquad (4.1)$$

The equilibrium solutions are

$$N_q^+ = \left(\frac{Q}{B}\right)^{1/2} \qquad \text{(a)}$$

$$N_q^- = \left(\frac{Q}{B}\right)^{1/2}\left(\frac{A}{A + F + \sqrt{QB}}\right) \qquad \text{(b)} \quad (4.2)$$

$$N_q = \left(\frac{Q}{B}\right)^{1/2}\left(\frac{F + \sqrt{QB}}{A + F + \sqrt{QB}}\right) \qquad \text{(c)}$$

where F, the complete detachment coefficient, is given by F = (C + D).

Profiles of N as functions of height and time may be derived using the information of the tables that have been given and interpolating where necessary. Two illustrative examples will be given.

The first of these is for an equinoctial day and a path lying around the equator. The sun will be overhead at local noon, and it is assumed, incorrectly but for simplicity in the computations, that the dip angle is zero over the entire equatorial path. Figure 4.1 is a contour representation of the electron distribution; it is, of course, symmetrical. Figure 4.2 shows profiles of N against height for the vertical paths and zenith angles indicated.

The second example, on Figs. 4.3 through 4.5 is for the winter solstice with noon over Capricorn and a meridional path. It is taken that the dip angle is equal to the geographic latitude. Evidently the combined effects of cosmic-ray and solar ionization introduce considerable asymmetries, especially at the lower heights.

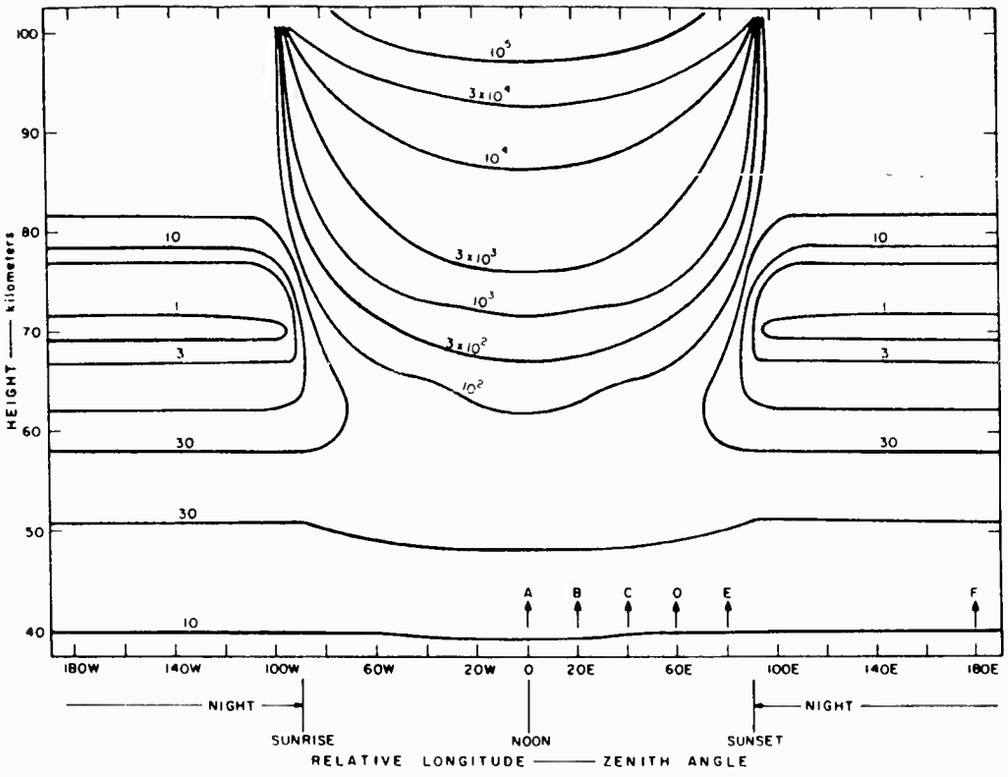

FIG. 4.1 EQUATORIAL PATH AT EQUINOX – ELECTRON DENSITY CONTOURS (cm^{-3})

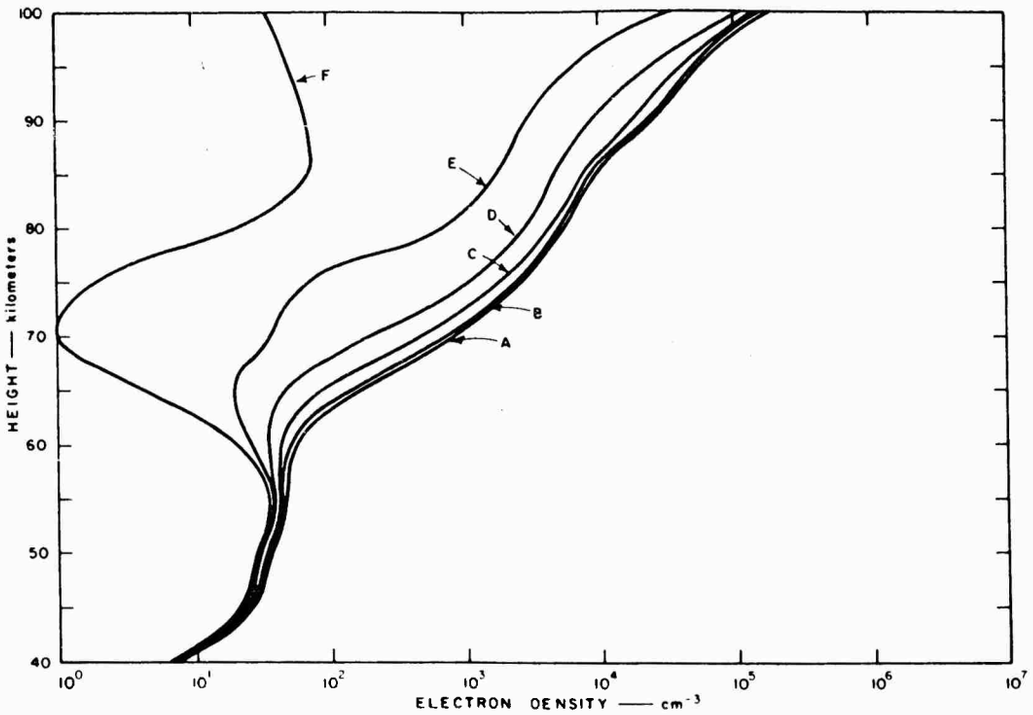

FIG. 4.2 PROFILES OF ELECTRON DENSITY vs. HEIGHT FROM FIG. 4.1

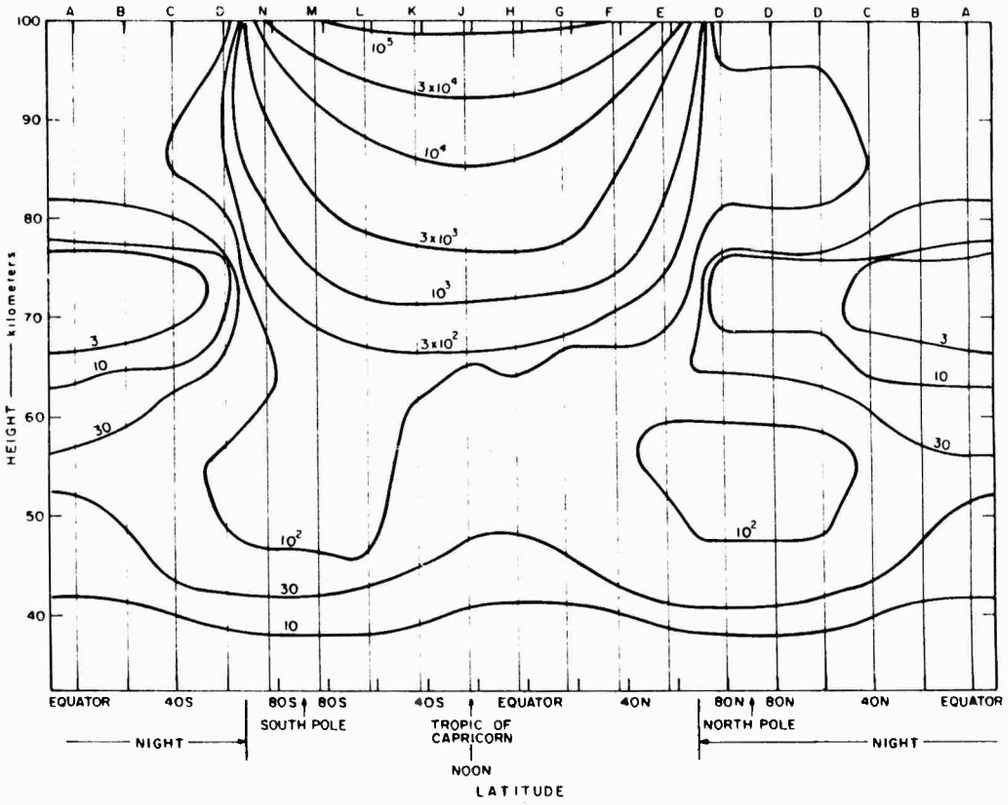

FIG. 4.3 MERIDIONAL PATH AT WINTER SOLSTICE – ELECTRON DENSITY CONTOURS (cm^{-3})

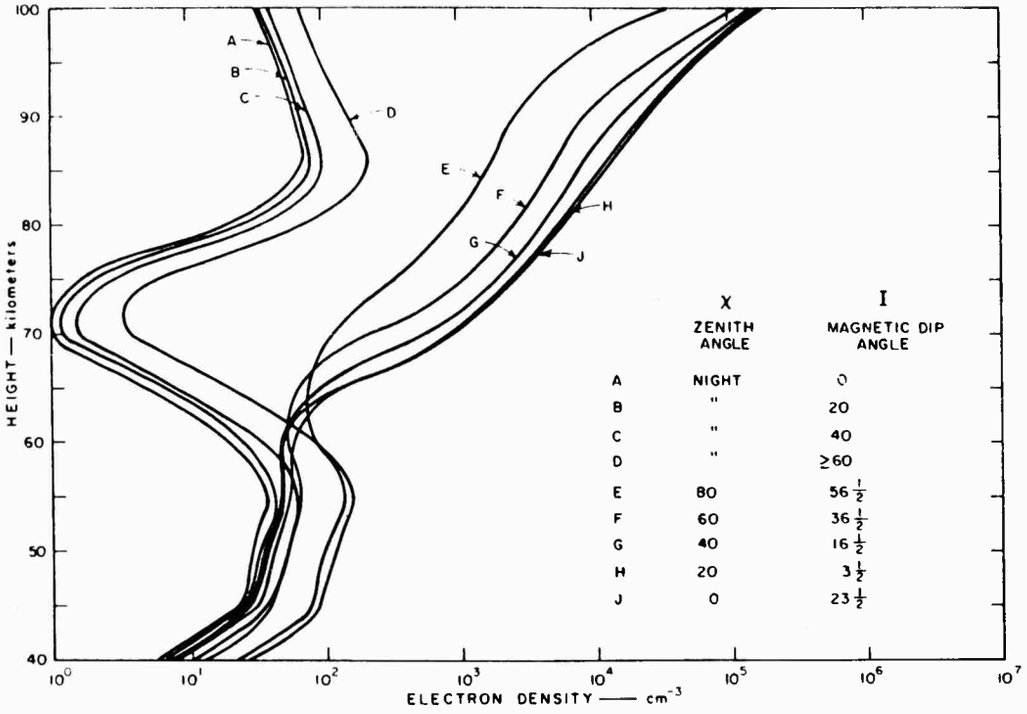

FIG. 4.4 PROFILES OF ELECTRON DENSITY vs. HEIGHT FROM FIG. 4.3

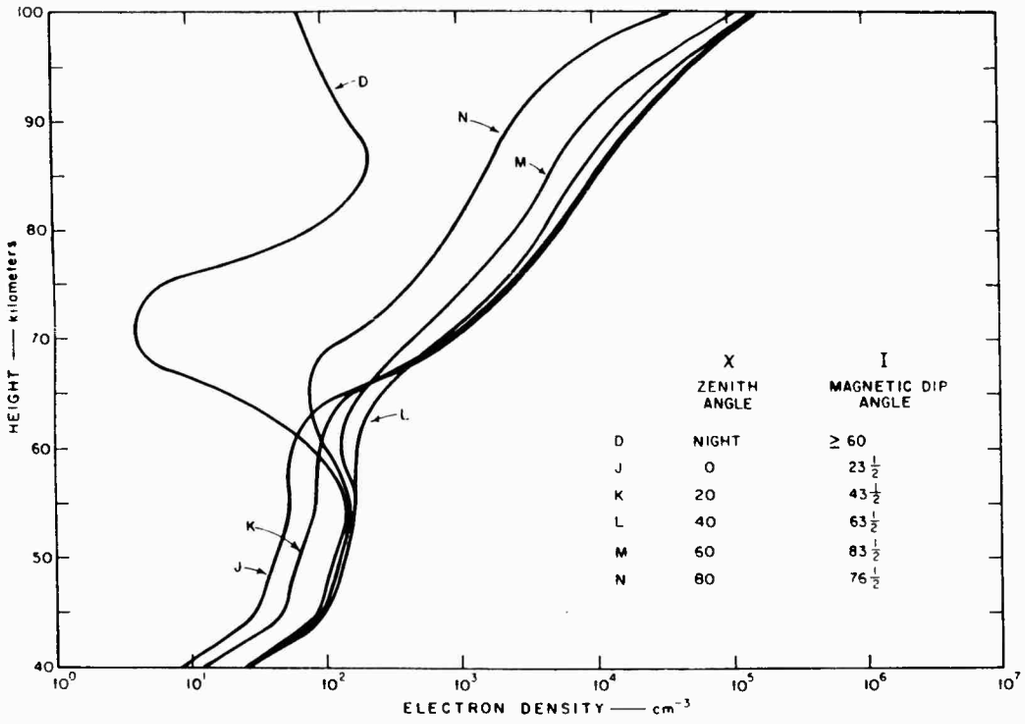

FIG. 4.5 FURTHER PROFILES OF ELECTRON DENSITY vs. HEIGHT FROM FIG. 4.3

4.2 DECAY OF IONIZATION AFTER SUNSET

The assumption that equilibrium is reached seems reasonably valid for daytime hours. Examination of the rate coefficients shows that after any daytime change equilibrium conditions are always re-approached fairly rapidly. Direct experimental evidence of D-layer effects, such as absorption [Bibl et al. (1961)] and VLF phase changes at near vertical incidence [Bracewell et al. (1951)] , indicates that a dependence on solar zenith angle is followed with little time-lag. This again confirms the concept that the quiet daytime D region is never far removed from an equilibrium state.

However, equilibrium is far from being attained at night, particularly at the greater altitudes. The ionization remaining after sunset decays slowly and the low equilibrium values are hardly approached before sunrise occurs. The contours of Figs. 4.1 and 4.3 have therefore been modified ignoring solar radiation for $\chi > 80°$. The values of the electron density have been obtained by considering the appropriate nighttime values of the parameters A, B, F, and Q for any position, and the time since $\chi = 80°$ at that position. The decay of ionization is essentially described by Eq. (3.1c) since the balance of attachment and detachment processes is achieved rapidly after sunset and the ratio N^-/N then remains constant and equal to A/F. This condition and the condition of electrical neutrality $N + N^- = N^+$ are sufficient to specify N, once the behavior of N^+ is known. Equation (3.1c) can be solved exactly, giving

$$N^+ = \frac{N_q^+ \left[2N_q^+ + N_o\left(1 + exp(-2\sqrt{BQ}\,t)\right)\right]}{2N_q^+ + N_o\left(1 - exp(-2\sqrt{BQ}\,t)\right)} \tag{4.3}$$

where N_q^+ is here the nighttime equilibrium value of ionization and $(N_o + N_q^+)$ is the equilibrium value existing at time t = o, when $\chi = 80°$. The modified distributions for N are shown on Figs. 4.6 and 4.8 together with cross sections on Figs. 4.7 and 4.9.

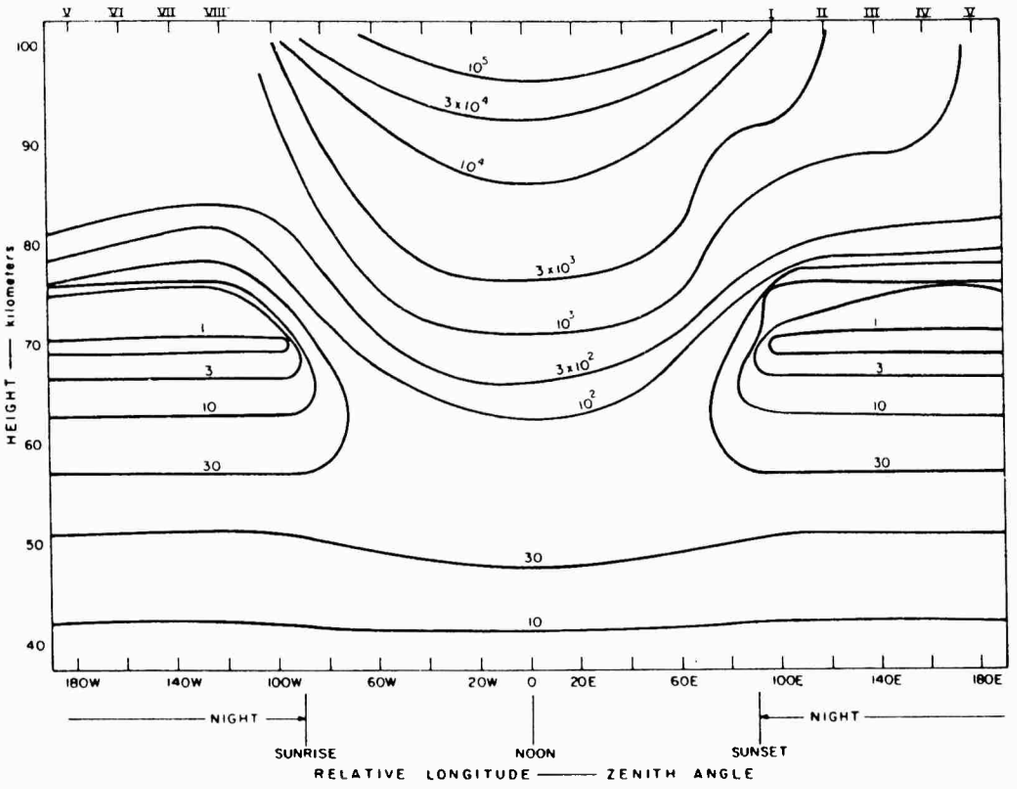

FIG. 4.6 EQUATORIAL PATH AT EQUINOX CONSIDERING NONEQUILIBRIUM AT NIGHT – ELECTRON DENSITY CONTOURS (cm^{-3})

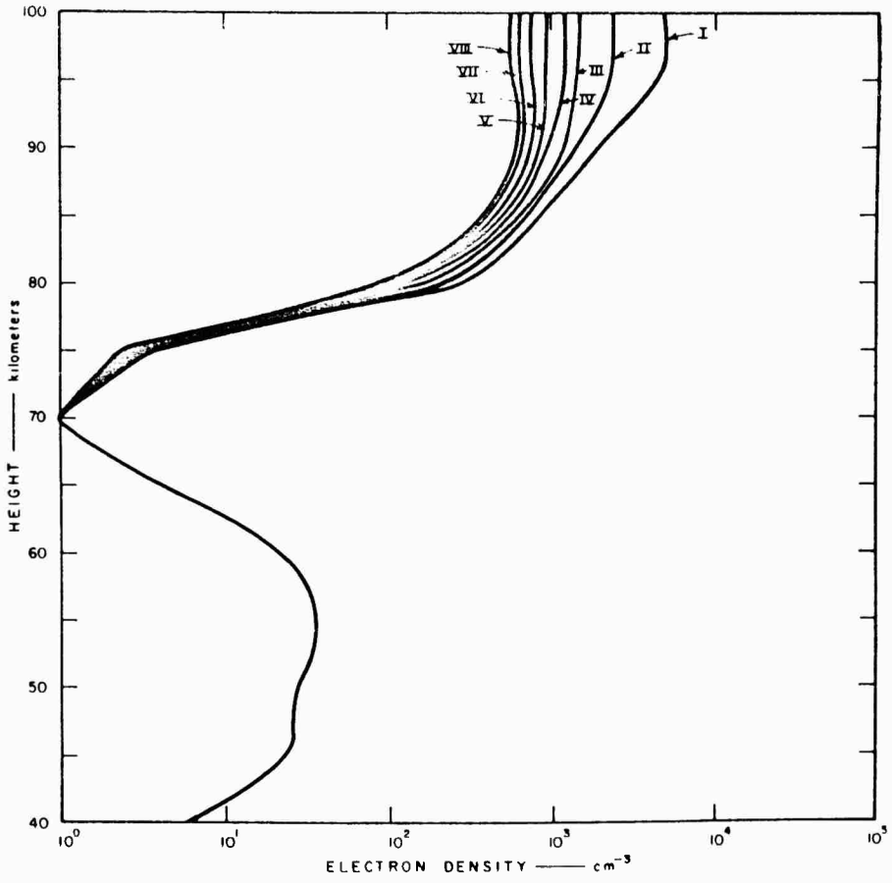

FIG. 4.7 PROFILES OF ELECTRON DENSITY vs. HEIGHT FROM FIG. 4.6

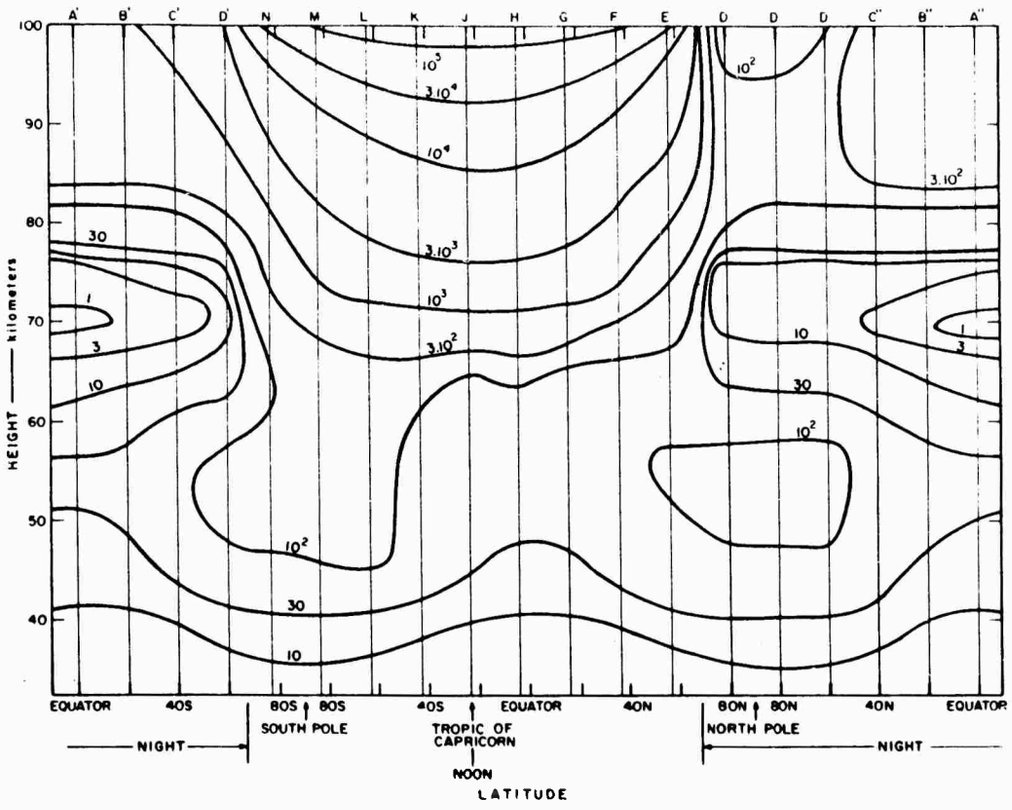

FIG. 4.8 MERIDIONAL PATH AT WINTER SOLSTICE CONSIDERING NONEQUILIBRIUM AT NIGHT – ELECTRON DENSITY CONTOURS (cm^{-3})

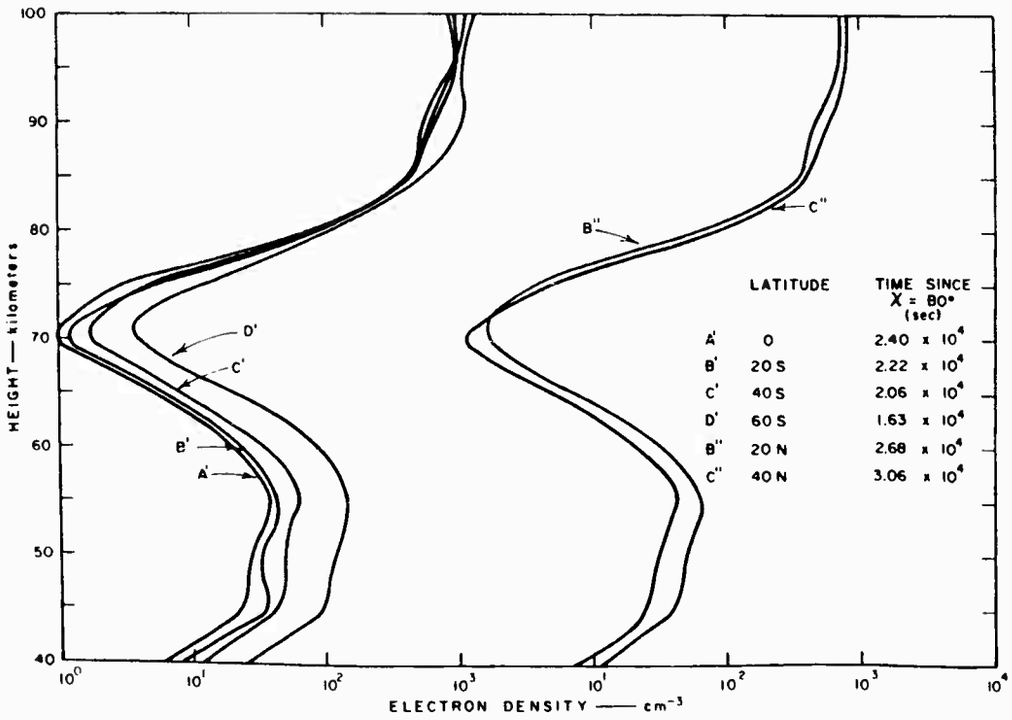

FIG. 4.9 PROFILES OF ELECTRON DENSITY vs. HEIGHT FROM FIG. 4.8

4.3 COMPARISON WITH EXPERIMENTAL OBSERVATIONS

Several theoretical models of electron density profiles in the lower ionosphere have been given, but actual experimental observations are very scanty. Profiles may be deduced by radio probing from the ground and examination of the partial reflections returned from the D region; this approach has been employed recently by Titheridge (1962). The direct method of measuring electron densities using rocket probes is difficult for heights below 100 km, since the density of the neutral particles is so much greater than that of the electrons. However Smith (1962) has reported three successful rocket flights. Some of the experimental results are given on Fig. 4.10 with the appropriate theoretical profiles deduced from Fig. 4.8 for comparison. The agreement is reasonably good. It would be surprising if it were exact, since the theoretical

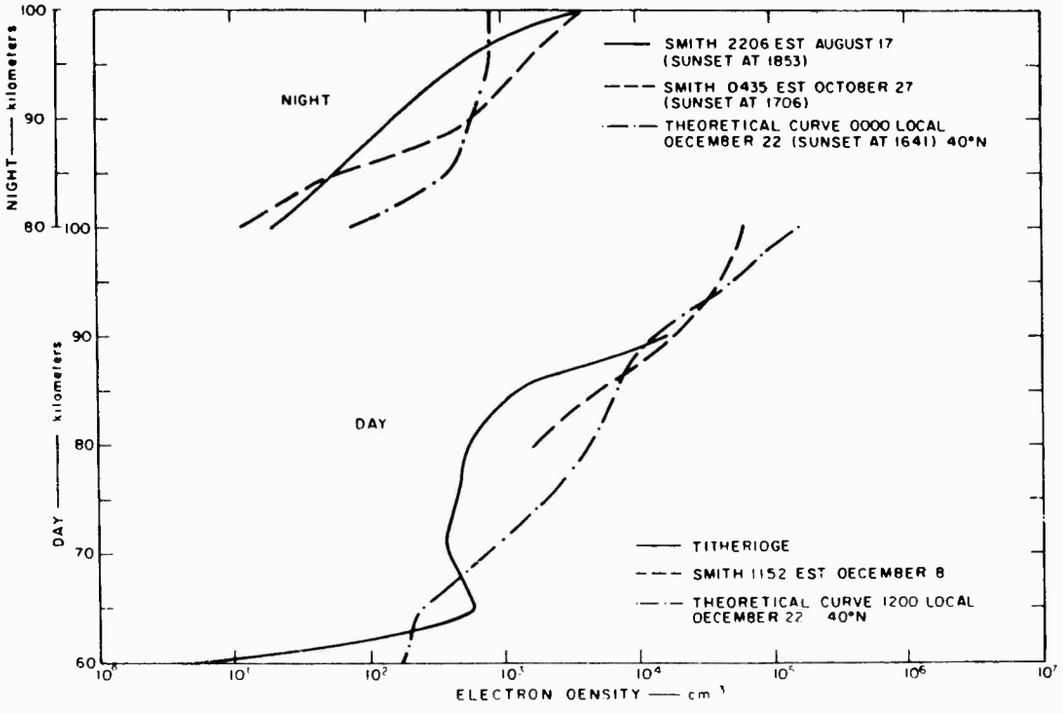

FIG. 4.10 COMPARISON OF EXPERIMENTAL AND THEORETICAL CURVES

work has completely ignored the vertical transport of electrons by diffusion or other processes. Perhaps the major difference between the theoretical and the experimental curves is the tendency of the former to give greater electron densities than the latter at heights near 80 km; this is true both by night and by day.

4.4 RELATION OF ELECTRON DENSITY PROFILES TO VLF PROPAGATION

The propagation characteristics for VLF radio waves in the quasi-waveguide formed by the surface of the earth and the lower ionosphere are chiefly determined by the variation in ionospheric conductivity with height. For this reason it is desirable to convert the contours of electron density into contours of the parameter ω_r. This parameter is directly related to ionospheric conductivity and is commonly employed in the development of the waveguide theory of VLF propagation. The equation

$$\omega_r = \frac{\omega_o^2}{\left(\nu^2 + \omega_L^2\right)^{1/2}} \tag{4.4}$$

defines ω_r ; in Eq. (4.4), ν is the electron collisional frequency, ω_L the longitudinal component of the electron gyrofrequency, and ω_o the plasma frequency. In mks units, $\omega_o^2 = N' e^2/\epsilon_o m$ where e is the electronic charge (1.6×10^{-19} c), m is the electronic mass (9.1×10^{-31} kg), $\epsilon_o = 8.85 \times 10^{-12}$, and N' is the number of electrons per m^3 ($N' = 10^6$ N). Hence $\omega_o^2 \approx 3.4 \times 10^9$ N. The quantity of ω_L is given by $(4\pi \times 10^{-7})$He/m where H (ampere-turn/meter) is the strength of the longitudinal component of the earth's magnetic field for the propagation. The best information upon collisional frequencies is in the report by Cook and Lorents (1961) (see Fig. 4.11) while the paper of Mlodnosky and Helliwell (1962) is useful in determining ω_L for meridional propagation.

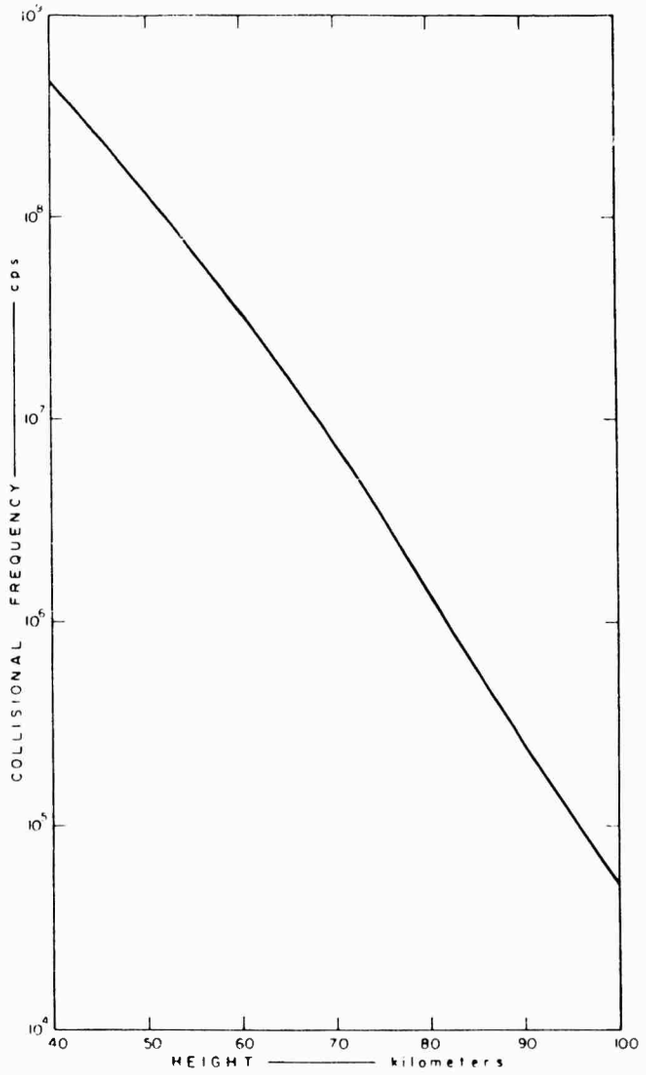

FIG. 4.11 ELECTRON COLLISIONAL FREQUENCY vs. HEIGHT

The electron densities shown on Figs. 4.6 and 4.8 have been converted to contours of ω_r ; the results are given on Figs. 4.12 through 4.19. For the equatorial case, ω_r was plotted for propagation along the equator ($\omega_L = 0$); the meridional case is given both for $\omega_L = 0$, and, more correctly, for the instance of propagation along the meridian (ω_L non-zero). In all cases the divergence between magnetic and geographic north is neglected.

It is noteworthy that the contours of ω_r are far from being parallel to the surface of the earth. This implies that in the waveguide theory of VLF propagation the guide must be considered to be of variable width. The effects are briefly discussed in Appendix II.

4.5 REFERENCES FOR SEC. 4

Bibl, K., A. Paul, and K. Rawer, "Absorption in the D and E Regions and Its Time Variation," J. Atmos. Terrest. Phys., Vol. 23, pp. 244-259 (1961).

Bracewell, R. N., K. G. Budden, J. A. Ratcliffe, T. W. Straker, and K. Weekes, "The Ionospheric Propagation of Low and Very-Low-Frequency Radio Waves over Distances Less than 1000 km," Proc. IEE (London), Vol. 98, Part III, pp. 221-236 (1951).

Cook, C. J., and D. C. Lorents, "Electron Collision Frequencies and Scattering Cross Sections in the Ionosphere," Final Technical Report 6, Part A, Contract DA-36-039 SC-85052, SRI Project PAU-3340, Stanford Research Institute, Menlo Park, California (1961).

Mlodnosky, R. F., and R. A. Helliwell, "Graphic Data on the Earth's Main Magnetic Field in Space," J. Geophys. Research, Vol. 67, pp. 2207-2214 (1962).

Smith, L. G., "Rocket Measurements of Electron Density and Temperature in the Nighttime Ionosphere," Technical Report 62-1-N, Contract NASW-98, Geophysical Corporation of America, Bedford, Massachusetts (1962).

Titheridge, J. E., "The Electron Density in the Lower Ionosphere," J. Atmos. Terrest. Phys., Vol. 24, pp. 269-282 (1962).

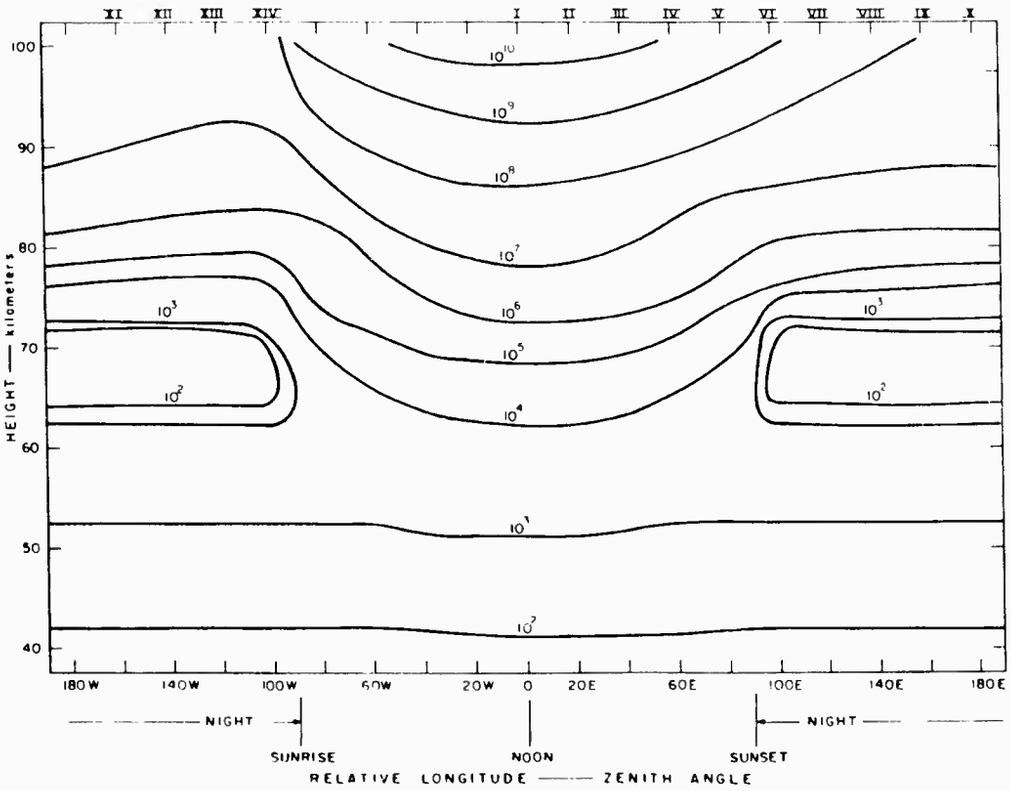

FIG. 4.12 EQUATORIAL PATH AT EQUINOX CONSIDERING NONEQUILIBRIUM AT NIGHT – CONTOURS OF ω_r (cps)

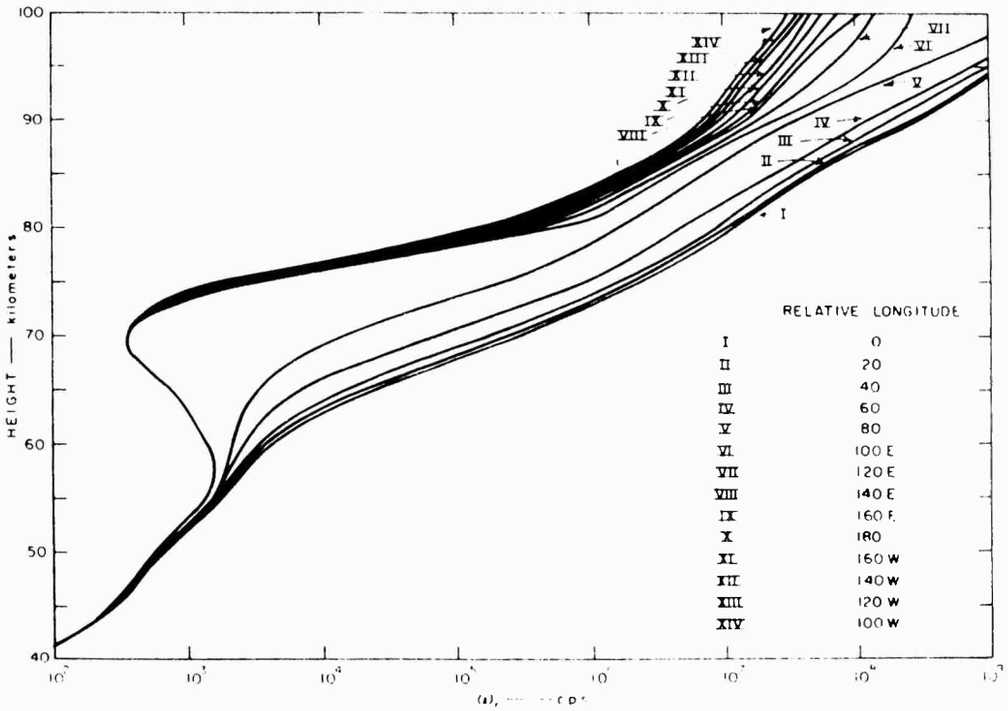

FIG. 4.13 PROFILES OF σ_T vs. HEIGHT FROM FIG. 4.12

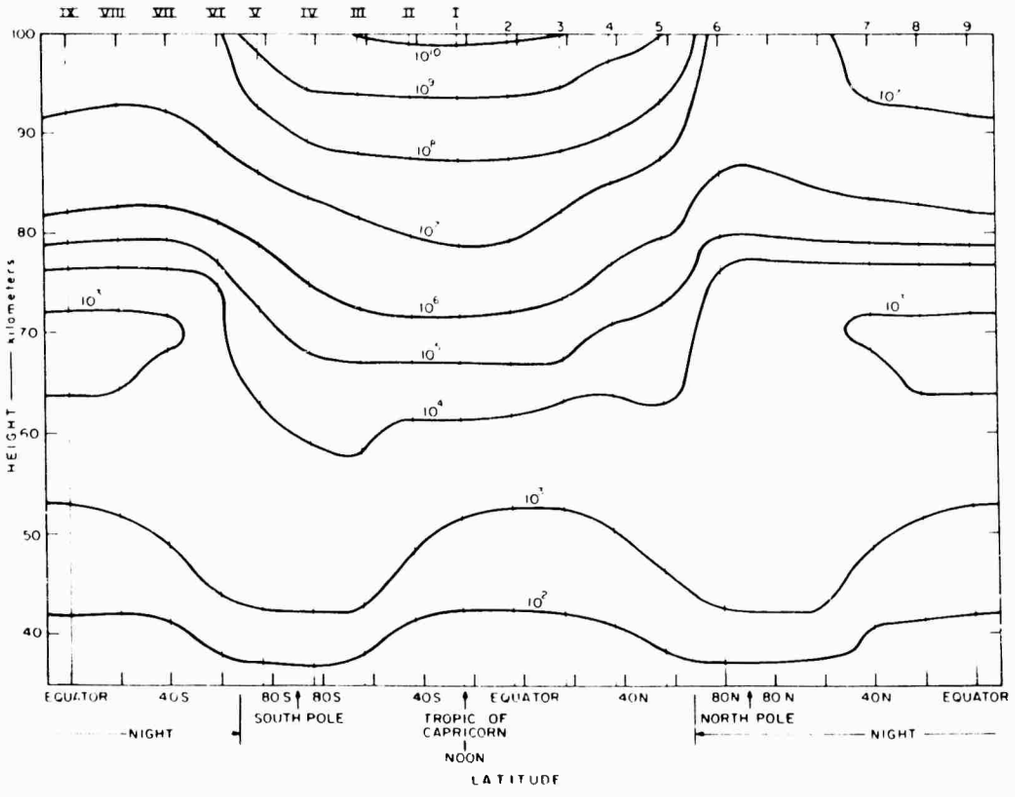

FIG. 4.14 MERIDIONAL PATH AT WINTER SOLSTICE CONSIDERING NONEQUILIBRIUM AT NIGHT – CONTOURS OF ω_r (cps) NEGLECTING EARTH'S MAGNETIC FIELD

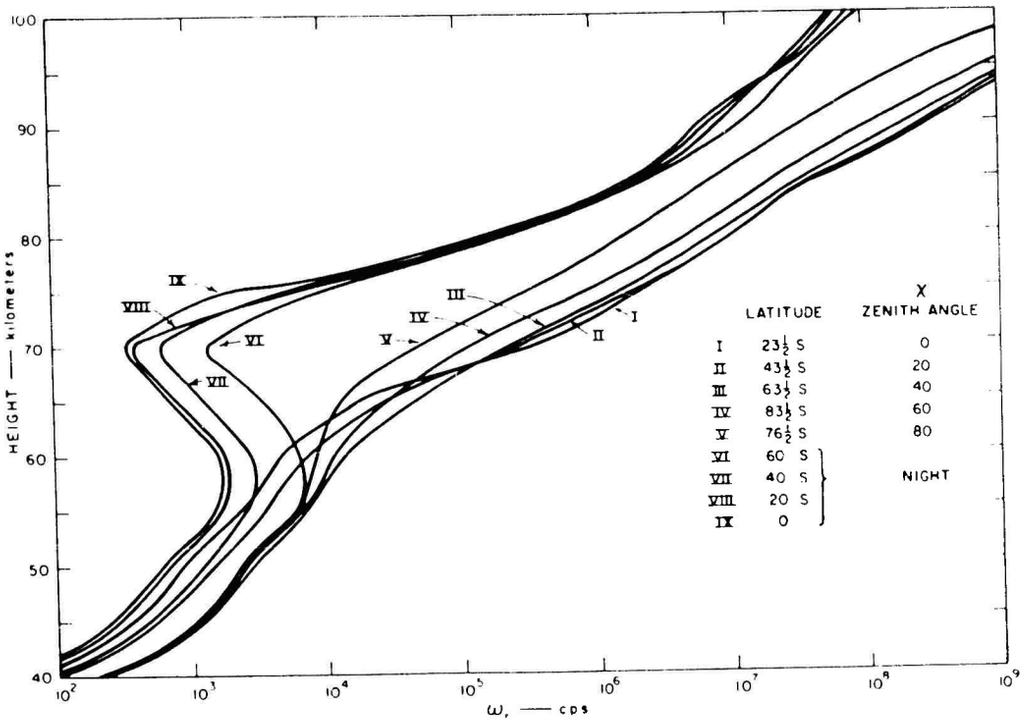

FIG. 4.15 PROFILES OF ω_r vs. HEIGHT FROM FIG. 4.14

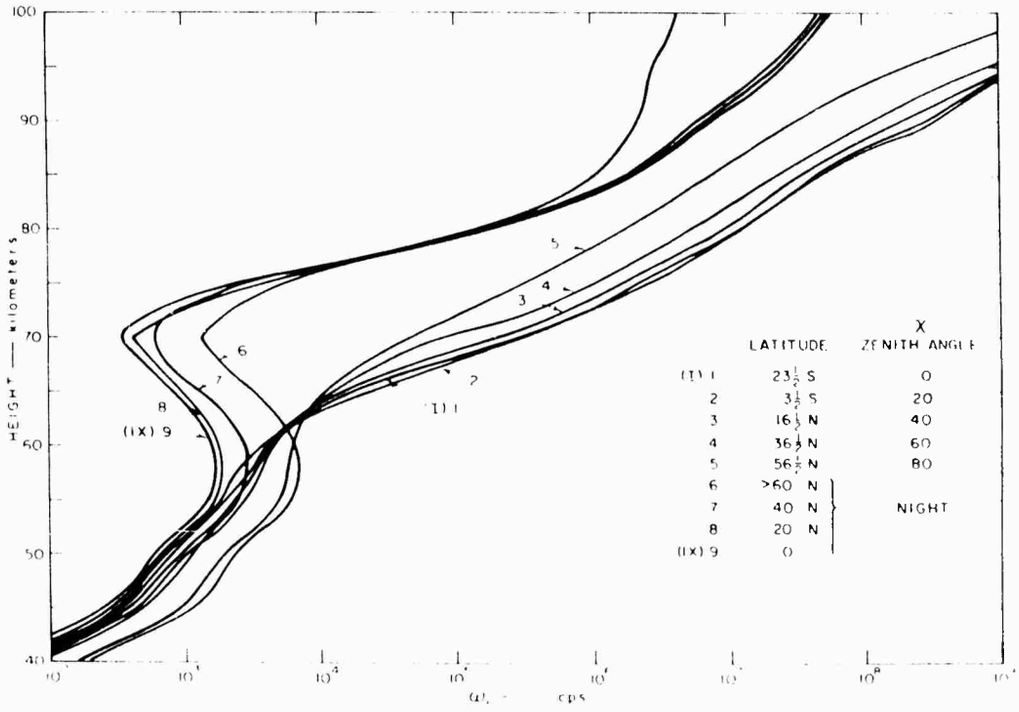

FIG. 4.16 FURTHER PROFILES OF α_i vs. HEIGHT FROM FIG. 4.14

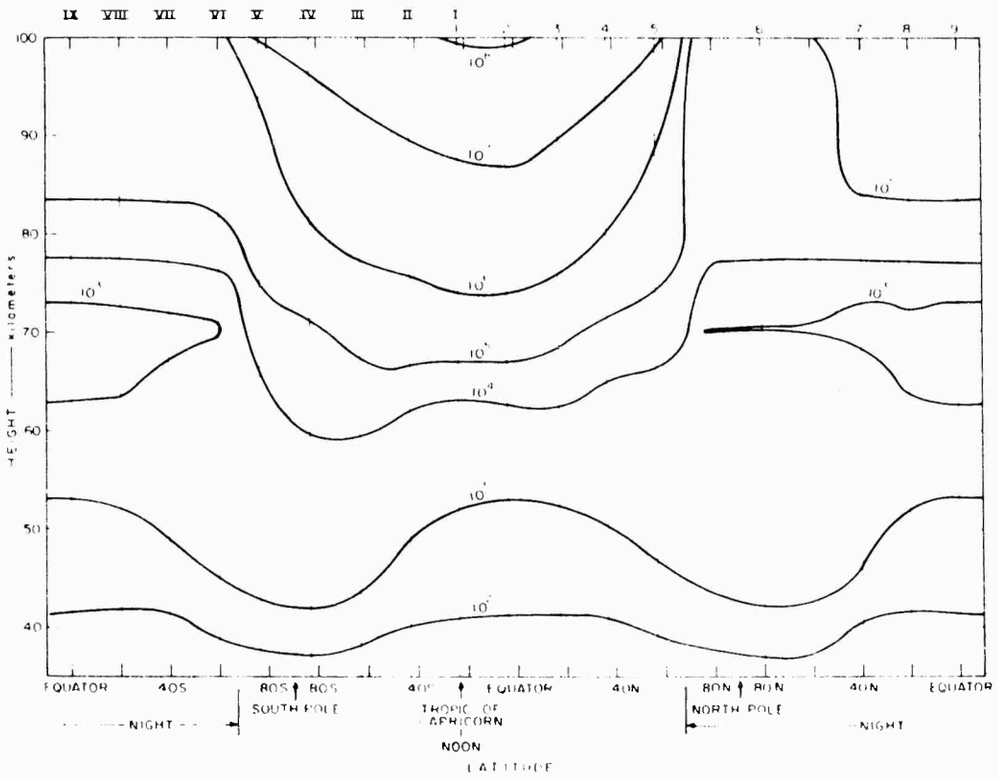

FIG. 4.17 MERIDIONAL PATH AT WINTER SOLSTICE CONSIDERING NONEQUILIBRIUM AT NIGHT – CONTOURS OF ν_r (cps) NOT NEGLECTING EARTH'S MAGNETIC FIELD

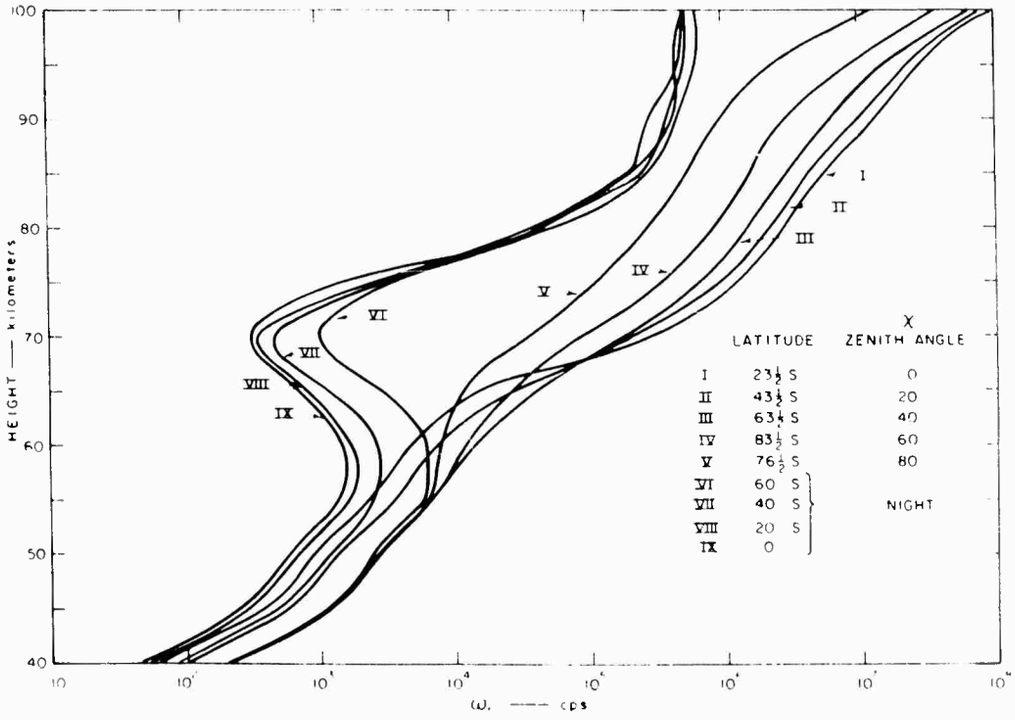

FIG. 4.18 PROFILES OF ν_r vs. HEIGHT FROM FIG. 4.17

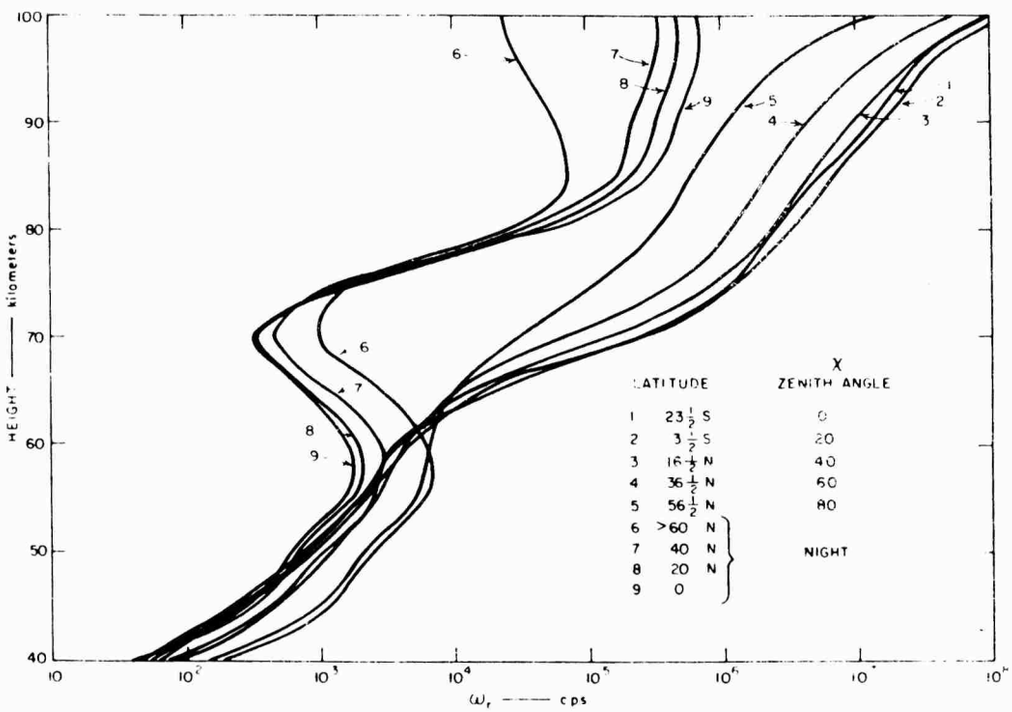

FIG. 4.19 FURTHER PROFILES OF α_r vs. HEIGHT FROM FIG. 4.17

5. THE SUDDEN IONOSPHERIC DISTURBANCE

The SID, as already indicated, is due to an increase in X-ray flux, that is, an enhancement of the flux given by Fig. 3.9. The intensity and spectral distribution of the X radiation undoubtedly varies between different SID incidents, but any investigation of such variation must await the analysis of extensive satellite data. Indeed, it can hardly be said that even the general behavior during an SID has yet been established.

5.1 SPECTRAL DISTRIBUTION OF X-RAY FLUX

Poppoff and Whitten (1961) have deduced the X-ray spectrum, associated with a Class 2+ flare, from rocket observations: the resulting D-layer electron distribution produces ionospheric absorption that is in reasonable agreement with that experimentally observed. Kreplin (1961) states that during a flare the X-ray emission in the 2 to 8Å band increases by a factor of ten to one hundred: it can be deduced from the same paper that over the wavelength range of 8 to 20Å the factor is three to twenty-five, while in the band between 44 and 60Å the SID flux is probably only about three times -- and certainly less than ten times -- as strong as that in undisturbed conditions. The satellite observations of Kreplin, Chubb, and Friedmann (1962) show that during a Class 2 flare accompanied by a short-wave fadeout (also of Class 2) the X-ray flux in the 2 to 8Å band is some 5×10^{-3} to 10^{-2} erg cm^2/sec.

The papers of Kreplin and his colleagues suggest that the Whitten-Poppoff X-ray spectrum is considerably more intense than that associated with a moderate flare. In order to reconcile the quiet-sun and solar-flare observations, it is necessary to reduce the magnitude of the X-ray flux indicated by Whitten and Poppoff by a factor of thirty, while retaining the same spectral distribution. This has been done and the result, plotted in Fig. 5.1, will be taken as representing the X-ray flux, additional to the quiet value, resulting from a moderate flare.

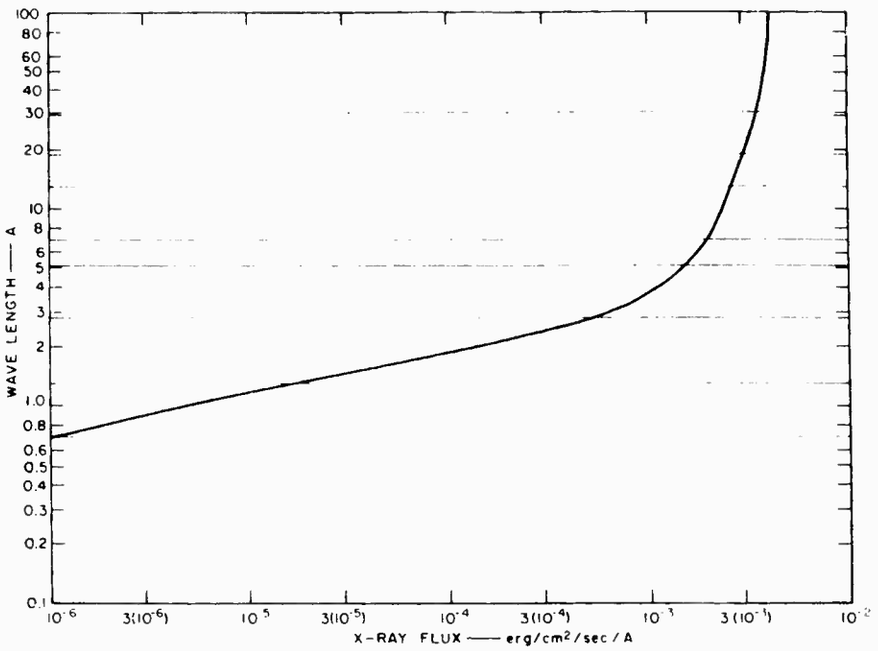

FIG. 5.1 ADDITIONAL X-RAY FLUX DUE TO A MODERATE FLARE

The X-ray flux during a flare rises rapidly to a maximum and then decays more gradually. It is probable that the predominant X radiation steadily becomes softer as time increases, but this effect will be ignored, in order to avoid considerable complexities, and the spectral distribution will be assumed constant throughout the flare.

5.2 TEMPORAL VARIATION OF X-RAY FLUX

The temporal variation of the X-ray flux during a flare has been estimated by Poppoff and Whitten (1961) to have the form shown on Fig. 5.2 rising to maximum intensity in about 300 sec and then decreasing to about 20 percent of its maximum value in a similar interval. Also shown on Fig. 5.2 is a plot of the function, Q(t), formulated by Poppoff and Whitten to fit this variation (this is the light continuous line on Fig. 5.2).

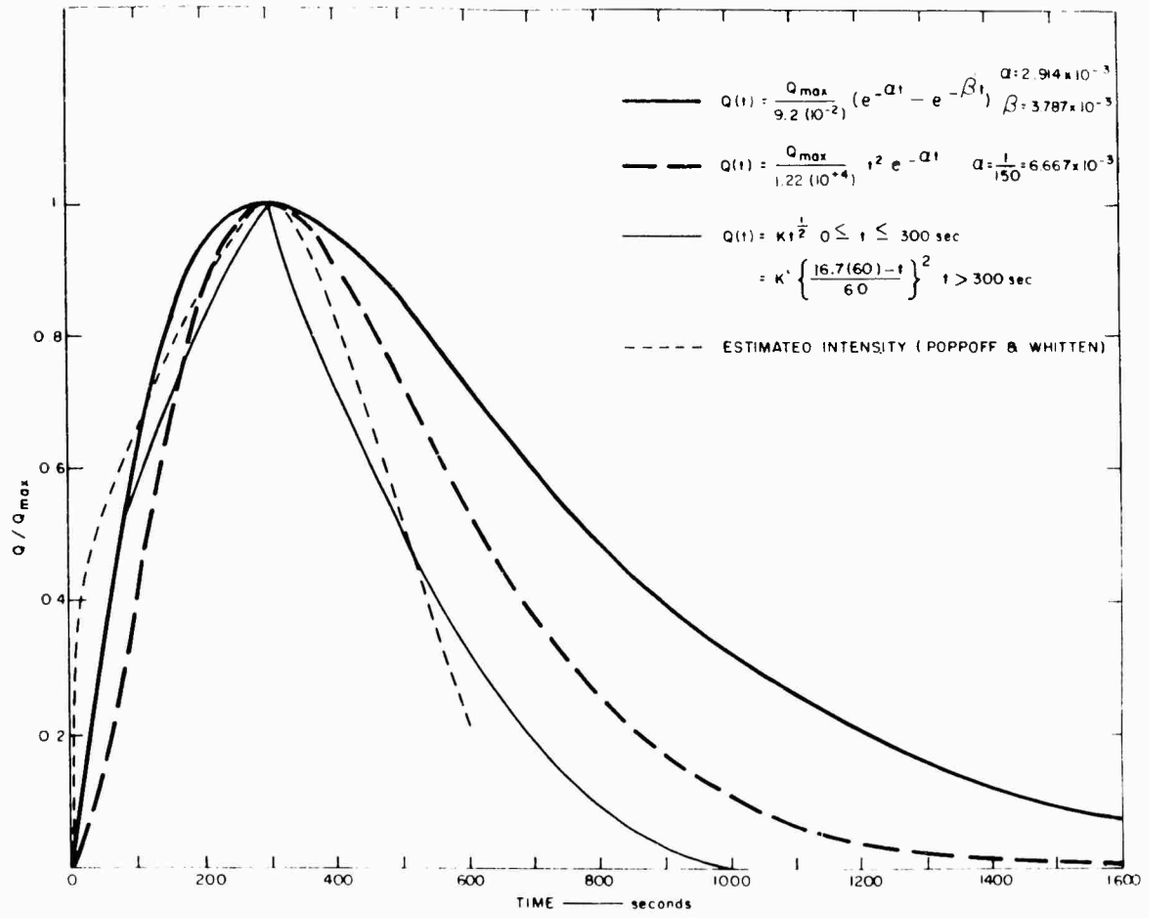

FIG. 5.2 TEMPORAL DEPENDENCE OF X-RAY FLUX IN A SOLAR FLARE

The statistics given in Sec. 2 suggest that the decay to normal of the X-ray flux takes rather longer than is indicated by Poppoff and Whitten. Also their form for Q(t), being two different functions in the intervals $0 \le t < 300$ and $t > 300$, seems somewhat artificial and is rather inconvenient to use for any calculations of the ionization it produces. For these reasons it was decided to find an expression for Q(t) giving a maximum intensity at t = 300 sec and a decay to Q = Q max/20 at t = 1200 sec. A function of the form

$$Q(t) = Q_0(e^{-\alpha t} - e^{-\beta t}) \tag{5.1}$$

where Q_0, α, and β are adjustable constants was first tried, but it was found that it is not possible to fit the above conditions with such a function. The closest approach to the required form is that plotted on Fig. 5.2, for $\alpha = 2{\cdot}914.10^{-3}$ and $\beta = 3{\cdot}787.10^{-3}$, which gives Q(1200) ≈ Q max/5 considerably larger than is desired. The conditions are more closely fitted by the function

$$Q(t) = Q_0' t^2 e^{-\alpha t}, \tag{5.2}$$

with $\alpha = 1/150$, which is also plotted in Fig. 5.2. For this function Q(1200) ≈ Q max/25, which is less than Q max/20 as required. The constants Q_0 and Q_0' of Eqs. (5.1) and (5.2) are adjusted to give Q(300) = Q max. This gives Q_0 = Q max $(9{\cdot}2\times10^{-2})^{-1}$ and Q_0' = Q max $(1.22\times10^{4})^{-1}$.

5.3 RESULTING HEIGHT AND ZENITH ANGLE DEPENDENCE OF IONIZING FLUX

The effect of an X-ray flare in causing an SID depends on the ionization produced at any position in the ionosphere. This is a function of height and zenith angle of the sun at the time of the flare as well as of the ionizing flux. However, the height and zenith angle dependence for a given X-ray flux has already been considered and Figs. 3.3 through 3.9 show the ionization produced per erg. cm^{-2} sec^{-1} of X-ray flux in terms of height, zenith angle, and wavelength. By using these and the spectral distribution given in Fig. 5.1, the ionization produced at the maximum of the flare, that is, by a flux Q max lasting for 1 sec, has been calculated, and the result plotted on Fig. 5.3. By using this and a temporal variation of the ionizing flux such as given by Eqs. (5.1) or (5.2). the ionizing flux during a moderate flare is completely specified: that is, a

possible form of the behavior of the ionizing flux, consistent with the available experimental observations, is defined.

The slight irregularities superimposed upon the curves of Fig. 5.3 are not of significance. In order to simplify the calculations, the X-ray flux, as indicated on Fig. 5.1, was split up into bands centered at 25, 16, 10, 6, 4, 2, and 1Å. The irregularities of Fig. 5.3 are the result of this subdivision.

5.4 SOLUTION OF THE BALANCE EQUATIONS DURING A FLARE

The equations of balance for the ionosphere are

$$\begin{aligned} \frac{dN}{dt} &= Q_q + Q(t) - AN - BNN^+ + FN^- \\ \frac{dN^-}{dt} &= AN - FN^- - BN^-N^+ \\ \frac{dN^+}{dt} &= Q_q + Q(t) - BN^{+2} \end{aligned} \tag{5.3}$$

where Q(t) is the ionizing flux during the flare and all other quantities are as previously defined, the suffix q representing quiet conditions before the flare. The solution of these equations is complicated, but all the necessary information has been given. An approximate solution expressing N^+ as a step function with 5-sec. intervals can be obtained and a computer program was set up to do this for a specific example, namely, the case when the flare occurs directly overhead at the equator. The temporal variation of the X-ray flux is taken as given by Eq. (5.2). The variation of N is then a series of steps followed by a rapid decay to regain the attachment-detachment balance $N_-/N = A/F$. This ratio is effectively attained in less than 5 sec, so that before each addition of further N^+, the value of N can be given as $N = F N^+/A+F$. This has also been computed for the case $\chi = 0$ and heights of 40 to 100 km in 5-km increments, and the

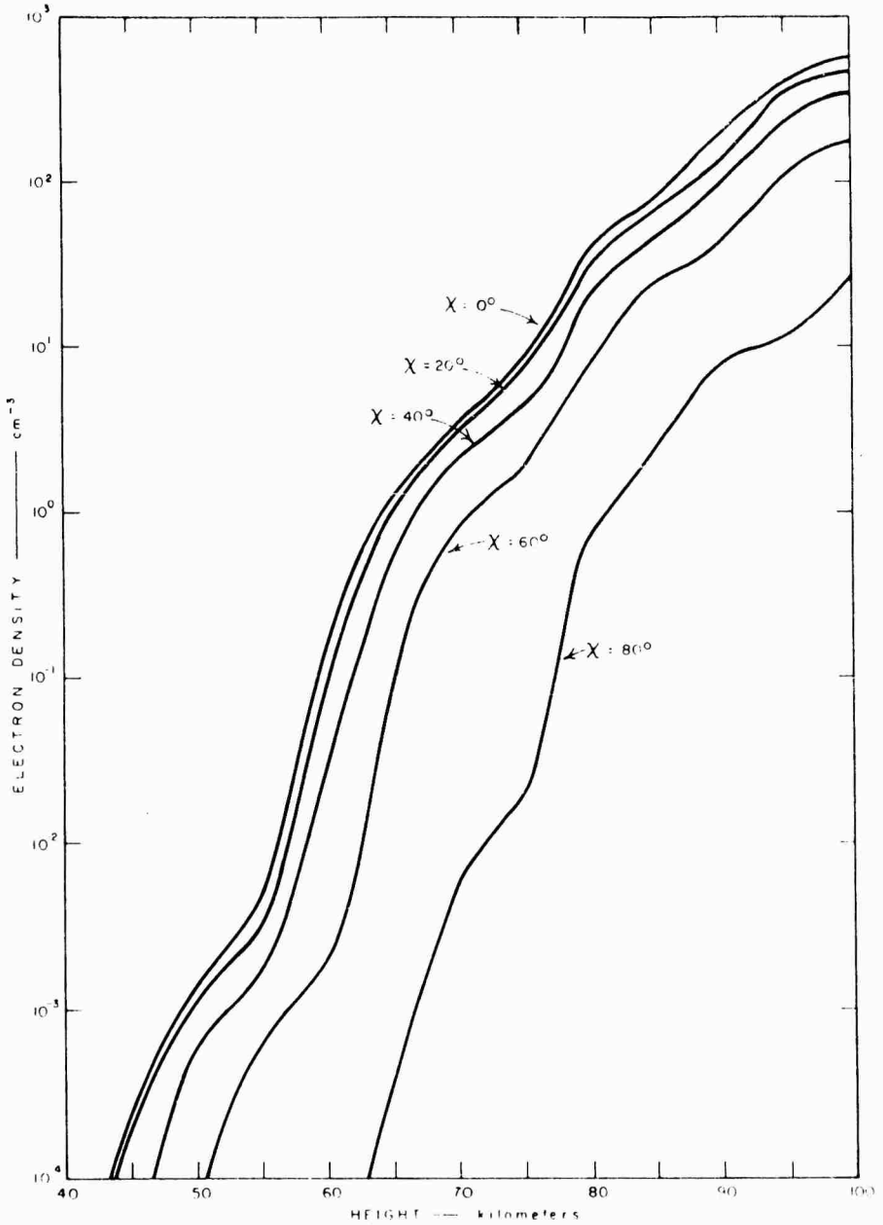

FIG. 5.3 IONIZATION PRODUCED PER SECOND AT FLARE MAXIMUM

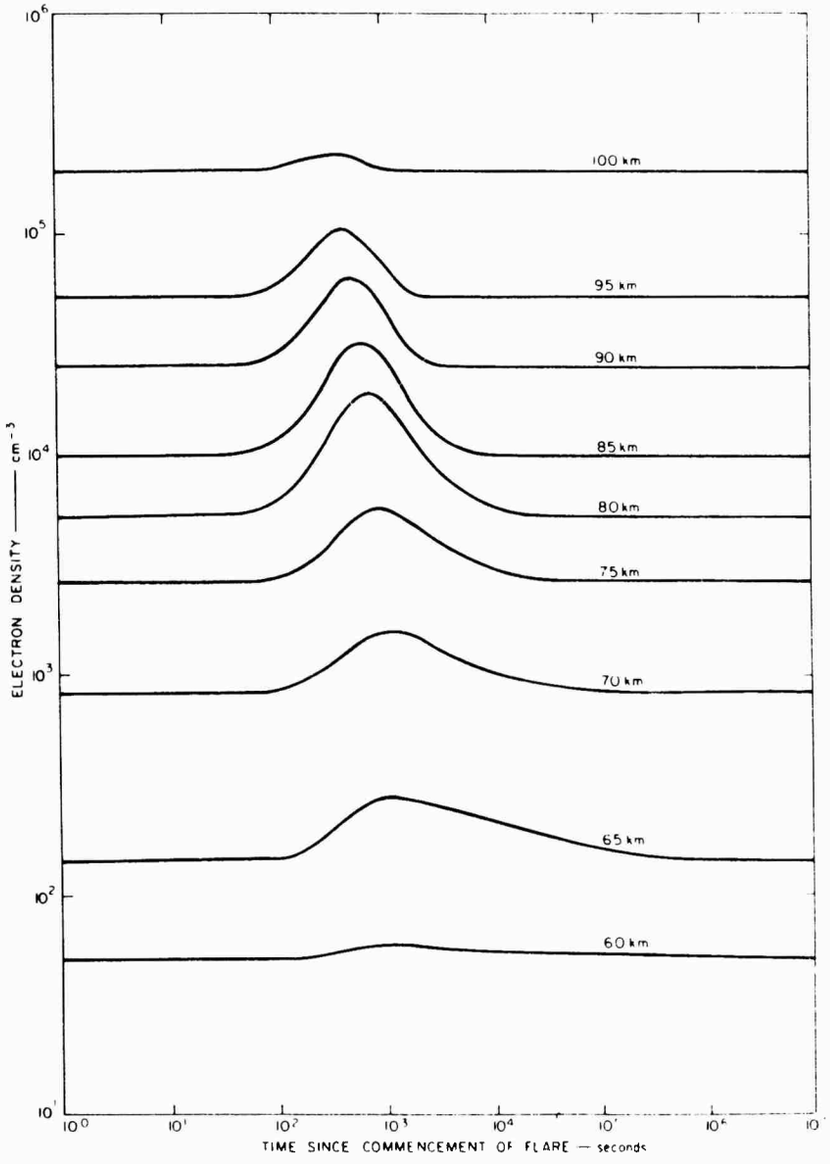

FIG. 5.4 VARIATION IN IONIZATION DURING AND AFTER A SOLAR FLARE

results plotted on Fig. 5.4. The quiet electron densities before and after the flare are those of profile A in Figs. 4.1 and 4.2; the simplification of neglecting the temporal change in solar zenith angle is adopted. The results of Fig. 4.2 suggest that this is not unreasonable for flares occurring within 3 hours ($\pm 10^4$ sec) of noon. However, for times exceeding some 10^4 sec the curves of Fig. 5.4 are unrealistic. Interesting features of Fig. 5.4 are that, proportionately, the maximum added ionization occurs at a height of about 85 km; that the onset time of the maximum increases as height decreases; and that, surprisingly enough, the persistence of the added ionization tends to decrease rather than increase with increasing height.

5.5 REFERENCES FOR SEC. 5

Kreplin, R. W., "Solar X-Rays," Ann. Geophys., Vol. 17, pp. 151-161 (1961).

Kreplin, R. W., T. A. Chubb, and H. Friedmann, "X-Ray and Lyman-Alpha Emission from the Sun as Measured from the NRL SR-1 Satellite," J. Geophys. Research, Vol. 67, pp. 2231-2253 (1962).

Poppoff, I. G., and B. C. Whitten, "A Model of Solar-Flare-Induced Ionization in the D Region," J. Geophys. Research, Vol. 66, pp. 2779-2786 (1961).

6. THE IONOSPHERIC DISTURBANCE DUE TO A NUCLEAR EXPLOSION IN SPACE

6.1 INTRODUCTION

Bollen and Dyce (1961) point out that most of the energy (60 to 80 percent) of a nuclear burst in space appears in the form of prompt X rays. This radiation, in a manner very similar to that of the flux of solar X rays during an SID, produces copious ionization in the lower ionosphere. There are, however, three differences between the disturbance due to a nuclear event and that caused by a natural SID. First, and most important, the time variations of the ionizing flux will be different; notably, the time from onset to maximum flux will be almost instantaneous for the nuclear burst as compared with that for the natural SID. Second, the spectral distribution of the incident X ray flux will not be the same; this will lead to differences in the ionization-height profile for the two types of incident. Third, since the burst will not be coincident with the sun, the dependence upon zenith angle will differ. This latter point is illustrated in the geometry of Fig. 6.1. Suppose the burst, N, occurs upon the line joining the center of the earth, O, and that of the sun, S. This situation is that likely to produce the greatest similarity between the nuclear and the solar zenith-angle dependence. Furthermore, for clarification, let C be an equatorial point, at the time of equinox, experiencing local noon: A and D are the poles. The solar zenith angle, χ is effectively equal to the latitude ϕ, since the solar distance, D, is very much greater than the radius of the earth, R. This is not true, however, for the nuclear angle, α, since, for the most likely situations, D >> R, where H is the height of the burst above the surface of the earth.

To show the variation of zenith angle with the height of a nuclear burst, the values of α for a burst at 10^5 km and for one at 10^4 km have been tabulated in

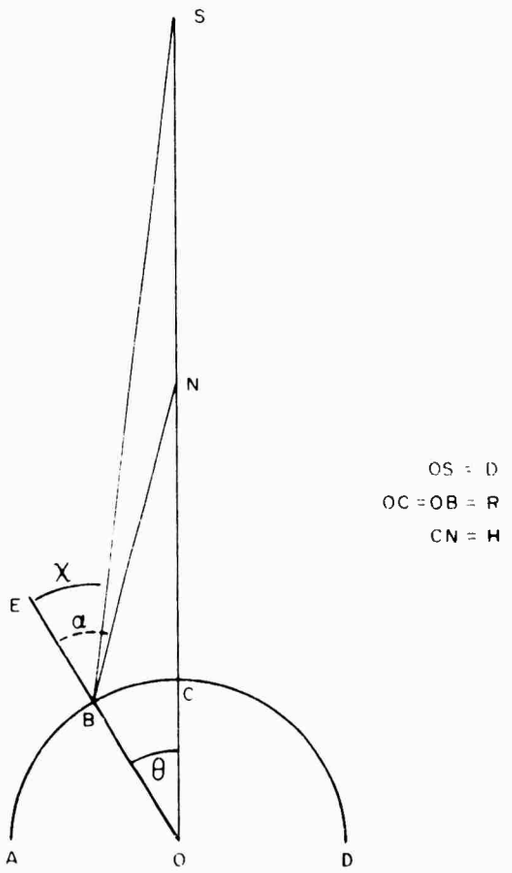

FIG. 6.1 GEOMETRY OF A BURST SITUATION

Table 6.1 as a function of θ, for the geometry of Fig. 6.1. It is clear that the zenith-angle variation from the solar value becomes appreciable for explosions fairly close to the earth.

Table 6.1

DIFFERENCE IN ZENITH-ANGLE DEPENDENCE FOR SOLAR AND NUCLEAR EVENTS

θ	θ (H = 10^5 km)	θ (H = 10^4 km)
0	0	0
10	10.8	16.3
20	21.4	32.2
30	32.2	16.4
40	42.8	59.0
50	53.4	72.2
60	63.6	83.1
70	73.7	90
80	83.8	
90	90	

6.2 SPECTRAL DIFFERENCES

It is usual to assume that a nuclear burst in space will radiate a pulse of X rays whose spectral distribution will correspond to that of a black body at a temperature characteristic of the explosion. Temperatures of between 0.16 and 1.25 kev have been considered by Bollen and Dyce (1961). According to the Wien displacement law, $\lambda_m T$ = constant where λ_m is the wavelength at which maximum energy is radiated. Temperatures of 1.25 and 0.16 kev correspond, respectively, to values of λ_m of about 2 and 16 Å.

In Fig. 6.2 the X-ray intensity incident at the surface of the earth for the conditions of a quiet sun and a moderate flare are replotted from the information of Sees. 3 and 5. For comparative purposes, the flux due to a 1.67KT burst (1 KT assumed as energy in prompt X rays), of 1-kev temperature, at a height

of 10^5 km, is also shown. this curve is for the sub-burst point at the earth, that is, for vertical incidence. It is evident that there are considerable differences between the form of the flare curve (B) and that for the burst (C). As the size and distance of the explosion are changed, the over-all magnitude of C will alter: if the temperature of the burst is modified, Curve C will slide up and down the wavelength axis upon Fig. 6.2. Similarly, Curve B will change in size according to the magnitude of the flare, and there may also be variations in the spectral distribution, although the knowledge of these, as emphasized in Sec. 5, is very scanty. However, it seems certain that a flare will always produce a flux monotonically increasing with increasing wavelength over the range of 0.1 to 100Å; for the same limits in wavelength the flux due to a burst will rise to a maximum (probably at a wavelength between 1 and 10Å) and then decrease as the wavelength further increases. Ignoring the temporal variation, although it may be conceivable for the X-ray flux from nuclear and solar disturbances to be

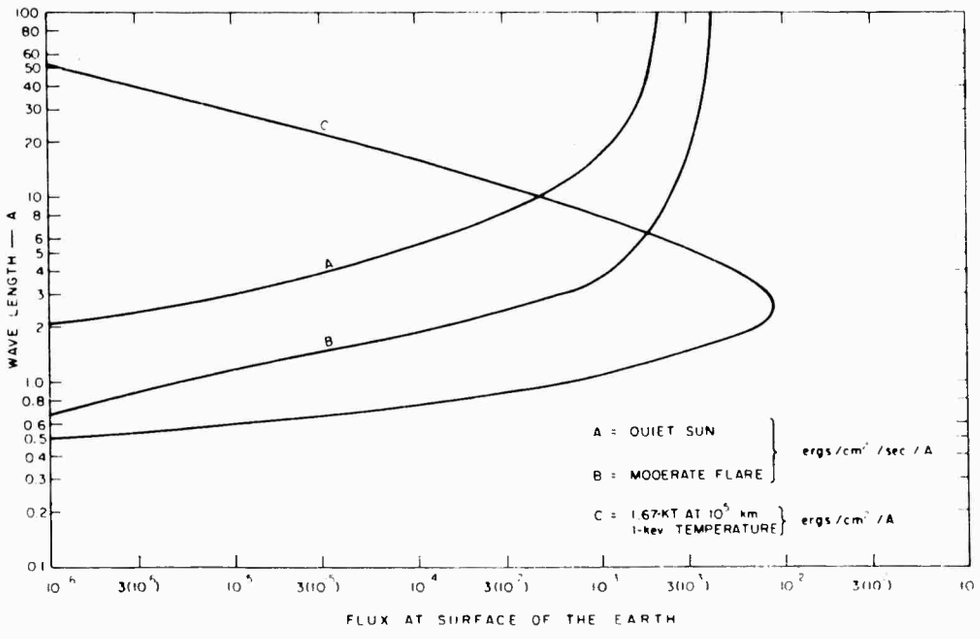

FIG. 6.2 X-RAY FLUX FOR THREE DIFFERENT TYPES OF SOURCE

similar over a wide range of wavelengths (for example, by an effective superposition of the lower parts of Curves B and C), it seems impossible for this similarity to extend over the whole wavelength band from 0.1 to 100Å. These differences in spectral distribution inevitably have ionospheric consequences which should be detectable.

As an example of the ionization differences that can result from a spectral variation, the electron densities produced by the nuclear flux (Curve C of Fig. 6.2) and during 1 sec by the flare-associated flux (Curve B of Fig. 6.2), assuming no losses by recombination or attachment, are plotted on Fig. 6.3. Both curves give maximum electron densities of the order of 10^2 for heights below 100 km, but the height of the maximum for the specific nuclear example is much less than that for the flare-produced ionization. This could have widely different consequences upon radio wave propagation. For instance, VLF propagation is controlled during daytime by an electron density of about 10^2 cm^{-3} at a height of some 70 km. The added ionization in a second at 70 km due to the flare is small compared with 10^2; thus the effects on VLF propagation would be minor. However, for the nuclear instance the enhancement in ionization at 70 km is comparable with that already present; in consequence, the modifications in VLF propagation would be very considerable.

The difference in spectral distribution of the flux due to a solar flare and that due to a nuclear burst will also result in considerable differences in zenith-angle dependence of the resulting ionization. A height of 10^5 km, as used by Bollen and Dyce (1961) for the nuclear burst, has been considered, for a 1.67KT nuclear burst at 1-kev temperature, which gives a 1-KT yield of X rays having the spectral distribution shown on Curve C of Fig. 6.2. Using this curve and interpolating from the curves of Figs. 3.3 through 3.8, the ionization produced at the angles, α, given on Table 6.1, corresponding to $\theta = 0°$, 20°, 40°, 60°, and 80° has been calculated for heights from 40 to 100 km and the results

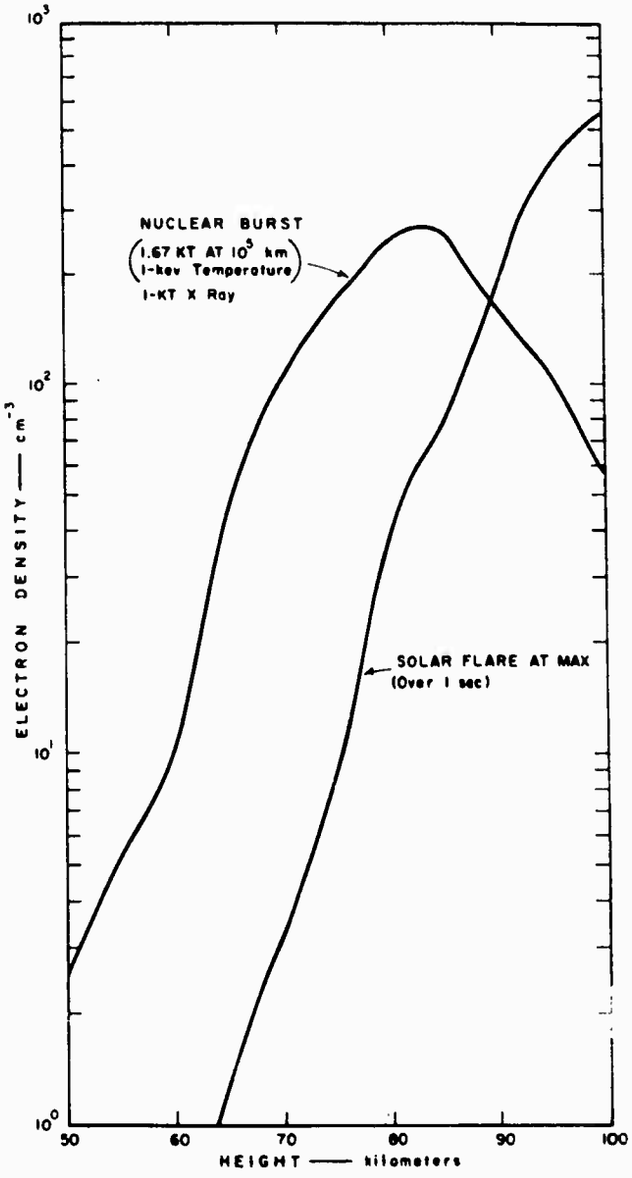

FIG. 6.3 IONIZATION DUE TO A FLARE AND TO A NUCLEAR SOURCE

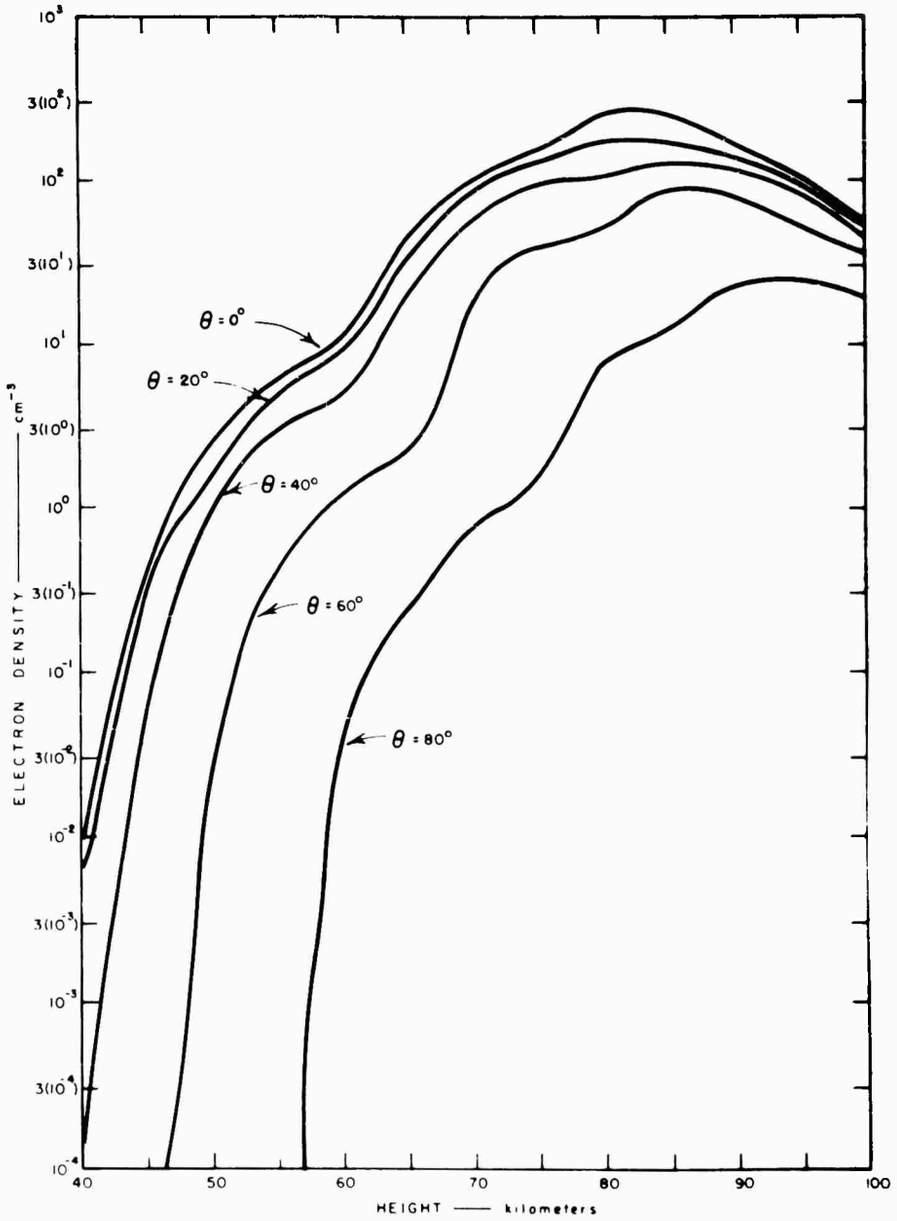

FIG. 6.4 IONIZATION DUE TO A 1.67-KT NUCLEAR BURST AT 10^5 km AND 1-kev TEMPERATURE

plotted on Fig. 6.4. The irregularities of Fig. 6.4 are probably introduced by approximating the continuous X-ray spectrum by a definite flux at each of several discrete wavelengths (the same is true of the calculations of the ionization due to a solar flare shown on Figs. 5.3 and 6.3). A comparison of the curves of Fig. 6.4 with those of Fig. 5.3 shows considerable differences in over-all behavior, in both the zenith-angle and height dependence of the ionization.

It may be concluded that, even if the X-ray flux during an unusually abrupt solar flare occurred in a burst of magnitude and duration, as observed by detectors at the earth, comparable with that associated with a nuclear burst in space, then differences in the spectral distribution of the X radiation would produce corresponding ionospheric variations which could be distinguished by radio methods.

6.3 THE DECAY OF IONIZATION FOLLOWING A NUCLEAR BURST IN SPACE

If the pre-existing ionization is neglected, and the deposition of ionization by the nuclear burst taken as instantaneous, with zero production before and after the explosion, then the ionospheric balance equations with B = E are of a very simple form:

$$\frac{dN}{dt} = -AN - BNN^{+} + FN^{-}$$

$$\frac{dN^{-}}{dt} = AN - FN^{-} - BN^{-}N^{+}$$

$$\frac{dN^{+}}{dt} = -BN^{+2}$$

with the solutions

$$N^+ = \frac{N_o}{1 + N_o \beta t}$$

$$N = \frac{N_o}{(A + F)(1 + N_o \beta t)} \left\{ F + A \exp\left(-(A + F)t\right) \right\}$$

$$N^- = \frac{N_o A}{(A + F)(1 + N_o \beta t)} \left\{ 1 - \exp\left(-(A + F)t\right) \right\}$$

where N_o is the positive-ion or electron density produced at time t = O.

The variation of N with time is plotted in Figs. 6.5 through 6.10 for values of N_o of 10^2, 10^3, 10^4, and 10^5, and heights at 10-km intervals between 60 and 100 km. Both day and night circumstances are shown. χ is taken as 0° during the day. It is evident that the decay of the electron density often has three main phases. Initially, the loss of electrons is primarily by attachment, until a quasi-balance of attachment and detachment processes has been established, with a corresponding partition, almost independent of N_o, of negatively charged particles between electrons and negative ions. Subsequently, there is a plateau during which the electron density remains approximately constant; the duration of the plateau depends upon the height and upon N_o. Finally, the decay phase of the negative and positive carriers by recombination takes over. There is then a strong tendency for the curves for different values of N_o to approach each other; in other words, the remaining electron density after a very long time is independent of N_o. It is noteworthy that the duration of the excess ionization does not increase entirely systematically as the height increases; this is exemplified on Fig. 6.10 for the night curves.

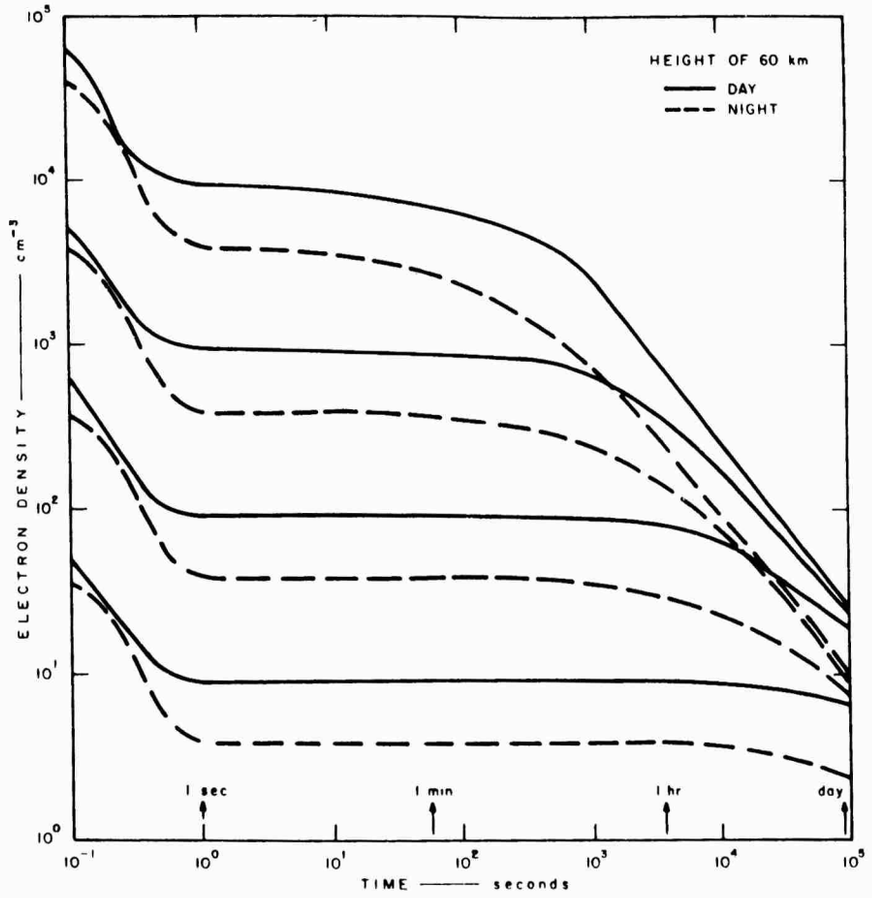

FIG. 6.5 DECAY OF NUCLEAR IONIZATION – HEIGHT 60 km

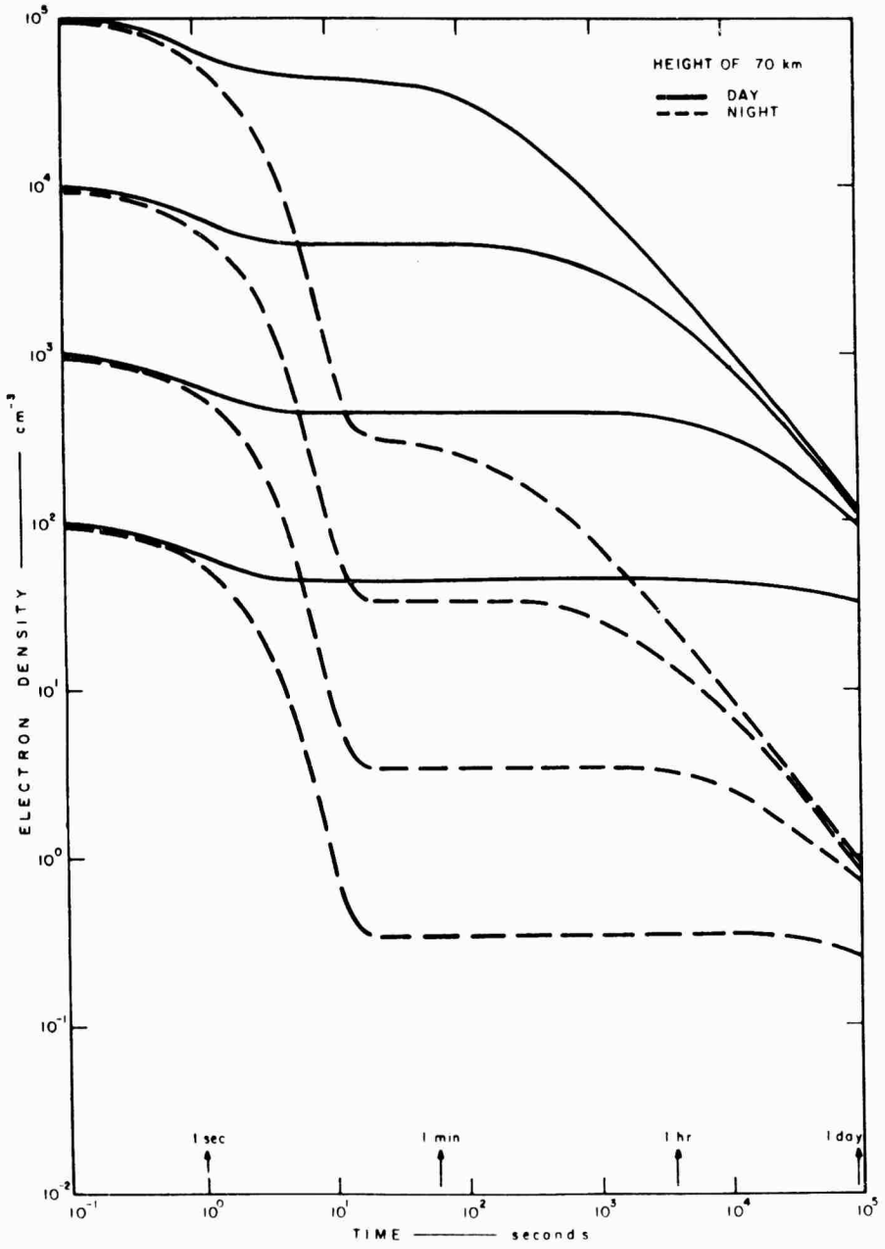

FIG. 6.6 DECAY OF NUCLEAR IONIZATION – HEIGHT 70 km

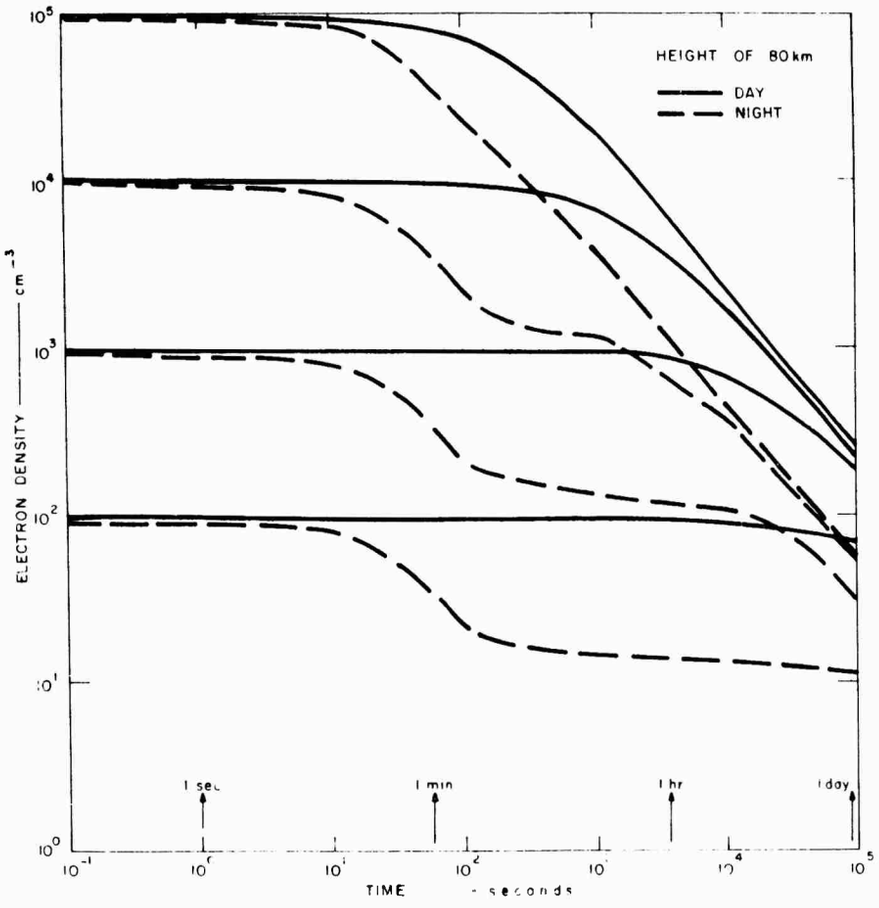

FIG. 6.7 DECAY OF NUCLEAR IONIZATION – HEIGHT 80 km

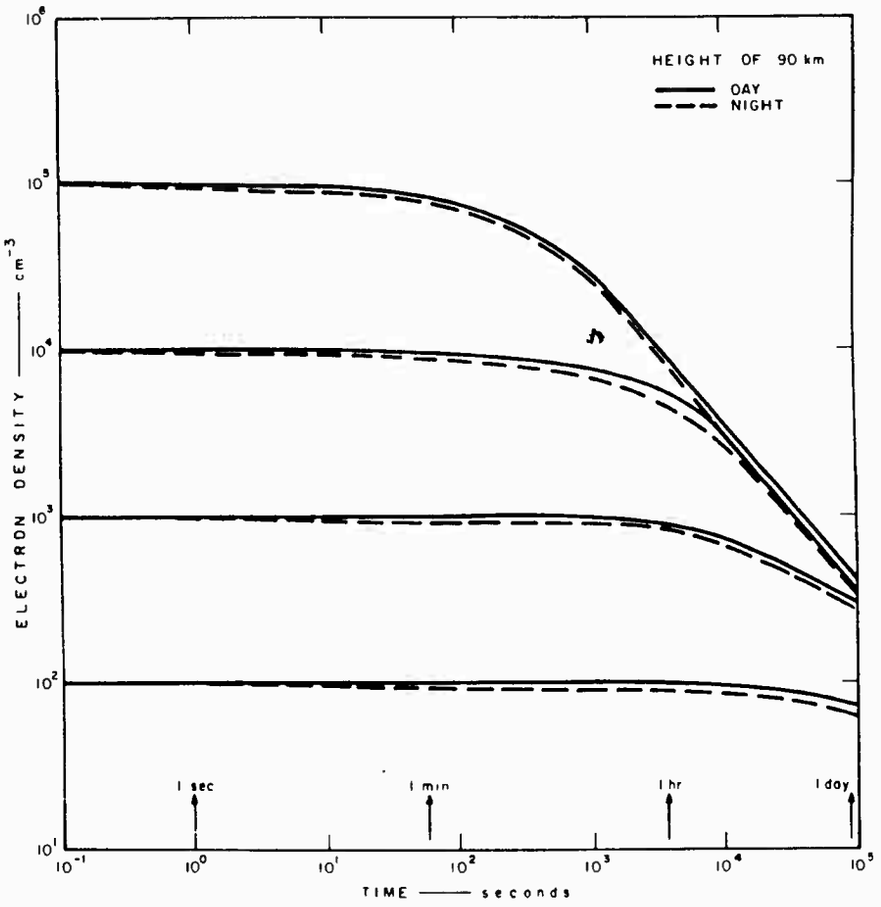

FIG. 6.8 DECAY OF NUCLEAR IONIZATION – HEIGHT 90 km

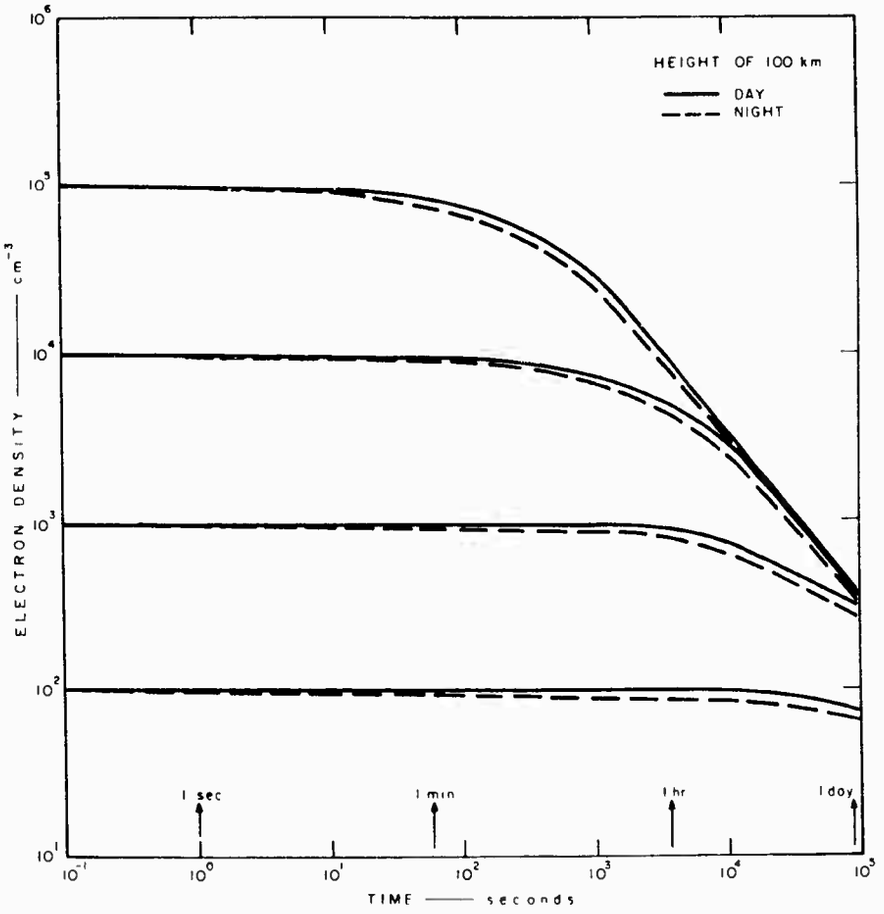

FIG. 6.9 DECAY OF NUCLEAR IONIZATION – HEIGHT 100 km

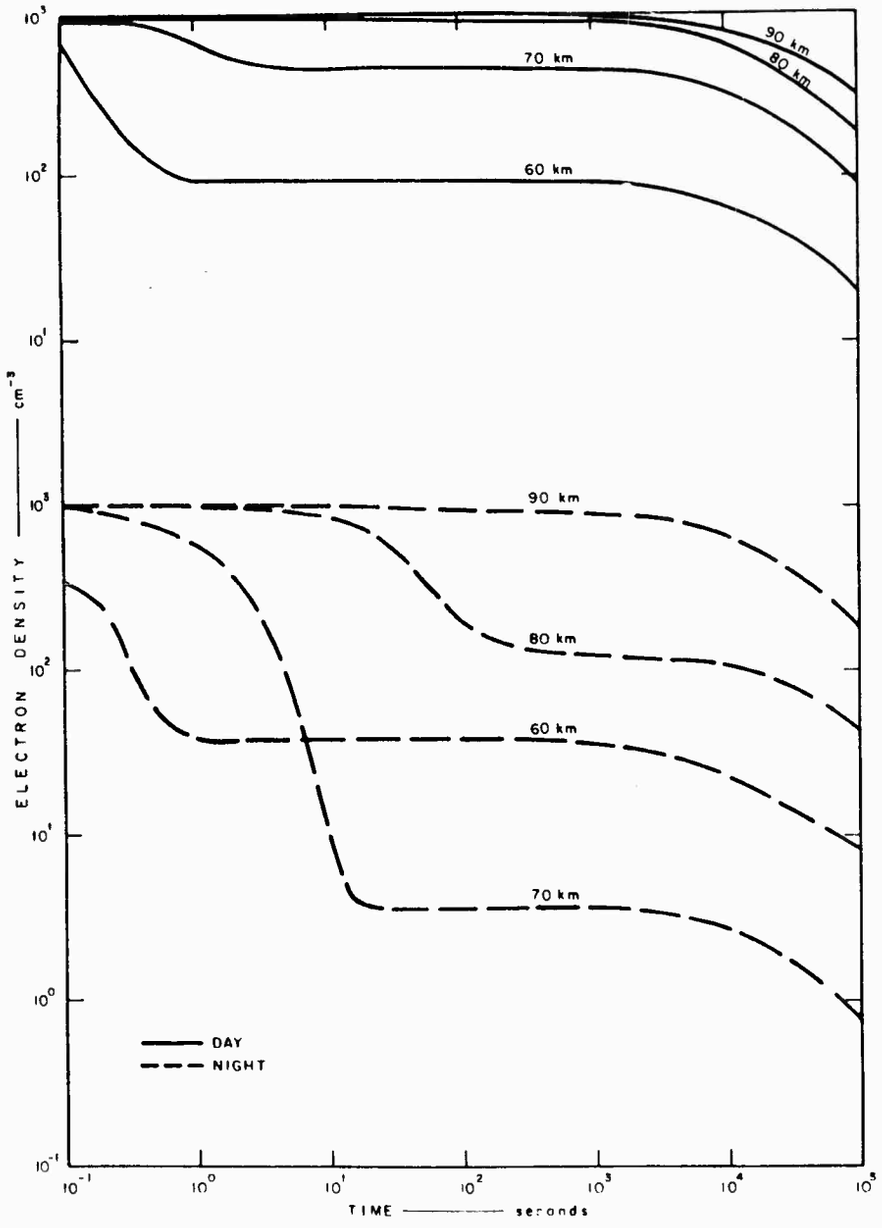

FIG. 6.10 DECAY OF NUCLEAR IONIZATION – $N_0 = 10^3$

The treatment is altered somewhat if, with all other conditions unchanged, the effects of a constant rate of production of ionization before and after the explosion and the resulting equilibrium value of the ionization are included. The appropriate equations are

$$\frac{dN}{dt} = Q - AN + FN^- - BNN^+$$

$$\frac{dN^-}{dt} = AN - FN^- - BN^-N^+$$

$$\frac{dN^+}{dt} = Q - BN^{+2}$$

with the initial conditions that $N = N_o + N_q$, $N^+ = N_o + N_q^+$, $N^- = N_q^-$ at time $t = o$. Suffix q gives the equilibrium values for the quiet-sun conditions which were considered in Sec. 3. By writing $N_o = KN_q$ and considering, for example, heights of 60-70 km, it is found that for $K < 100$ it is possible to solve these equations approximately by considering two separate stages in the return to equilibrium conditions, as suggested by Swift (1961). In the first stage, the effects of recombination and the steady ionization are neglected so that N^+ remains sensibly constant while there is a rapidly achieved balance of attachment and detachment resulting in the ration $N^-/N = A/F$, which is then maintained. The second stage consists of a slow decay of electrification to the equilibrium values, by recombination. The solutions are then, for the first stage

$$N = \frac{N_q}{A+F}\left[(K+1)F + A\left(1 + Ke^{-(A+F)t}\right)\right],$$

$$N^+ = N_o + N_q^+ = KN_q + \frac{A+F}{F} \cdot N_q = \left[(K+1)F + A\right]\frac{N_q}{F},$$

and $$N^- = N^+ - N;$$

and for the second stage

$$N^+ = \frac{N_q^+\left[2N_q^+ + N_o\left(1 + e^{-2\sqrt{BQ}\,t}\right)\right]}{2N_q^+ + N_o\left(1 - e^{-2\sqrt{BQ}\,t}\right)},$$

$$N = \frac{FN^+}{A+F},$$

and $$N^- = \frac{AN^+}{A+F}.$$

For the above treatment to be valid, it is necessary that N^+ does not change appreciably during the short time during which the ratio N^-/N is becoming insignificantly different from A/F. Two conditions are involved. The first is that

$$e^{-(A+F)t} \ll \frac{F(K+1)+A}{AK}$$

which gives

$$t \gg \frac{1}{A+F} \ln \frac{AK}{A+(K+1)F} .$$

The second condition is satisfied when

$$e^{-2\sqrt{BQ}\,t} \gg \frac{N_o^2 + N_o(1-N_q^+) - 2N_q^+}{N_o(N_o+N_q^++1)} > 1 - \frac{3(A+F)^2}{K^2F^2+(A+F)^2}$$

which is obeyed for t such that

$$2\sqrt{BQ}\,t \ll \frac{3(A+F)^2}{K^2F^2+(A+F)^2} .$$

These together require K to be such that

$$\frac{AK}{A+(K+1)F} \ll exp\left\{\frac{3(A+F)^3}{2\sqrt{BQ}\left(K^2F^2+(A+F)^2\right)}\right\} .$$

With K<100 and values of the parameters A, F, B, and Q appropriate for heights of 60 to 70 km, the above inequality is certainly satisfied.

The solutions for K = 1 and K = 10 at heights of 60, 65, and 70 km have been plotted in Figs. 6.11 and 6.12 using the values of the constants for zenith

angle and magnetic dip angle both zero, that is, neglecting any variation in Q and F due to changing zenith angle during the time of the return to equilibrium. For comparison, the curve obtained neglecting Q for a similar initial value of total ionization has also been drawn (Fig. 6.11) corresponding to the case K = 10 and a height of 70 km. It is seen to be almost identical in the initial stages, but differs greatly as t increases so that the effect of the steady Q begins to show. The differences are in the later recombination stage rather than in the earlier stage of partition of the negative carriers between electrons and negative ions. Further calculations showing the importance of considering pre-existing ionization are included in Appendix I, in which the relevance of the present work to two recent reports by Westfall and by LeLevier is considered.

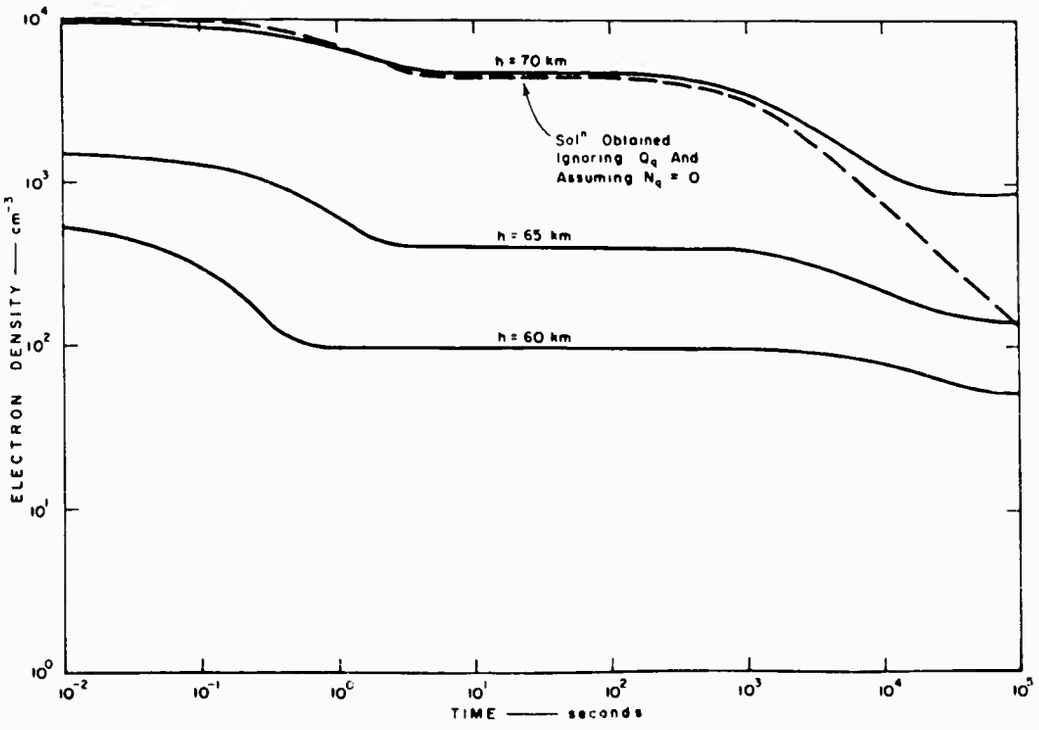

FIG. 6.11 DECAY OF NUCLEAR IONIZATION WHEN PRE-EXISTING IONIZATION IS CONSIDERED (K = 10)

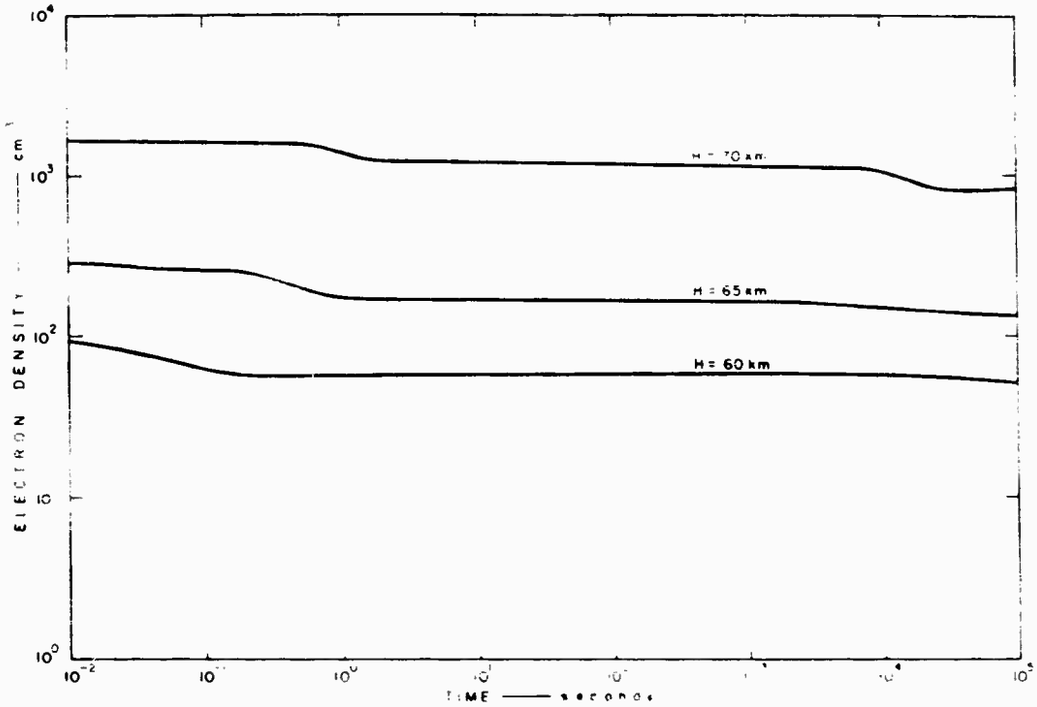

FIG. 6.12 DECAY OF NUCLEAR IONIZATION WHEN PRE-EXISTING IONIZATION IS CONSIDERED (K = 1)

6.4 REFERENCES FOR SEC. 6

Bollen, R. L., and R. B. Dyce. "Procedure for Calculating Ionospheric Absorption Resulting from a Nuclear Burst in Space," Monograph 1 Contract AF 49(638)-989 (May 1961). SRI Project 3498, Stanford Research Institute, Menlo Park, California (May 1961).

Swift, D. W., "The Effect of Solar X-Rays on the Ionosphere," J. Atmos. Terrest. Phys., Vol. 23, pp. 29-56 (1961).

7. SUMMARY AND CONCLUSIONS

This report is primarily designed to provide a survey of the phenomenology of SEAs and a background of ionospheric theory for use in further work. It is not intended to be a self-contained and complete entity. However, it is still desirable to summarize the major points that have emerged. These are:

(1) There is an association but no rigid interconnection between the various SID phenomena accompanying a solar flare.

(2) SEAs have an average rise time of about 10 min. Rise times of less than 2 min are relatively rare, but occur upon the average at a rate of perhaps one every two months.

(3) SEAs due, respectively, to a solar disturbance and to a local thunderstorm have considerable similarity. The best way of differentiation is to use the fact that an SEA produced by thundery activity gives an enhancement at all frequencies; the SEA accompanying an SID has an enhancement at frequencies exceeding 20 kc and a decrease in noise for frequencies less than 10 kc.

(4) There are considerable differences in the temporal behavior during an SEA at frequencies of 10 and 27 kc. It seems probable that the 10-kc noise is influenced by ionization at a lower level than is the case for a frequency of 27 kc. This implies that the significant ionizing radiations and the speed of ionospheric recovery are different for the two frequencies.

(5) The interesting behavior as a function of frequency during an SEA suggests that simultaneous observations at many frequencies in the VLF band would be valuable.

(6) A survey of information on the rate coefficients for the lower ionosphere suggests that the values of the attachment coefficient are well established. As regards detachment, photodetachment is dominant by day at heights exceeding 60 km; below this level, collisional detachment seems significant. At night collisional detachment dominates below 70 km while associative detachment is probably important at greater heights. The electron-ion and ion-ion recombination coefficients are of comparable magnitude and do not vary much with height. Consequently, the considerable simplification in ionospheric theory of regarding the two recombination coefficients as equal and constant seems valid.

(7) The major ionizing agencies in the lower ionosphere are solar X rays, solar Lyman α, and cosmic rays. The latter is the only significant influence at night, and even by day is dominant below 60 km. In daytime and for heights between 60 and 80 km, the three agencies are of comparable strength; above 80 km, X rays are most important. These conclusions are for a period near solar maximum; there are indications that the significance of solar X rays relative to solar Lyman α may decrease with sunspot number.

(8) The balance equations for the lower ionosphere can be solved easily, assuming no vertical transport of ionization and equating the recombination coefficients. By day the equilibrium condition corresponding to a very slow rate of change of ion density is closely approached; at night, however, decay of the ionization from an equilibrium daytime value must be considered. There are considerable global asymmetries in electron density contours. Generally speaking, however, two electron layers can be identified at night; one centered at about 55 km is due to cosmic rays, while above some 80 km ionization produced during the day persists throughout the night. With the onset of daytime conditions, the ionization above 65 km increases rapidly.

(9) A parameter, ω_r, which may be considered as an effective ionospheric conductivity, defines the upper boundary of the earth-ionosphere waveguide system involved in VLF propagation. Conversion of electron density contours into contours of ω_r shows that these are not parallel to the surface of the earth, particularly by day. For meridional propagation the contours of ω_r are very different according to whether the term in ω_r involving the earth's magnetic field is included or neglected.

(10) During a moderate solar flare the flux of X rays affecting the lower ionosphere increases by a factor of perhaps twenty. The flux rises to its maximum in a time of some 5 minutes; the subsequent decay occupies about 15 minutes. The X-ray flux produces its greatest proportionate increase in ionization (by a factor of about four) at a height near 80 km. The time to reach maximum electron density varies between 300 and 1000 sec. according to height; the greatest lag is at the lower heights. Surprisingly enough, the rate of decay of the added ionization tends to increase with increasing height.

(11) A nuclear burst in space emits a flux of X rays that differs in three significant respects from the flux associated with a solar flare. First,--and most important--the onset is immediate. Second, the spectrum of the nuclear flux is concentrated more towards energetic X rays than is the solar flux. Third, the zenith-angle dependences are different. The more energetic spectrum implies the production of ionization at low levels in the ionosphere. Combined with the sudden onset, this means that the ionization changes at a height of 70 km, a

controlling level in daytime VLF propagation, are far more rapid during a nuclear burst than during a solar flare.

(12) After the sudden deposition of ionization in the lower ionosphere by a nuclear burst in space, three decay phases can often be identified: the establishment of an initial partition of negative carriers between electrons and negative ions; a plateau stage during which there is little change in electron density; and a final phase in which recombination processes control the decay. The pre-existing ionization has considerable influence upon the decay, especially during the recombination phase.

(13) If a specific electron density is suddenly deposited, as by a nuclear burst, at different levels in the ionosphere, there are apparent anomalies in the decay of the ionization. When account is taken of the pre-existing ionization, the rate of decay does not decrease systematically as height increases, as might be anticipated. The exact specification of this anomalous behavior depends critically upon the values assumed for the rate coefficients and for the quiet-state ion production. An example, for heights of 70, 75, and 80 km, shows that in the attachment-detachment phase electrons are lost more rapidly at the lower heights. The contrary is the case for the recombination phase, so that ultimately the greatest electron density exists at 70 km.

(14) It is shown that the departures from parallelism of the earth and ionosphere boundaries for the waveguide theory of VLF propagation have significant implications. The true attenuation coefficient can differ from an average value, deduced for an ionospheric boundary of constant height, by 10 percent or more according to the time of day.

APPENDIX I

REPORTS BY WESTFALL AND LELEVIER

APPENDIX I

REPORTS BY WESTFALL AND LELEVIER

I.1 GENERAL

Since the completion of much of the work of this report, two important relevant reports have become available, and it is worthwhile comparing their results with those already stated. The first of these, by Westfall (1962) deals with the variation of the electron density in the ionosphere caused by an SID, in particular as observed in the sudden phase anomaly (SPA) occurring in VLF propagation. From observations of this phenomenon it is possible to calculate the changes in the effective height of reflection for a given frequency, which can then be related to electron density at that height. Two points arise that are of interest here. The first is that, as for the SCNA and SEA statistics considered in Sec. 2, the SPA observations did not indicate that there is any close correlation between the visible Hα-flare and the ionizing flux, either in temporal behavior or magnitude. A lack of correlation is also noted in comparing the ionizing flux to 2800-Mc solar noise bursts, although all three phenomena are generally related and are products of a disturbed state of the sun. Second, Westfall's deductions of spectral behavior during a flare are worth noting. The relation between X-ray flux and electron density produced is considered to be that given by Pierce and Swift (1960). The rate coefficients used in that report are considerably different from those given in Sec. 3 of this report, but the same general behavior, a nonlinear decrease in electron production with increasing solar zenith angle and decreasing ionospheric height, is found with the modified parameters as was obtained with the Pierce and Swift (1960) values. The solar zenith-angle dependence of the electron density caused by an SID is largely related to the spectral content of a flare. Because the relationship between solar zenith-angle difference and the difference in change of height of reflection

between two paths during a flare varies for different flares, Westfall concludes that the spectral content of the X-ray flux is variable. The treatment of Sec. 5 assumes, for simplicity, a specific spectral distribution although stating that this is not necessarily maintained, even during the course of a single flare. Variations in spectral distribution between individual flares are certainly to be anticipated and would account for Westfall's observations. There are, however, other factors involved which could also be considered in explaining the variations noted. For example, the actual zenith angle and the latitude of the path will cause differences in the original pre-flare reflection height over that path, and the change in height caused by a given X-ray flux is height dependent.

A second and more closely related report is that of R. E. LeLevier (1962) which covers essentially the material of Sec. 6.3. A summary of the rate coefficients involved in determining ionospheric balance conditions is made, but it is not as detailed as that of Sec. 3. A brief comparison of the values obtained is made here.

I.2 ATTACHMENT (A)

LeLevier considers A to be solely due to a three-body attachment process whereas in Sec. 3 it is found that, above about 80 km, radiative attachment to O_2 and also attachment to atomic oxygen become significant. Figure I.1 gives an approximate comparison of the two sets of values.

I.3 ELECTRON-ION RECOMBINATION (B)

LeLevier uses the value of 4×10^{-7}, corresponding to recombination with O_2^+, which is approximately the upper bound given in Sec. 3. This is an order of ten greater than that used throughout this report ($B = 4 \times 10^{-8}$), a difference which considerably modifies the results obtained when considering the decay of ionization. The reasons for the value employed in this report are given in Sec. 3.

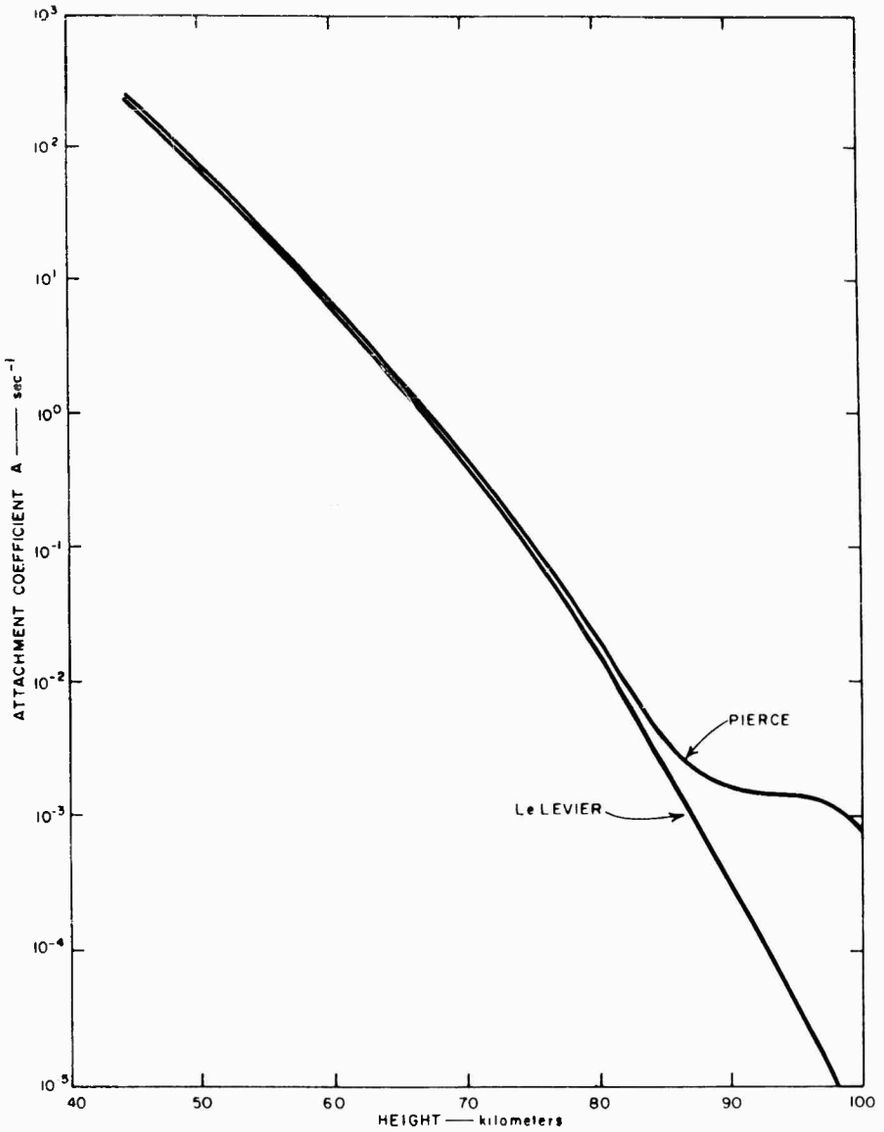

FIG. I.1 COMPARISON OF VALUES OF PIERCE AND LE LEVIER FOR THE ATTACHMENT COEFFICIENT

I.4 ION-ION RECOMBINATION (E)

In most of the calculations of this report E is taken as equal to B, and is therefore given by 4×10^{-8}. LeLevier carries out his analysis twice, in one case equating E to B, and in the other using E = O. However the difference in B already noted results in a different E even when the same assumption (i.e., E = B) is made.

I.5 DETACHMENT (F)

In this report F = C + D where C is the term due to photodetachment and D is the sum of collisional and associative detachment. The figures given show D to be significant below about 70 km, whereas LeLevier considers it is negligible and includes only photodetachment from the O_2^- ion. This differs even from the C term of this report, because above 80 km the contribution of detachment from the O^- ion is appreciable. LeLevier makes no mention of zenith-angle dependence, implicitly assuming a zenith angle of zero in his value of the photodetachment coefficient.

The values of the ambient electron density (N_q) have been shown in Sec. 3 to vary with latitude and zenith angle as well as with height. In Fig. I.2 LeLevier's assumed electron density profile is compared with that obtained for quiet-sun conditions and latitude and zenith angle both zero.

LeLevier obtains an exact solution for the decay of ionization after a sudden deposition of ions which gives the same result as the approximate solution of Sec. 6.3. This is true during both stages of the decay, in all the cases considered, using either set of parameters, since the most important condition, $\sqrt{BQ} << A + F$, holds. Thus any differences in results obtained are due to the different choice of values for the parameters. Choosing the height 67 km, at which the ambient electron densities of Fig. I.2 are equal, the decay of ionization after a deposition of 10^3 electrons/cm^3 has been calculated using both sets of parameters. The excess ionization ($N-N_q$) is plotted on logarithmic scale in

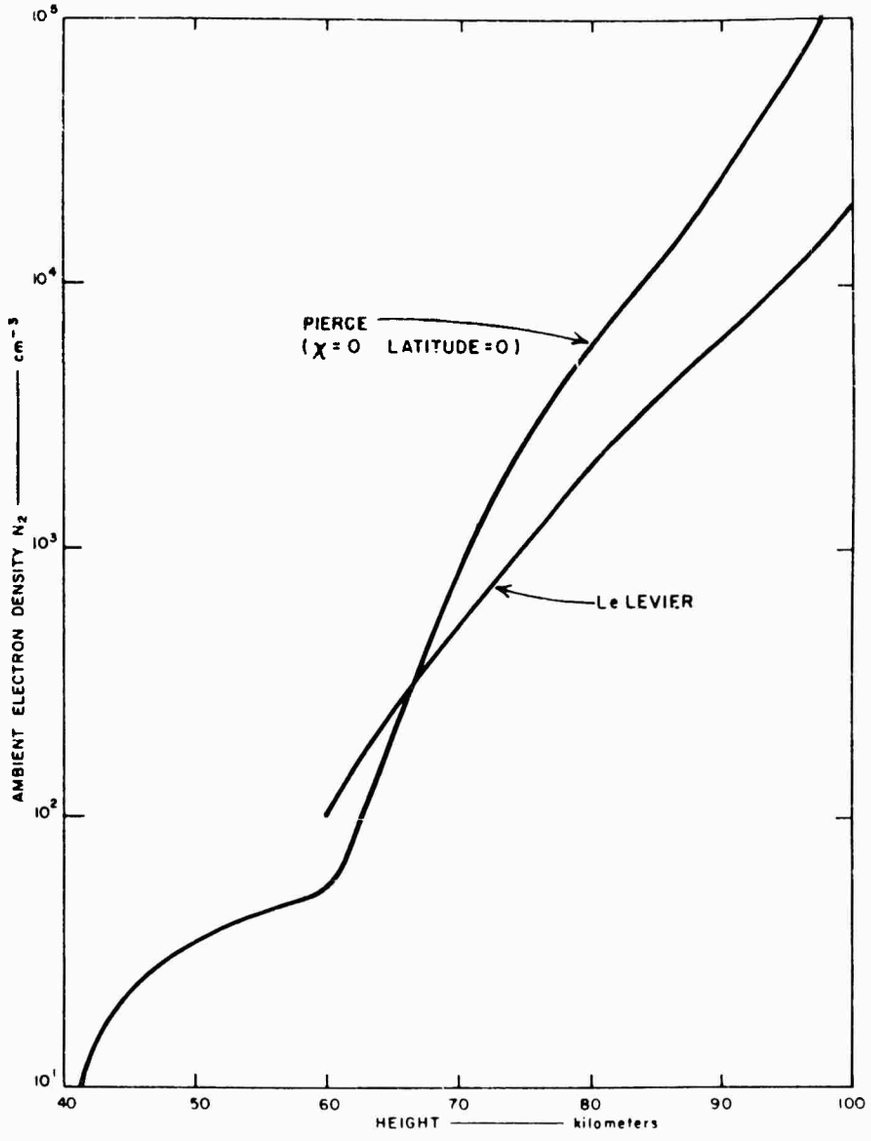

FIG. 1.2 COMPARISON OF QUIET SUN ELECTRON DENSITY PROFILES AS GIVEN BY PIERCE AND BY LE LEVIER

Figure I.3. Figure I.4 shows the total electron densities for comparison with earlier figures in this report.

One of the most interesting features of LeLevier's work is his confirmation of an effect originally noted by Booker and Crain (1962). This work showed that if a certain density of electrons is suddenly added at different levels in the lower ionosphere, then the rate of decay of the additional ionization does not decrease steadily as height increases, as might be expected. There are regions where the persistence of the ionization is greater than the levels above or below. Booker and Crain found that these apparently anomalous persistence effects are especially marked when account is taken--as it obviously should be--of any pre-existing steady ionization. Figure 6.10 (night) shows, however, that these anomalies can be present even when the pre-existing ionization is ignored.

For daytime conditions and with the parameter $B = E = 4 \times 10^{-7}$ LeLevier gives curves showing that the decay of an added 10^3 electron/cm^3 is less rapid at 75 km than it is at 70 or 80 km. A similar analysis has been performed with the parameters of the present report (notably $B = E = 4 \times 10^{-8}$) and the results are shown in Fig. I.5, those of LeLevier also being given for comparison. During the phase in which the attachment-detachment balance is being established, that is up to between perhaps 10 and 100 sec, both sets of results show that the proportion of the ionization persisting increases with increasing height. However, for times between 10^3 and 10^4 sec when the ion decay phase has taken over, LeLevier's parameters, as already mentioned, lead to a greater electron density at 75 km than at 70 or 80 km. When the Pierce parameters are employed, the even more surprising result is obtained that the persisting electron density in the ion decay phase becomes greater at 70 km than it is at either 75 km or 80 km.

It is evident that these apparently anomalous persistence effects are quite common. Also, it is difficult to establish their exact magnitude and significance without precise knowledge of such quantities as the ambient electron density,

the quiet-state ion production, and--most important--the rate coefficients.

REFERENCES FOR APPENDIX I

Booker, H. G., and C. M. Crain, "The Effects of Nuclear Bursts in Space on the Propagation of High-Frequency Radio Waves Between Separated Earth Terminals," R-394-PR, The RAND Corporation, Santa Monica, California (February 1962).

LeLevier, R. E., "The Response Time of the Lower Ionosphere to a Pulse of Ionization," Memorandum RM-3204-PR, The RAND Corporation, Santa Monica, California (August 1962).

Pierce, E. T., and D. W. Swift, "Study of Spontaneous Ionospheric Disturbances," Technical Report RAD-TR-14-60-7, Part 1, Avco Corporation, Wilmington, Massachusetts (1960).

Westfall, W. D., "Factors Which Control Solar Flare Induced Ionospheric Height Changes as Observed with VLF Radio Waves over Long Paths," USNEL Problem M4-1, ARPA Order 164-62, Amendments, U. S. Navy Electronics Laboratory, San Diego, California (1 July 1962).

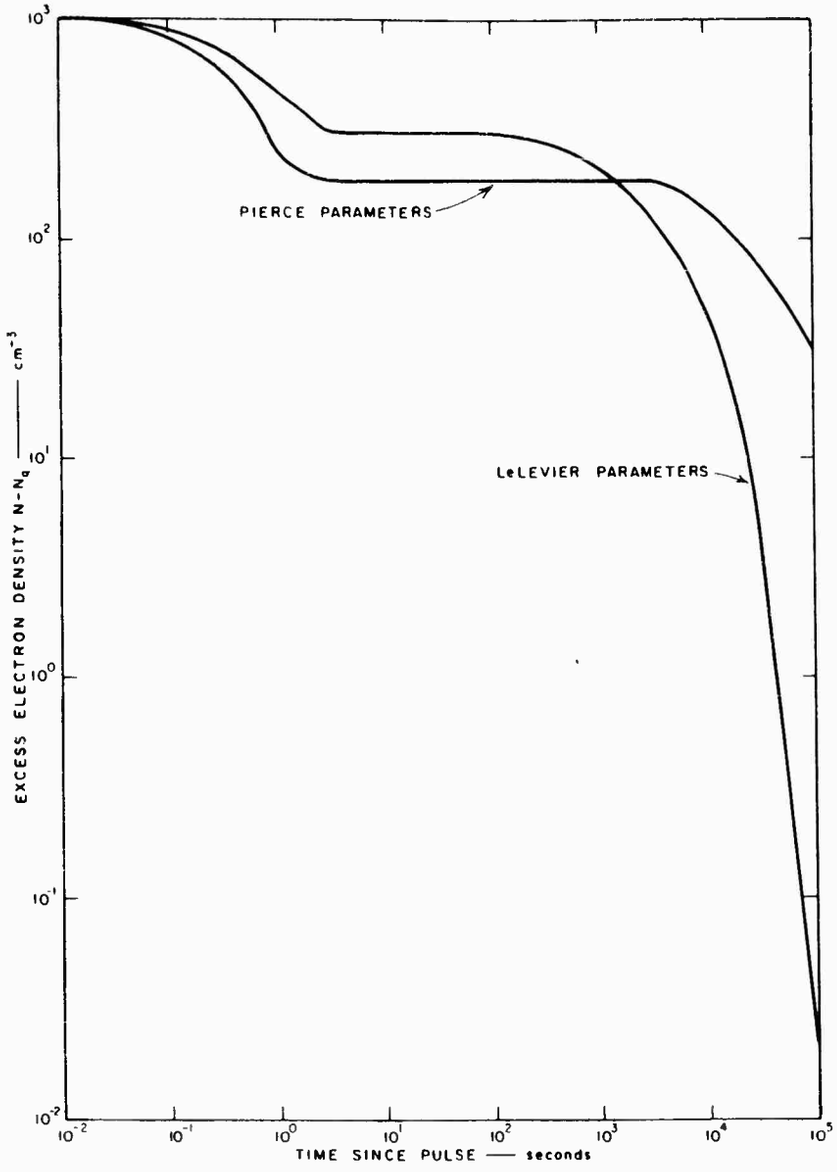

FIG. I.3 EXCESS ELECTRON DENSITY vs. TIME AFTER DEPOSITION OF 10^3 ELECTRONS/cm^3

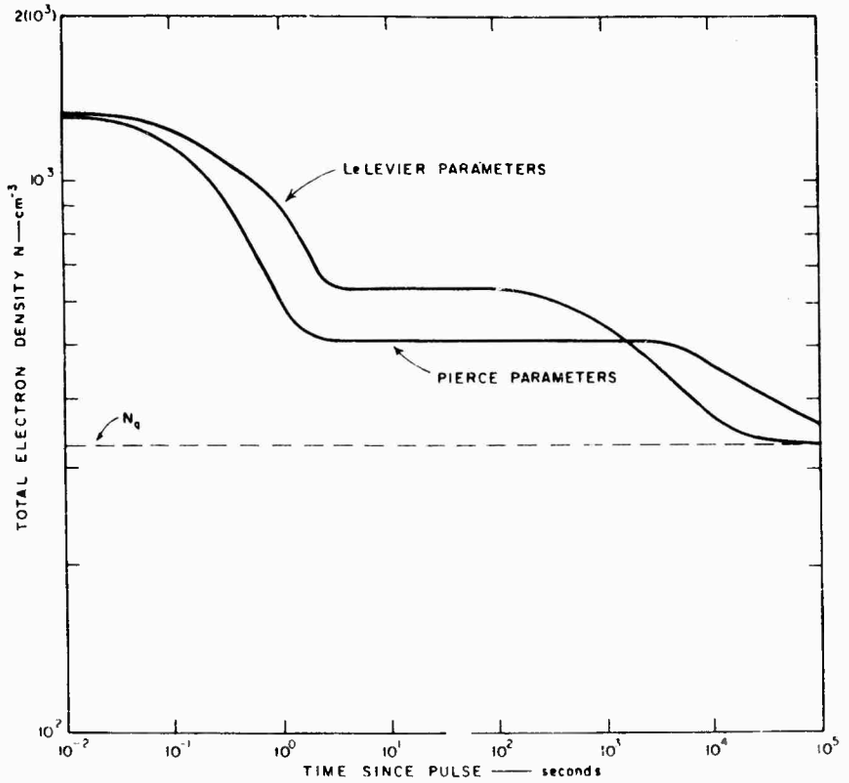

FIG. I.4 TOTAL ELECTRON DENSITY vs. TIME AFTER DEPOSITION OF 10^3 ELECTRONS/cm^3

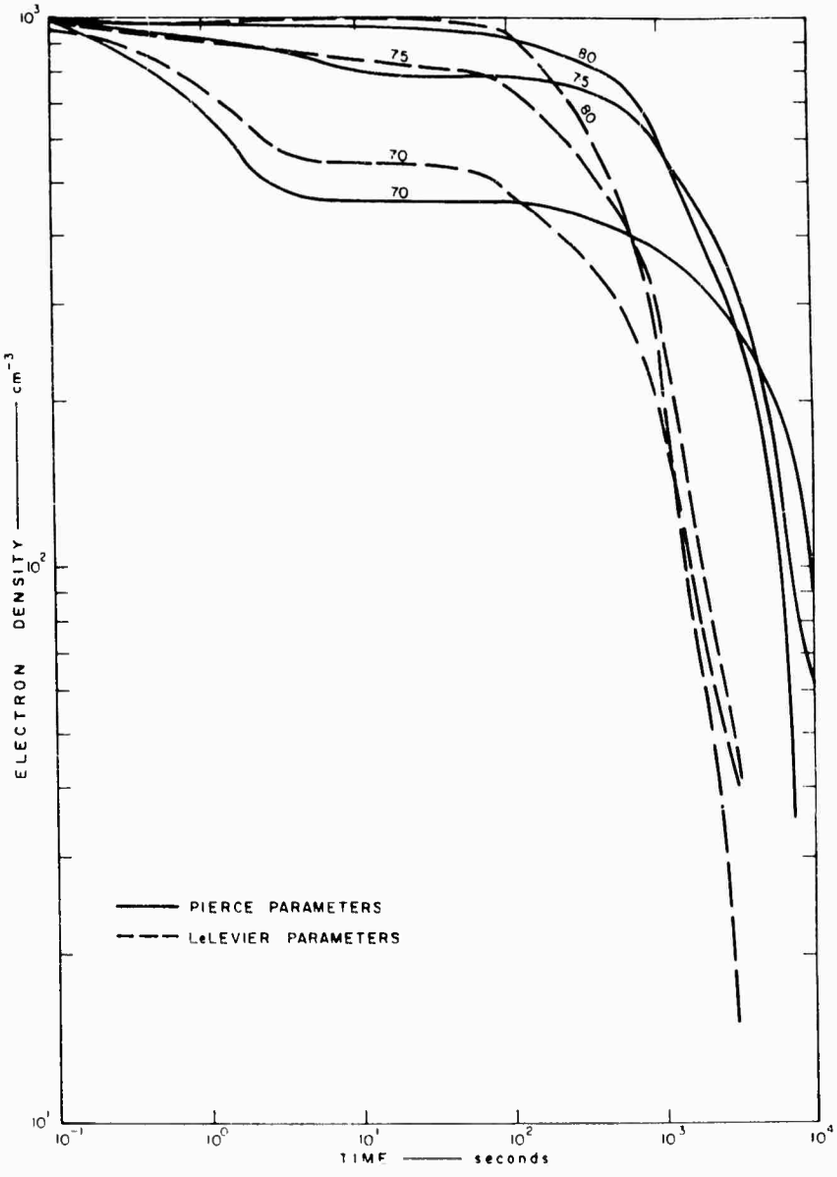

FIG. I.5 DECAY OF DEPOSITED ELECTRONS – COMPARISON OF LE LEVIER AND PIERCE PARAMETERS

APPENDIX II

THE EFFECT OF VARIABLE IONOSPHERIC HEIGHT ON VLF PROPAGATION

Appendix II

THE EFFECT OF VARIABLE IONOSPHERIC HEIGHT ON VLF PROPAGATION

The waveguide mode theory of VLF propagation has been largely formulated in terms of an ionosphere parallel to the surface of the earth. Comparatively little consideration has been given to analysis of the influence of variable ionospheric height, although Wait (1961) has examined the influence of a local perturbation. Wait (1962) has also treated the case of transition from day to night propagation, by conceiving the problem to be of propagation in two parallel-plate waveguide regions connected by a tapered section.

It is evident from the results deduced in Secs. 4, 5, and 6 of this report that contours of equal electron density in the lower ionosphere are not parallel to the earth's surface. This is true both for quiet conditions and also when the ionosphere is disturbed either by natural or nuclear events. The deviations from parallelism are comparatively gradual except near a sunrise zone. Nevertheless, when propagation over great distances is involved, as is commonly the case at VLF, the deviations certainly have appreciable influence.

A specific value of the parameter ω_r, which is directly related to the ionospheric conductivity, is convenient in defining the upper boundary of the waveguide. Suppose ω_r is chosen to be 10^5 cps. Then the earth-ionosphere guide is taken to be sharply bounded at the height for which $\omega_r = 10^5$: above this height the ionospheric conductivity is assumed to be uniform, while below the level of $\omega_r = 10^5$, ω_r is taken to be zero. In order to illustrate the variation in height of the contour $\omega_r = 10^5$, Fig. II.1 has been constructed. This shows the level $\omega_r = 10^5$ as a function of zenith angle (relative longitude) for propagation around the equator at an equinox and under quiet ionospheric conditions. The results used in preparing Fig. II.1 were derived in Sec. 4. It is noteworthy that the curve for height versus zenith angle is asymmetric, with the greatest slope at sunrise.

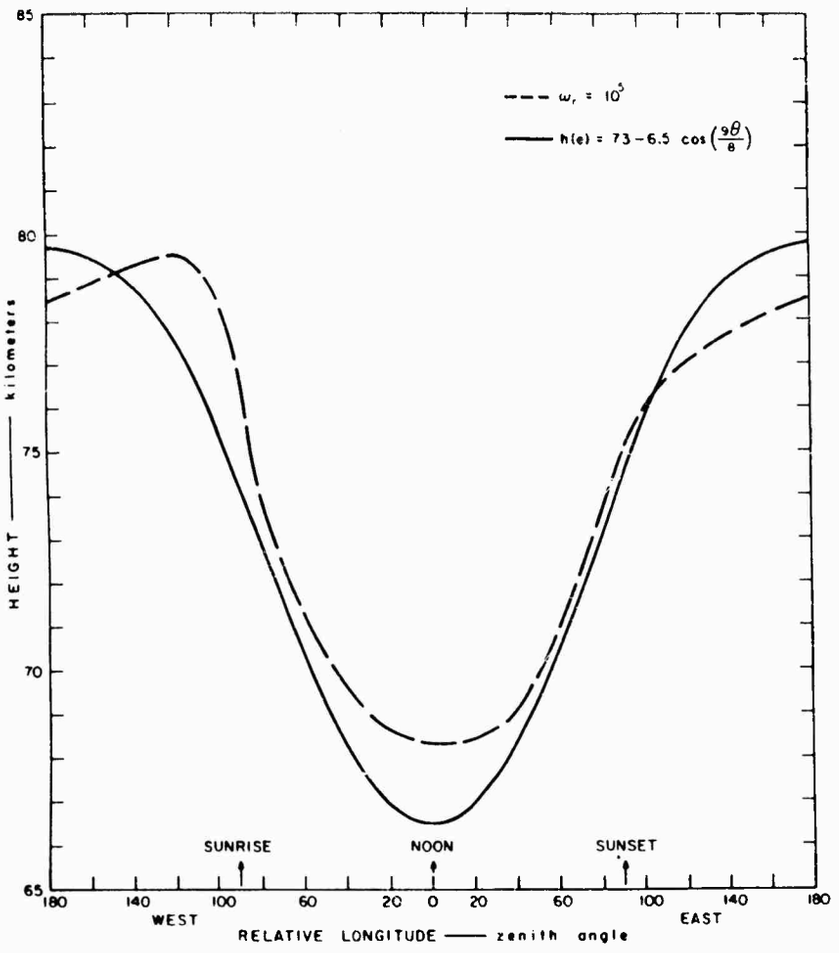

FIG. II.1 VARIATION OF EFFECTIVE IONOSPHERIC HEIGHT WITH TIME OF DAY

Wait (1961) treated a local perturbation by postulating a cosine function for the variation of ionospheric height with horizontal distance. The same type of approach can legitimately be applied over much greater distances to obtain order of magnitude estimates for the influence of the ionospheric height variability. Some calculations have been made for the height variation represented by

$$h(\theta) = a - b\cos\left(\frac{90}{8}\theta\right) \tag{II.1}$$

where θ is the zenith angle (relative longitude) in degrees. This curve is plotted on Fig. II.1 for the values of the constants a = 73 and b = 6.5, h (θ), the height, being in kilometers. In the mode theory of VLF propagation, the major contribution to the decrease in amplitude with distance in a mode arises from a factor exp ($-\alpha x$), where x is the distance and α the attenuation coefficient. For the least attenuated mode (n = 1), the attenuation factor, α, is given approximately (Wait 1957) by

$$\alpha = \left(\sqrt{\frac{\omega}{\omega_r}} + \sqrt{\frac{\omega_r}{\omega}}\right)\frac{\lambda^2}{16\sqrt{2}\cdot h^3} \quad nepers/km \tag{II.2}$$

where ω is the angular frequency being propagated, λ the corresponding wavelength, and h the ionospheric height.

When the ionospheric height is variable, Eq. (II.2) must be modified by the inclusion of an integral. The attenuation factor between x and x_2 is then given by

$$x_1 \alpha x_2 = \left(\sqrt{\frac{\omega}{\omega_r}} + \sqrt{\frac{\omega_r}{\omega}} \right) \frac{\lambda^2}{16\sqrt{2}} \cdot \frac{1}{(x_2 - x_1)} \cdot \int_{x_1}^{x_2} \cdot \frac{dx}{(h(x))^3} \qquad \text{(II.3)}$$

If the height variation of Eq. (II.1) is adopted, the integral can be evaluated in closed form ($x = \theta R$, where R is the radius of the earth). The results obtained at a frequeney of 10 ke are given in Table II.1.

Table II.1

INFLUENCE OF VARIABLE IONOSPHERIC HEIGHT ON ATTENUATION COEFFICIENT

θ_1 (degrees)	θ_2 (degrees)	h_1 (km)	h_2 (km)	α (db/1000 km)
0	40	66.5	68.4	2.34
40	60	68.4	70.5	2.24
60	80	70.5	73.1	1.91
80	100	73.1	75.7	1.75
100	120	75.7	77.6	1.58
120	140	77.6	79.0	1.44

For a height of 70 km, which is that eommonly adopted in daytime VLF propagation, the attenuation coefficient as derived from Eq. (II.2) is 2.08 db/1000 km. A comparison of this value with the figures in Table II.1 shows that the attenuation coefficient ean differ according to the time of day by some ±10 percent from the average daytime value. The same result ean be derived very simply from Eq. (II.2). Since the $\omega_r = 10^5$ level shown in Fig. II.1 is about 68.5 km at noon and near 71 km at 16.00 ($\theta = 60°$), it follows from Eq. (II.2) that the ratio of attenuation coefficients at these times is $(71/68.5)^3 \approx 1.1$.

Obviously the asymmetric curve of Fig. II.1 for a level of constant ω_r can be better approximated by expressions other than that of Eq. (II.1). However, the above analysis is perhaps sufficient to indicate the potential errors implicit in assuming the attenuation coefficient to be constant throughout the day (or night, for that matter). Certainly with a long path, for which the solar zenith angle is significantly different from the average value over the day, the use of a mean daytime attenuation coefficient can lead to appreciable inaccuracies.

REFERENCES FOR APPENDIX II

Wait, J. R., "The Mode Theory of VLF Ionospheric Propagation for Finite Ground Conductivity," Proc. IRE, Vol. 45, pp. 760-767 (1957).

Wait, J. R., "Expected Influence of a Localized Change of Ionospheric Height on VLF Propagation," J. Geophys. Research, Vol. 66, pp. 3119-3123 (1961).

Wait, J. R., "An Analysis of VLF Mode Propagation for a Variable Ionosphere Height, " J. Research NBS, Vol. 66D, pp. 453-461 (1962).

STANFORD
RESEARCH
INSTITUTE

MENLO PARK
CALIFORNIA

Regional Offices and Laboratories

Southern California Laboratories
820 Mission Street
South Pasadena, California

Washington Office
808 17th Street, N.W.
Washington 5, D.C.

New York Office
270 Park Avenue, Room 1770
New York 17, New York

Detroit Office
The Stevens Building
1025 East Maple Road
Birmingham, Michigan

European Office
Pelikanstrasse 37
Zurich 1, Switzerland

Japan Office
911 Iino Building
22, 2-chome, Uchisaiwai-cho, Chiyoda-ku
Tokyo, Japan

Representatives

Honolulu, Hawaii
Finance Factors Building
195 South King Street
Honolulu, Hawaii

London, England
19 Upper Brook Street
London, W. 1, England

Milan, Italy
Via Macedonio Melloni 40
Milano, Italy

London, Ontario, Canada
P.O. Box 782
London, Ontario, Canada